University of Crete
Heraklion

Multiple Excitations In Structured Radiation Reservoirs

Georgios M. Nikolopoulos

Ph.D Thesis

2001

Ph.D Thesis

MULTIPLE EXCITATIONS IN STRUCTURED RADIATION RESERVOIRS

COMMITTEE

Prof. P. Lambropoulos (Supervisor)

Prof. E. N. Economou

Assoc. Prof. D. Charalambidis

Assoc. Prof. G. C. Psaltakis

Prof. A. T. Georges

Assoc. Prof. I. E. Perakis

Prof N. Papanikolaou

University of Crete
Physics Department
Heraklion, 2001

To my family

This thesis is submitted in partial satisfaction of the requirements for the degree of *Doctor of Philosophy* in the Department of Physics at the University of Crete.

I am indebted to my supervisor Prof. P. Lambropoulos, for his guidance during my Ph.D-studies, as well as for his valuable contributions to the work presented here. I want to thank him for our four-year collaboration and the knowledge I gained through the discussions we had. The most important aspect of our collaboration, however, is that he has been the exemplar of a scientist to me. His ideas in the context of scientific research, have influenced me in an irreversible way.

The main part of my Ph.D work has been performed at the Physics Department of the University of Crete. In addition, it has been a great pleasure for me to work in the Max-Planck Institut für Quantenoptic (MPQ) for one year. For the first six months I had the opportunity to collaborate with Dr. Søren Bay, who helped me at the beginning of my Ph.D-studies and I would like to thank him for the fruitful discussions we had. My adaption to the life in Germany would have been rather difficult without the help of the Theory Group secretary, Renate Weise-McKnight, who used to deal with all bureaucratic problems, while simultaneously she was creating a very warm atmosphere in the Institute, during the rainy days of winter.

The help of my diploma-thesis supervisor Prof. A. T. Georges has been invaluable to me. It was him who taught me the basics on atom−laser interactions when I was still an undergraduate student at the University of Patras, while his guidance has helped me more than one can imagine.

Many thanks also go to all the academic staff of the Physics Department and especially to Prof. D. Charalambidis since I had the pleasure to be teaching-assistant in his course for three academic semesters. Finally I thank all my friends both in Crete and Munich, who made my stay in Physics Department and MPQ respectively, a rather pleasant experience.

The present Ph.D work has resulted in a number of publications [86, 87, 89, 88], while I have also contributed to a review paper[64].

Georgios M. Nikolopoulos, Heraklion, February 7, 2001

Contents

Chapter 1

Introduction

Spontaneous emission is a fundamental process in atomic physics, resulting from the interaction between radiation and matter. In its simplest form the problem consists of an initially excited one-electron, two-level atom (TLA), which through the coupling to the vacuum electromagnetic field decays into its ground state emitting a photon. In the spirit of open (dissipative) quantum systems, the vacuum electromagnetic field acts as a *reservoir* or *bath* (infinitely many quantal degrees of freedom) into which the *small atomic system* (few quantal degrees of freedom) deposits its excitation in the form of radiation. The atom−reservoir coupling leads to fluctuating forces reflecting the modal structure of the vacuum electromagnetic field. Thus, the *photonic density of states* (DOS) does not only characterize the photonic reservoir but it determines the atomic dynamics as well.

For example, as is well known, a photonic DOS which varies smoothly over the spectral range of the atomic transition (*flat continuum*), results in a *vacuum shift* (Lamb shift) of the atomic levels as well as an *irreversible spontaneous decay* which renders all excited states unstable. Both spontaneous decay and vacuum shift appear in all texts of quantum electrodynamics (QED). As a result, for many decades they were considered to be inherent and unavoidable phenomena associated with matter. This view, however, overlooks the fact that spontaneous emission is a property of the combined system "atom + field" rather than of the isolated atom, and as such can be strongly modified by changing the atom−field coupling or by modifying the structure of the continuum.

Abrupt changes in the modal density in the vicinity of the atomic transition (*structured reservoir*), can affect significantly not only the magnitude but the nature of spontaneous decay as well. For instance, consider an atom excited to some Rydberg state, placed in a high-Q, high finesse cavity. In this case, spatial boundary conditions imposed on the radiation field determine the coupling constant between the atom and the field as well as the photonic DOS which exhibits sharp peaks, each corresponding to a reso-

nant cavity-mode. If the transition frequency to a lower atomic state (with which a nonzero electric dipole matrix element exists) lies between any of these peaks, spontaneous decay is strongly suppressed. On the contrary, if the transition frequency matches one of the cavity resonances, spontaneous decay is strongly enhanced due to the large DOS available to the emitted photon. Furthermore, spontaneous emission displays features of reversibility which appear as periodic exchange of energy between atom and cavity, known as *vacuum Rabi oscillations*, an unusual generalization of the more traditional *Rabi oscillations*, induced by an externally imposed field.

Quite recently it has been realized that strong modification in the photonic DOS can be achieved by means of photonic crystals (PCs). These are artificial dielectric structures exhibiting periodic spatial modulation of the dielectric constant. Under favorable circumstances, the spectrum of the electromagnetic field they support, may exhibit allowed bands and forbidden gaps, in analogy to the electronic band-structure in semiconductors. Inside a *photonic band-gap* (PBG), photonic modes and zero-point fluctuations are absent.

The material in this thesis deals with the interaction of small atomic systems with structured radiation reservoirs, which is of central importance in a number of areas including cavity QED (CQED), nanostructures, semiconductors, atom lasers and molecular physics. We will focus on the dynamics of few-level atoms or collections thereof, embedded in PCs. The first motivation for these studies was the fact that the unconventional photonic DOS associated with such materials, has been shown to be accompanied by a variety of novel phenomena such as: *inhibition* of spontaneous decay of an atom with transition frequency within the gap, strong *localization* of the emitted radiation at the site of the atom, *vacuum Rabi splitting*, formation of *"photon + atom" bound state*.

A fundamental difficulty in the theoretical description of such phenomena stems from the invalidation of the *Born* and *Markov* approximations, essential in obtaining a *master equation*, which is the standard tool in quantum optics problems involving flat photonic continua. As long as only one photon is exchanged between the small system and the reservoir, the problem can be handled through the direct solution of the respective time-dependent Schrödinger equation. The direct extension of this approach, however, to situations involving more than one photon in the reservoir does not seem tractable. The development of a technique capable of circumventing this mathematical difficulty, was the second motivation for the work presented in this thesis.

Closing this introductory section, we outline the remainder of this thesis. The following chapter (Chap. 2) is dedicated to a brief presentation of PCs, its fabrication and possible applications. In Chap. 3, after a brief introduction to elementary QED, we discuss various quantum optical phenomena in the context of open space and cavities. In Chap. 4 we focus on

quantum optics in PCs and in particular on various DOS models which have been adopted in the literature for the description of the modified radiation reservoir associated with PCs. We additionally review the major ideas in the state of the art right up to the work presented in this thesis. Finally, we set a **Research Question** to be answered in the following chapters.

In Chap. 5, we present the *discretization approach*, the validity and the limitations of which are discussed in the context of photonic continua of various DOS. Given the discretization, in the chapters that follow 5 we address problems involving multiple excitations in structured radiation reservoirs, and as such are not amenable to other techniques.

In Chap. 6, we study spontaneous emission in an atomic ladder system, with both transitions near-resonantly coupled to the edge of a PBG continuum. Studying the atomic dynamics in terms of the relative atomic detunings from the band-edge frequency, we find that the interaction of the atom with the strongly localized photons is accompanied by a variety of novel phenomena. Specifically, we predict the formation of a *"two-photon + atom" bound state* and a competition between a "direct" two-photon process and a stepwise one.

In Chap. 7, we consider a TLA coupled to the edge of a PBG and a defect-mode. The defect-mode acts as a photon source that can pump the atom. Propagating the wavefunction of the system, we obtain results pertaining to the problem of two and three photons in the reservoir, for various states of the defect-field. For a wide range of parameters we find that part of the total initial excitation remains *trapped* to the atom and the defect-mode in the long-time limit.

In Chap. 8, we investigate the dynamics of a small collection of two closely-spaced TLA, near-resonantly coupled to the edge of a PBG. Both atoms are considered to be initially excited, and the role of the dipole-dipole interaction in the *enhancement* of the collective decay is investigated.

Part I

Basics on Photonic crystals and Quantum Optics

Chapter 2

Photonic Crystals

In 1987, John and independently Yablonovitch, suggested that structures with periodic variation in dielectric constant could influence the properties of photons, in much the same way semiconductors affect the properties of electrons [51, 52, 125]. In semiconductors, it is the Bragg-like diffraction of the electrons from the atoms of the lattice which results to gaps in allowed energies, for which the electron's propagation is forbidden. In contrast to semiconductors, PCs do not exist naturally and need to be fabricated. One has to create somehow a periodic lattice, consisting now of dielectric matter (rods, spheres, slabs, etc) instead of atoms, with periodicity on the scale of the wavelength of light. Under appropriate conditions, a complete PBG in frequency may then open up, for which electromagnetic-wave propagation, irrespective of direction and polarization, is forbidden. Strictly speaking, linear-wave propagation is absent in a gap, while nonlinear propagation effects do exist in the form of solitary waves. In analogy to valence and conduction bands in semiconductors, the allowed bands above and below a PBG, are also referred to as "air band" and "dielectric band", respectively. In this chapter we present an outline of the theory underlying these interesting objects (Sec. 2.1). Furthermore, in Sec. 2.2 we present the state of the art in their fabrication while future applications are discussed in Sec. 2.3.

2.1 Ab-initio Calculations

From a theoretical point of view, Maxwell's equations can give a complete description of the field in a PC [49]. In the absence of any external currents and sources, we have:

$$\nabla \cdot \mathbf{B} = 0, \tag{2.1}$$

$$\nabla \cdot \mathbf{D} = 0, \tag{2.2}$$

$$\nabla \times \mathbf{E} = -\frac{1}{c}\frac{\partial \mathbf{B}}{\partial t}, \tag{2.3}$$

$$\nabla \times \mathbf{H} = \frac{1}{c}\frac{\partial \mathbf{D}}{\partial t}, \tag{2.4}$$

where c is the speed of light, $\mathbf{E}$ and $\mathbf{H}$ are the electric and magnetic fields, while $\mathbf{D}$ and $\mathbf{B}$ are the displacement and the magnetic induction fields, respectively.

In general, $\mathbf{D}$ is related to $\mathbf{E}$ via a rather complicated power series. For materials and fields under consideration, it is a very good approximation to keep only the linear term, i.e., $\mathbf{D}(\mathbf{r},\omega) = \epsilon(\mathbf{r},\omega)\mathbf{E}(\mathbf{r},\omega)$. Furthermore, considering macroscopic, isotropic and low-loss materials, $\epsilon(\mathbf{r},\omega)$ is purely real and practically constant over the frequency-range of interest. We thus obtain $\mathbf{D}(\mathbf{r}) = \epsilon(\mathbf{r})\mathbf{E}(\mathbf{r})$ where $\epsilon(\mathbf{r})$ is the macroscopic dielectric constant. A similar expression relates $\mathbf{H}$ to $\mathbf{B}$, but for the dielectric materials of interest, magnetic permeability is close to unity and thus, $\mathbf{H}(\mathbf{r}) = \mathbf{B}(\mathbf{r})$.

With all these assumptions Maxwell's equations become:

$$\nabla \cdot \mathbf{H}(\mathbf{r},t) = 0, \tag{2.5}$$

$$\nabla \cdot \epsilon(\mathbf{r})\mathbf{E}(\mathbf{r},t) = 0, \tag{2.6}$$

$$\nabla \times \mathbf{E}(\mathbf{r},t) = -\frac{1}{c}\frac{\partial \mathbf{H}(\mathbf{r},t)}{\partial t}, \tag{2.7}$$

$$\nabla \times \mathbf{H} = \frac{\epsilon(\mathbf{r})}{c}\frac{\partial \mathbf{E}(\mathbf{r},t)}{\partial t}. \tag{2.8}$$

It is worth noting here that Maxwell's equations are exact and thus provide, the band-structure of a PC from first principles (ab-initio). This may be the most exciting aspect of the field and results to excellent agreement between theory and experiment. Another aspect of Maxwell's equations is that there is no fundamental length. This ensures that a PC designed at one length will exhibit the same electromagnetic properties at any other length scale.

The fields entering Maxwell's equations have time and spatial dependence. Taking full advantage of the linearity of the equations, we may separate the two dependences by expanding the fields into a set of harmonic modes. Since we are looking for eigenmodes of the system, we may write a harmonic mode as a certain field spatial pattern times a complex exponential, i.e.,

$$\begin{pmatrix}\mathbf{H}\\ \mathbf{E}\end{pmatrix}(\mathbf{r},t) = \begin{pmatrix}\mathbf{H}\\ \mathbf{E}\end{pmatrix}(\mathbf{r})e^{i\omega t}. \tag{2.9}$$

Substituting Eq. (2.9) into (2.7)-(2.8) we may obtain a *master equation* which governs the magnetic field pattern:

$$\mathbf{\Theta H}(\mathbf{r}) = \left(\frac{\omega}{c}\right)^2 \mathbf{H}(\mathbf{r}), \tag{2.10}$$

under the *transversality condition* $\nabla \cdot \mathbf{H}(\mathbf{r}) = 0$. The operator $\mathbf{\Theta}$ is Hermitian and is given by

$$\mathbf{\Theta} \equiv \nabla \times \left(\frac{1}{\epsilon(\mathbf{r})}\nabla \times\right). \tag{2.11}$$

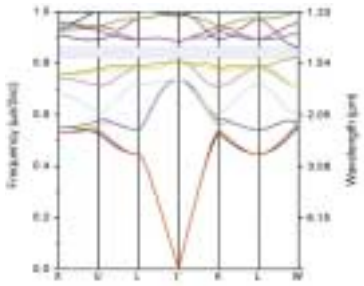

Fig. 2.1: A typical band-structure coming out from theoretical calculations. It corresponds to the inverse opal depicted in Fig. 2.5. The shaded region corresponds to the photonic band-gap [10].

A similar master equation can be obtained for the electric field, but in that case, the corresponding operator is non-Hermitian complicating thus the solution of the problem.

In a typical PC, the dielectric constant is periodically modulated with lattice vector $\mathbf{R}$, i.e., $\epsilon(\mathbf{r}) = \epsilon(\mathbf{r} + \mathbf{R})$. Using the Bloch-Floquet theorem, we may expand both field pattern and dielectric constant in plane waves whose wavevectors are reciprocal lattice vectors. For instance, the Fourier expansion for the field will be of the form:

$$\mathbf{H}_{\omega}^{\mathbf{k}}(\mathbf{r}) = \sum_{\mathbf{G},\lambda} h_{\mathbf{G},\lambda} \mathbf{e}_{\lambda} e^{i(\mathbf{k}+\mathbf{G})\mathbf{r}}, \tag{2.12}$$

where $\mathbf{e}_{\lambda}$ is the polarization vector and $\mathbf{G}$ are reciprocal lattice vectors. Each mode is thus identified by the wavevector $\mathbf{k}$ while the transversality condition requires that $\mathbf{e}_{\lambda} \cdot (\mathbf{k} + \mathbf{G}) = 0$. Substituting the expansion for both field and dielectric constant into (2.10), the problem is reduced to the solution of a system of linear equations on $h_{\mathbf{G},\lambda}$. Given that Θ is Hermitian, the eigenvalue problem can be solved in different ways and its solution provides the allowed mode-frequencies for a given crystal, whose wavevectors are associated with each one of these modes. In other words, we obtain the band-structure, $\omega(\mathbf{k})$ (Fig. 2.1).

In analogy to quantum mechanics, the Hermiticity of Θ ensures that its eigenvalues are real, while its eigenvectors (modes) can be obtained by means of a variational principle and they are orthogonal to each other. Using the "electromagnetic analogue" of the variational theorem, one can show that *a mode tends to concentrate its displacement field in regions of high dielectric constant, lowering thus its frequency, while remaining orthogonal to modes below it in frequency* [49].

2.2 State of the Art in Fabrication of Photonic Crystals

2.2.1 Two-dimensional Photonic Crystals

The traditional multilayer film is the simplest possible PC in which one can always observe a complete gap in one direction, between every set of bands [9, 26, 27, 32, 49, 102, 103, 104, 105, 115, 116]. It consists of periodically arranged dielectric layers, with alternating high and low dielectric constants. The medium is periodic in one direction and homogeneous in the other two. The simplest departure from the multilayer film is the two-dimensional (2D) photonic structure, consisting of a square lattice of dielectric rods or veins [Fig. 2.2(a) and (b)]. An alternative 2D configuration is the triangular lattice of air cylinders in dielectric medium [Fig. 2.2(c)] or even the so-called honeycomb lattice of dielectric rods. Such 2D systems, are homogeneous in only one direction (periodic in the other two) and they are convenient from both theoretical and experimental point of view [49, 50, 70, 71, 73, 76].

The structure of dielectric columns [Fig. 2.2(a)] has been shown to support gaps only for TM modes but not for TE modes, whereas for the structure of dielectric veins [Fig. 2.2(b)] it is the other way around. This behavior can be explained if we examine the field patterns for the two structures. Recall that the fields for either the dielectric- or air-band TE and TM modes tend to be concentrated in the $high-\varepsilon$ (dielectric) regions. The degree of this concentration is given by the fill factor

$$f = \frac{\langle \mathbf{E}(\mathbf{r})\mathbf{D}(\mathbf{r})\rangle_{high-\varepsilon}}{\langle \mathbf{E}(\mathbf{r})\mathbf{D}(\mathbf{r})\rangle_{low-\varepsilon}}, \tag{2.13}$$

which measures the electrical energy distributed inside the $high-\varepsilon$ regions, with respect to that in $low-\varepsilon$ regions, while we have introduced the notation

$$\langle AB\rangle \equiv \int_V A^* B d^3\mathbf{r}. \tag{2.14}$$

In the structure of the dielectric columns [Fig. 2.2(a)], the fill factor of the dielectric-band TM mode is much larger than that of the corresponding air-band mode, while there is not so large contrast between the fill factors for the two TE modes. This big difference between the fill factors of the two TM modes, is responsible for the large TM PBG. On the other hand, in the structure of dielectric veins [Fig. 2.2(b)], there is a big difference between the fill factors of the two consecutive TE modes but not for the TM modes and thus only TE gaps may appear. Summarizing we can say that: *TM band-gaps are preferable in lattices consisting of isolated* $high-\varepsilon$ *regions while TE band-gaps are preferable in connected lattices.*

In a triangular lattice [Fig. 2.2(c)] both isolated spots and connected $high-\varepsilon$ regions co-exist. As a result, such a structure exhibits band-gaps

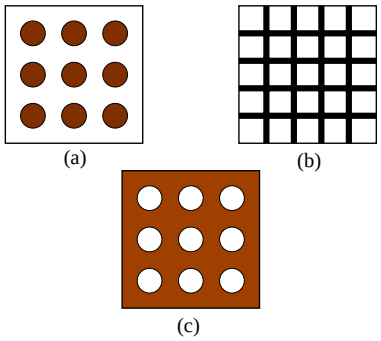

Fig. 2.2: Two-dimensional photonic structures.

for both polarizations, and by adjusting the dimensions of the lattice, one may arrange band-gaps to overlap, obtaining thus a complete PBG in two dimensions. Two-dimensional PCs fabricated by electrochemical etching technique, have reached gaps around $\lambda = 5\mu m$ and the technique seems to be capable of providing PCs at even smaller wavelengths.

2.2.2 Three-dimensional Photonic Crystals

Ho, Chan and Soukoulis [45] were the first theorists to correctly predict that a particular three-dimensional (3D) crystal would exhibit a complete gap. Their structure was a diamond lattice consisting of either dielectric spheres in air or air spheres embedded in a dielectric medium. Following their predictions, Yablonovitch [126, 127, 128] demonstrated the first 3D PC exhibiting a complete PBG. Starting with a dielectric slab and mechanically drilling cylindrical holes in it, Yablonovitch created a diamond-like configuration. The resulting structure, known as Yablonovite, indeed supported a complete gap in the microwave regime.

Since then, the efforts have been focused on realizing large-scale 3D PCs exhibiting complete gaps for shorter wavelengths in the optical or near-infrared regimes [22, 50]. To construct such photonic structures, many challenges exist. First of all, the lattice constant, must be comparable to the wavelength of the light of interest. For instance, for a PC operating at $1.5\mu m$, which is the wavelength currently used in telecommunications, the lattice constant must be of the order of μm! Furthermore, both constituent materials of the crystal must be topologically interconnected, while additionally, a large contrast in their dielectric constants is desired. Finally, the fraction of the volume occupied by the high-dielectric material must be as low as possible. There are two approaches currently used to create PCs in micrometer length scale [65]. The first one, is the microengineering and involves various microlithography schemes, such as electron beam lithogra-

phy and X-ray lithography. For instance, Yablonovitch has continued his technique of drilling holes into a dielectric slab but, for optical wavelengths the "drill" is a beam of ions and the appropriate material is GaAs. In 1996, Yablonovitch and co-workers reported a band-gap in near-infrared ($1.1 - 1.5\mu m$) [20]. The main drawback of their method, however, is that only crystals up to a few unit cells can be produced.

A layer-stacking design was proposed by Iowa group in 1994 [46] and since then has been extensively studied both theoretically and experimentally. Based on this design, Lin and Fleming have developed a multistep process involving photopatterning, etching and plasma enhanced deposition by means of which they created a seven-layer structure [Fig. 2.3(a)] which exhibits a gap around $1.5\mu m$ [31, 72]. The attenuation they measured was about 99% (1% transmition) while they believe that a ten-layer structure might give 0.1% transmition. Noda and Yamamoto followed an alternative multistep process involving electron beam lithography and reactive ion etching to stack semiconductor rods with micrometer dimensions [90]. They have reported an attenuation of 99.9% between 6 and $9\mu m$, for an eight-layer structure which is grown within ten days in the laboratory. Both Lin's and Noda's fabrication methods are believed to be very promising for any future mass production of PCs since they combine low cost with high reliability. A new layered structure has been recently proposed by Joannopoulos and co-workers (Fig. 2.3) for achieving full 3D band-gaps. Its main advantage over the previous layer-stacking design is that it allows the building of a 2D crystal in three dimensions.

The second approach to microfabrication of PCs, involves 3D self-assembling systems such as colloidal crystals [77, 120] and artificial opals [11]. The latter are structures of SiO_2 or TiO_2 spheres (opal) arranged in a close-packed face-centered cubic lattice (Fig. 2.4). Intersphere voids form a network which can be impregnated with materials of low or high refractive index. Although both colloids and opals have excellent long-range periodicity required for photonic band-structures, it has been difficult to achieve high index contrast and the correct network topology in order to support complete gaps. Closely related structures are the so-called inverse opals(crystals) which have been shown to exhibit sizable PBGs [15]. They consist of air (low dielectric) spheres, embedded in a connected high dielectric network (Fig. 2.4) and the recipe for their fabrication is the following.

An opal structure is used as a template and its void regions are infiltrated with a material of high dielectric constant, such as Ge, Si or GaP. Subsequently, the original template is removed by chemical or heat treatment, leaving behind a connected network (macroporous sample or Swiss cheese structure) with high dielectric contrast, which is essential in obtaining larger gaps. Furthermore, the void regions in macroporous crystals allow the injection of atoms or dye molecules making thus quantum optical experiments feasible. Experimental realization of such a type of "inverted" opal

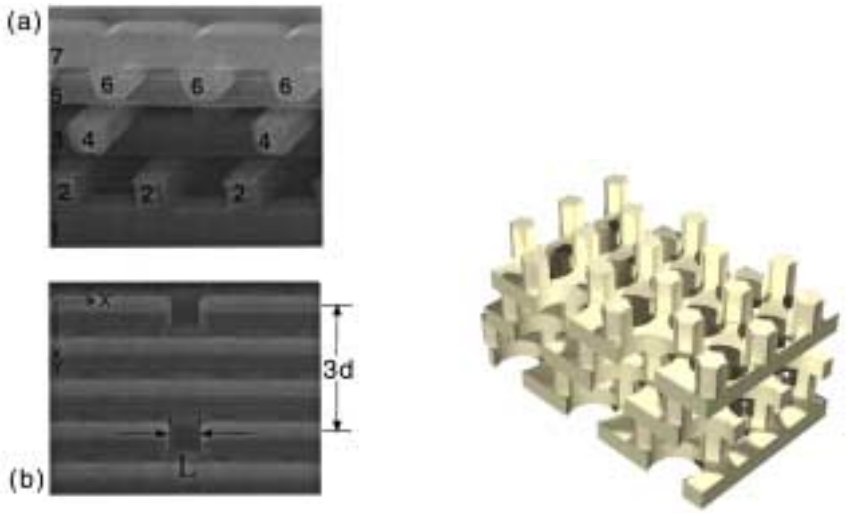

Fig. 2.3: On the left, a scanning electron microscopy image of a seven-layer three-dimensional photonic crystal. A vacancy defect has been created in the fourth layer and acts as a defect-cavity; $L = 2\mu m$ [72]. On the right, a layered structure proposed by Joannopoulos and co-workers for achieving a full three-dimensional band-gap.

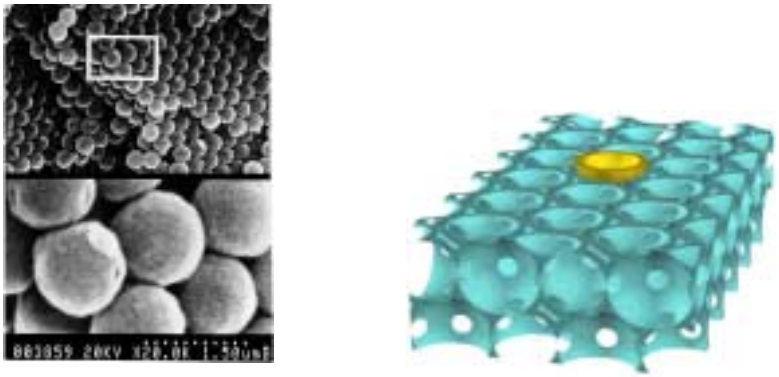

Fig. 2.4: On the left, electron microphotograph of an opal sample [11]. On the right, view of an inverse opal backbone resulting from incomplete infiltration of silicon in air voids of an artificial opal. The inner surface of each sphere (only one is shown) is "covered" by a nematic liquid crystal and thus a tunable PBG is obtained [15, 16].

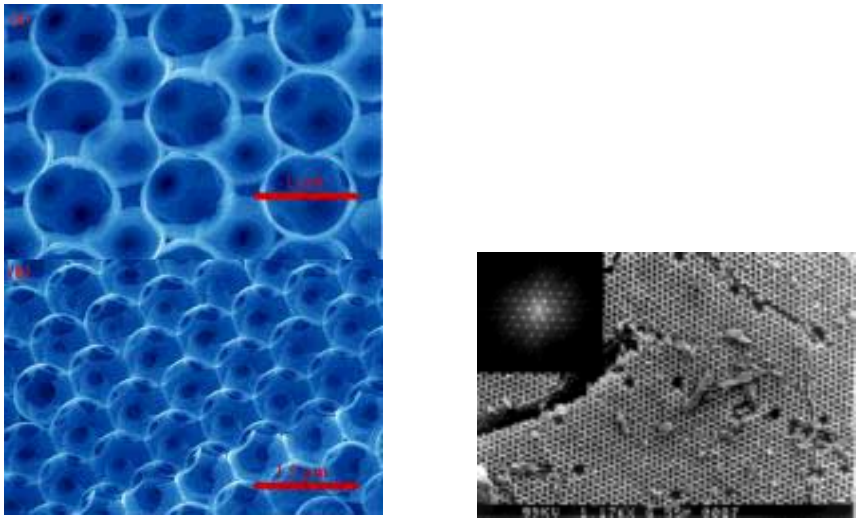

Fig. 2.5: A crystal of air spheres in (a) silicon (on the left) and (b) TiO_2 (on the right).

structures (Fig. 2.5) has been reported in the literature [10, 123]. Busch and John have gone one step further, coating the internal surfaces of the macroporous structure with a nematic liquid crystal [16]. As they calculated, the resulting structure (Fig. 2.4) exhibits a completely tunable PBG. Specifically, the 3D PBG can be opened or closed by applying an external electric field which affects the orientation of the nematic molecules.

2.3 Applications

Once we have a PC, it is possible to create *point-defects* by destroying locally the periodicity of the lattice of the crystal. Such imperfections may involve changes to the dielectric constant (or equivelantly refractive index) of one of the "dielectric atoms", modification of its size or even its removal from the lattice of the crystal. The point-defect can then "pull" a mode (or group of modes) inside the otherwise forbidden gap. The resulting photonic state known as *defect-mode* is strongly localized and decays exponentially in the bulk [76], while its frequency and symmetry can be controlled [49, 50, 119]. In analogy to atomic physics, depending on their symmetry, defect-modes can be labeled as s, p, d, etc. For instance, in Fig. 2.6 we show a p-like photonic state (it has two nodes) in a 2D PC. The crystal surrounding a defect acts as highly reflecting mirror. The quality factor Q of such a defect-cavity is a measure of the losses, while its size is of the order of the cubic wavelength of light λ^3. Clearly, if losses can be controlled, a high-Q microcavity can be obtained, operating at optical or even near-infrared wavelengths, where the

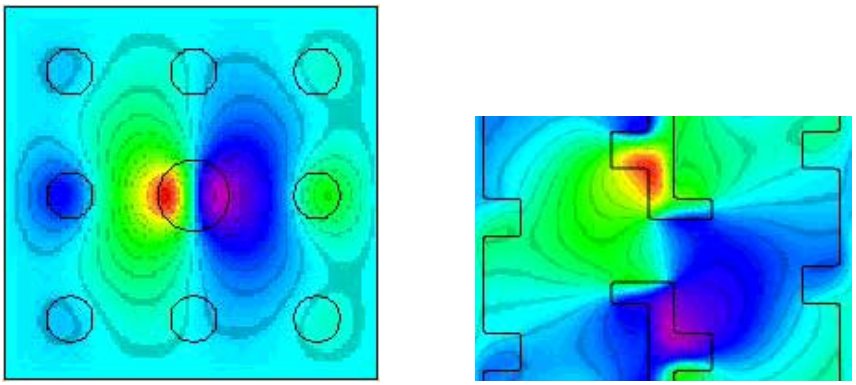

Fig. 2.6: Magnetic field pattern in the vicinity of a defect-mode in a (a) two-dimensional photonic crystal (on the left) and (b) three-dimensional photonic crystal (on the right). Dark and light regions, correspond to field maxima.

ordinary cavities used in quantum optical experiments are getting lossy. To this end, we need 3D PCs exhibiting large complete band-gaps (along all directions in 4π steradiants), isolating thus the defect-mode from the continuum into which it can dissipate its energy. In Fig. 2.6, we present the distribution of the magnetic field around a defect in a 3D PC. The necessary criteria for achieving large gaps are well-known and have been discussed in the previous section. We additionally need large scale crystals for the elimination of losses through the surrounding walls. It has been shown both theoretically and experimentally that the Q factor of the defect-cavity increases exponentially with the size of the crystal, without presenting any saturation [72, 119]. For the time being, the highest value of Q ($\sim 10^4$) has been reported by Lin and co-workers in a 2D defect-cavity [73] while, the first 3D defect-cavity has been realized in a seven-layer structure [Fig. 2.3(b)] [72].

PBG microcavities can be used to control spontaneous emission, which is the heart of all light-emitting devices in optoelectronics. In light-emitting diodes (LEDs) for example, spontaneous emission takes place during the radiative recombination of holes and electrons in a $p-n$ junction. Surrounding a LED by an optical cavity supporting a single mode, we may obtain single-mode light-emitting diode (SMLED) which, in analogy to an above threshold semiconductor laser, exhibits coherence properties while simultaneously is thresholdless and much more reliable. Schener and co-workers have demonstrated the first "PBG defect-mode laser" operating at wavelengths $\sim 1.5\mu m$ [66, 92]. The laser microcavity was formed by a point defect in a 2D photonic crystal fabricated in $InGaAsP$. A point defect can be finally used as a narrow-band polarization-selector [72].

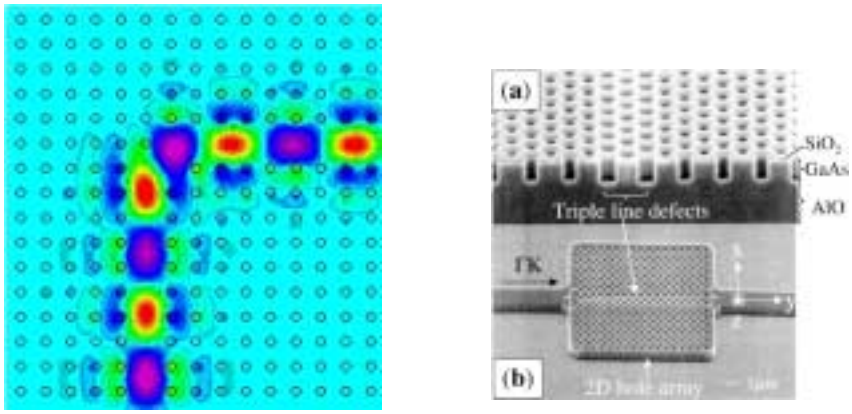

Fig. 2.7: On the left, electric field pattern in the vicinity of a bend in a two-dimensional photonic crystal [78]. Dark and light regions, correspond to maxima of the freely propagating field. On the right, scanning electron microscope view of a fabricated triple-line defect in a triangular two-dimensional photonic crystal [71].

Instead of a point-defect one can also introduce *line-defects* in an otherwise perfect photonic structure. The defect may then support a mode within the band-gap and as such is forbidden from propagating in the bulk crystal. Such defects can be used as "lossless" waveguides. In conventional dielectric waveguides (fiber-optic cables) currently used in telecommunications, the total internal reflection is responsible for the confinement of light. If, however, a fiber curves tightly, a significant portion of light will be lost, since the angle of incidence is then too large for total internal reflection to occur. In PBG waveguides, on the other hand, the situation is substantially different. As long as the frequency of the defect-guiding-mode lies within the gap, it is impossible for the light to escape, i.e., to propagate in the bulk crystal, even around tight corners (Fig. 2.7). A highly efficient waveguiding through a triple-line-defect embedded in a 2D triangular photonic structure, has been demonstrated (Fig. 2.7) by Lin and co-workers [71]. Although the structure does not exhibit a large band-gap, the authors have reported a near-perfect waveguiding at $1.5\mu m$.

Combining both line- and point-defects, the creation of channel-drop filters is possible. Such filters usually consist of two parallel waveguides (line-defects) and an "optical resonator system" which involves one or more point-defects. Calculations have shown that by means of PBG channel-drop filters, it is possible to transfer 100% of a selected frequency channel from one of the waveguides into the other in the forward or backward propagation direction [29, 30].

2.4 Summary

Light has several advantages over electrons. It is not only that it travels much faster than electrons, but it can carry much larger amount of information per second while heating problems are practically absent, since photons do not interact so strongly as electrons. It would thus be desirable to construct all-optical circuits which can replace their conventional electronic counterparts and open the door towards high-speed data transfer and computing. Such optical devices, however, require structures that can trap, bend and split light beams efficiently. Many scientists believe that the answer lies in PCs and they have already begun imagining photonic metropolises in micrometer length scales. In this thesis we deal with another field of applications involving small quantum systems (atoms, molecules, ...) embedded in PCs.

Chapter 3

Radiative Processes

The investigation of atomic radiative processes requires the description of the atom, the radiation field and the interaction between the bound atomic electrons and the field. It is the purpose of this chapter to review standard tools used in quantum optics for the investigation of the atomic dynamics as long as the atom is weakly coupled to a flat radiation reservoir, into which it can dissipate its energy. Furthermore, we give a brief overview of basic quantum optical phenomena associated with QED in open space and cavities which are discussed later on, in the context of PBG materials.

3.1 Interaction of Radiation with Atoms

For the sake of simplicity, let us consider a single-electron atom interacting with the radiation field. The source-free radiation field (R) , can be described by the vector potential $\mathbf{A}(\mathbf{r},t)$ with the constraint $\nabla\cdot\mathbf{A}=0$. The interaction between the electron and the field is then described by the following non-relativistic Hamiltonian

$$\mathcal{H}=\frac{1}{2m}\left(\mathbf{p}-e\mathbf{A}\right)^2+e\Phi(\mathbf{r})+\mathcal{H}_R, \tag{3.1}$$

where the electron's spin has been neglected, $\Phi(\mathbf{r})$ is the Coulomb potential which keeps the electron bound to the atom, while m, e and $\mathbf{p}$ are the mass, the charge and the momentum of the electron, respectively. Expanding the first term in Eq. (3.1) and using the Coulomb gauge condition[1], we obtain

$$\mathcal{H}=\frac{\mathbf{p}^2}{2m}+e\Phi(\mathbf{r})+\mathcal{H}_R-\frac{e}{m}\mathbf{A}\cdot\mathbf{p}+\frac{e^2}{2m}\mathbf{A}^2. \tag{3.2}$$

The first two terms constitute the Hamiltonian of the isolated atom, namely,

$$\mathcal{H}_A=\frac{\mathbf{p}^2}{2m}+e\Phi(\mathbf{r}), \tag{3.3}$$

[1] Since $\nabla\cdot\mathbf{A}=0$ and $\mathbf{p}\sim\nabla$, we have $\mathbf{p}\cdot\mathbf{A}=\mathbf{A}\cdot\mathbf{p}$.

while $\mathcal{H}_R$ is the Hamiltonian for the source-free radiation field in the absence of the atom. Finally, the last two terms in Eq. (3.2) represent the interaction between atom and field, i.e.,

$$\mathcal{V} = -\frac{e}{m}\mathbf{A}\cdot\mathbf{p} + \frac{e^2}{2m}\mathbf{A}^2. \tag{3.4}$$

In the following sections, we discuss these three parts of the Hamiltonian separately.

3.1.1 Quantization of the Electromagnetic Field

In many QED problems, it is rather convenient to envisage the electromagnetic field as confined in a volume similar to a cavity. This allows us to deal with a discrete set of variables rather than the whole continuum [75, 100, 108]. Specifically, the field is represented by a set of infinitely many but discrete modes indexed by λ, whose dynamics are described in terms of the corresponding creation and annihilation operators $a_\lambda^\dagger$ and a_λ respectively, obeying the commutation relations

$$[a_\lambda, a_{\lambda'}^\dagger] = \delta_{\lambda\lambda'}, \quad [a_\lambda, a_{\lambda'}] = 0 = [a_\lambda^\dagger, a_{\lambda'}^\dagger]. \tag{3.5}$$

The Hamiltonian of the radiation reservoir is that of a set of infinitely many independent harmonic oscillators and denoting by ω_λ the frequency of the λ mode, we have in Scrödinger picture

$$\mathcal{H}_\mathcal{R} = \sum_\lambda \hbar\omega_\lambda \left(a_\lambda^\dagger a_\lambda + \frac{1}{2}\right), \tag{3.6}$$

while the vector potential is given by

$$\mathbf{A}(\mathbf{r}) \;=\; \sum_\lambda \sqrt{\frac{\hbar}{2\epsilon_0\omega_\lambda}}\left(a_\lambda \mathbf{u}_\lambda(\mathbf{r}) + a_\lambda^\dagger \mathbf{u}_\lambda^*(\mathbf{r})\right), \tag{3.7}$$

where ϵ_0 is the electric permitivity of the vacuum. For each mode λ, the corresponding mode-function $\mathbf{u}_\lambda(\mathbf{r})$, satisfies the wave-equation under the transversality condition,

$$\nabla^2\mathbf{u}_\lambda(\mathbf{r}) + \frac{\omega_\lambda^2}{c^2}\mathbf{u}_\lambda(\mathbf{r}) = 0, \quad \nabla\cdot\mathbf{u}_\lambda(\mathbf{r}) = 0, \tag{3.8}$$

where c is the speed of light. Additionally, the mode-functions form a complete and orthonormal set and depend on the boundary conditions applied to the electromagnetic field. In the following sections we discuss various types of mode-functions. For the time being, what should be kept in mind is that the mode-index λ, is usually an abbreviation for a set of four numbers, namely, the three cartesian components of the propagation vector $|\mathbf{k}_\lambda| \equiv \omega_\lambda c^{-1}$ and the corresponding polarization index σ, i.e,

$\lambda \equiv \{k_x, k_y, k_z, \sigma\}$. Thus, any sum over λ must be understood as a shorthand notation for

$$\sum_{\lambda} \equiv \sum_{\mathbf{k}} \sum_{\sigma=1}^{2} . \tag{3.9}$$

•Fock or Number States: Since each mode λ of the radiation field is independent, the Hamiltonian (3.6) can be written as a sum over sub-Hamiltonians for each mode, i.e., $\mathcal{H}_{\mathcal{R}} = \sum_{\lambda} h_{\lambda}$, where

$$h_{\lambda} = \hbar\omega_{\lambda} \left(\mathcal{N}_{\lambda} + \frac{1}{2} \right) , \tag{3.10}$$

while we have introduced the *number operator* $\mathcal{N}_{\lambda} \equiv a_{\lambda} a_{\lambda}^{\dagger}$. The $\mathcal{N}_{\lambda}$ is Hermitian and has a discrete set of eigenstates $\{|n_{\lambda}\rangle\}$ (*Fock or Number States*) [74], while its eigenvalues are $n_{\lambda} = 0, 1, 2, \ldots, \infty$. Accordingly, $|n_{\lambda}\rangle$ are also eigenstates of the Hamiltonian (3.10), with eigenvalues $E_{\lambda} = \hbar\omega_{\lambda} \left(n_{\lambda} + \frac{1}{2} \right)$. The effect of a_{λ} and $a_{\lambda}^{\dagger}$ on the number states is:

$$a_{\lambda}|n_{\lambda}\rangle = \sqrt{n_{\lambda}}|n_{\lambda} - 1\rangle, \quad a_{\lambda}^{\dagger}|n_{\lambda}\rangle = \sqrt{n_{\lambda} + 1}|n_{\lambda} + 1\rangle, \tag{3.11}$$

and thus $\mathcal{N}_{\lambda}|n_{\lambda}\rangle = n_{\lambda}|n_{\lambda}\rangle$, i.e., $\mathcal{N}_{\lambda}$ counts the number of photons in mode λ. The vacuum state of mode λ is defined by, $a_{\lambda}|0_{\lambda}\rangle = 0$ and its energy is $\frac{1}{2}\hbar\omega_{\lambda}$, while the higher excited states can be obtained by

$$|n_{\lambda}\rangle = \frac{\left(a_{\lambda}^{\dagger}\right)^{n_{\lambda}}}{\sqrt{n_{\lambda}!}}|0_{\lambda}\rangle. \tag{3.12}$$

The number states are orthogonal and complete, i.e.,

$$\langle n_{\lambda}|m_{\lambda}\rangle = \delta_{nm}, \quad \sum_{n_{\lambda}=0}^{\infty} |n_{\lambda}\rangle\langle n_{\lambda}| = 1, \tag{3.13}$$

and as such, they form a complete set of basis vectors for a *Hilbert space.*

The state-vectors of the entire field are defined in the tensor product space of the *Hilbert spaces* for all the modes; that is, a state-vector of the radiation field may be written in the form:

$$|\{n_{\lambda}\}\rangle \equiv |n_1\rangle|n_2\rangle \ldots |n_{\infty}\rangle \equiv |n_1, n_2, \ldots, n_{\infty}\rangle, \tag{3.14}$$

and

$$\mathcal{H}_{\mathcal{R}}|n_1, n_2, \ldots n_{\infty}\rangle = \sum_{\lambda} \hbar\omega_{\lambda} \left(n_{\lambda} + \frac{1}{2} \right) |n_1, n_2, \ldots n_{\infty}\rangle. \tag{3.15}$$

The lowest eigenenergy, is $\frac{1}{2}\sum_{\lambda}\hbar\omega_{\lambda}$ and corresponds to the ground (vacuum) state of the field which is given by the normalized vector $|\{0_{\lambda}\}\rangle \equiv$

$|0,0,\ldots,0\rangle$. It is known as *zero-point energy* and can be omitted in our calculations, since it does not affect the atomic dynamics. Each state-vector can be constructed from the vacuum state in the following way

$$|n_1,n_2,\ldots n_\infty\rangle = \frac{\left(a_1^\dagger\right)^{n_1}\left(a_2^\dagger\right)^{n_2}\ldots}{\sqrt{n_1!n_2!\ldots}}|0,0,\ldots,0\rangle. \tag{3.16}$$

Note additionally that the state-vectors (3.14) are orthogonal and complete too, i.e.,

$$\begin{aligned}\langle n_1,n_2,\ldots,n_\infty|m_1,m_2,\ldots,m_\infty\rangle &= \delta_{n_1m_1}\delta_{n_2m_2}\ldots,\\ \sum_{n_1,n_2,\ldots,n_\infty}|n_1,n_2,\ldots,n_\infty\rangle\langle n_1,n_2,\ldots,n_\infty| &= 1,\end{aligned} \tag{3.17}$$

while, application of the creation and annihilation operators to them yields

$$\begin{aligned}a_\lambda|n_1,n_2,\ldots,n_\lambda,\ldots,n_\infty\rangle &= \sqrt{n_\lambda}|n_1,n_2,\ldots,n_\lambda-1,\ldots,n_\infty\rangle,\\ a_\lambda^\dagger|n_1,n_2,\ldots,n_\lambda,\ldots,n_\infty\rangle &= \sqrt{n_\lambda+1}|n_1,n_2,\ldots,n_\lambda+1,\ldots,n_\infty\rangle,\\ \mathcal{N}_\lambda|n_1,n_2,\ldots,n_\lambda,\ldots,n_\infty\rangle &= n_\lambda|n_1,n_2,\ldots,n_\lambda,\ldots,n_\infty\rangle.\end{aligned} \tag{3.18}$$

•**Coherent States:** A more appropriate basis for many optical fields is that of coherent states [74, 75, 121]. Consider again a single mode of the radiation field denoted by λ. A coherent state $|\alpha_\lambda\rangle$ is defined as eigenstate of the non-Hermitian annihilation operator a_λ, i.e., $a_\lambda|\alpha_\lambda\rangle = \alpha_\lambda|\alpha_\lambda\rangle$, where α_λ is the corresponding complex eigenvalue. We may expand the coherent state in terms of the Fock states $|n_\lambda\rangle$ as follows,

$$|\alpha_\lambda\rangle = e^{-|\alpha_\lambda|^2/2}\sum_{n_\lambda=0}^{\infty}\frac{(\alpha_\lambda)^{n_\lambda}}{\sqrt{n_\lambda!}}|n_\lambda\rangle. \tag{3.19}$$

The number of photons in the mode λ is then uncertain, but the statistical properties of the field are well defined with mean number of photons $\bar{n}_\lambda \equiv |\alpha_\lambda|^2$ and a Poissonian photon number distribution

$$\mathcal{P}_c(n_\lambda) \equiv |\langle n_\lambda|\alpha_\lambda\rangle|^2 = \frac{\bar{n}_\lambda^{n_\lambda}}{n_\lambda!}e^{-\bar{n}_\lambda}, \tag{3.20}$$

while the uncertainty is $\Delta n_\lambda = \sqrt{\bar{n}_\lambda}$. The set $\{|\alpha_\lambda\rangle\}$ is continuous, normalized but not orthogonal. Coherent states are minimum uncertainty states, while the variation of the electric field in the limit of high excitation, approaches that of classical wave of stable amplitude and fixed phase. The field generated by a single-mode laser operating well above threshold is, to a good approximation, a coherent state. In analogy to Eq. (3.14), a state-vector of the radiation field can be written in terms of coherent states as

$$|\{\alpha_\lambda\}\rangle \equiv |\alpha_1\rangle|\alpha_2\rangle\ldots|\alpha_\infty\rangle \equiv |\alpha_1,\alpha_2,\ldots,\alpha_\infty\rangle. \tag{3.21}$$

•**Thermal Field:** Coherent states are pure states since they can be expressed as a linear superposition of Fock states [see Eq. (3.19)]. There are states, however, which are not expressible in this way. Such a case, is a thermally-excited mode [74, 75, 121] where the photon number distribution is given by

$$\mathcal{P}_t(n_\lambda) = \frac{1}{1+\bar{n}_\lambda}\left(\frac{\bar{n}_\lambda}{1+\bar{n}_\lambda}\right)^{n_\lambda}, \tag{3.22}$$

while the mean number of photons is temperature-dependent as is determined by

$$\bar{n}_\lambda = \frac{1}{exp\left[\hbar\omega_\lambda/K_BT\right]-1}, \tag{3.23}$$

with uncertainty $\Delta n_\lambda = \sqrt{\bar{n}_\lambda^2+\bar{n}_\lambda}$, while T is the temperature and K_B is the Boltzman constant.

3.1.2 Atomic Hamiltonian

Let's consider the atomic levels $|a\rangle$, $|b\rangle$, $|c\rangle$, ..., and the atomic Hamiltonian $\mathcal{H}_A$, which is given by Eq. (3.3). Each of the atomic states satisfies the following eigenvalue problem

$$\mathcal{H}_A|j\rangle = \hbar\omega_j|j\rangle, \quad j \in \{a,b,c,\ldots\}, \tag{3.24}$$

where $\hbar\omega_j$ is the eigenenergy corresponding to the eigenstate $|j\rangle$. Let us further assume that the atomic states are orthonormal and complete, i.e,

$$\langle i|j\rangle = \delta_{ij}, \quad \sum_j |j\rangle\langle j| = 1, \tag{3.25}$$

where $\sum_j$ is a sum over all eigenstates of $\mathcal{H}_A$. For a couple of atomic levels, we may define the so-called *atomic dyadic operator*, $\sigma_{ij} \equiv |i\rangle\langle j|$ [74, 121]. The orthonormality of the atomic eigenstates implies that

$$\sigma_{ij}|l\rangle = |i\rangle\delta_{jl}. \tag{3.26}$$

In other words, operation of σ_{ij} on the atom prepared in state $|j\rangle$, removes it from that state and puts it in state $|i\rangle$. That's why these operators are also referred to raising and lowering atomic operators or even electronic creation and annihilation operators.

Both, atomic Hamiltonian and electronic momentum can be expressed in terms of σ_{ij}. Using Eqs. (3.24) and (3.25), we have

$$\mathcal{H}_A = \sum_i |i\rangle\langle i|\mathcal{H}_A\sum_j |j\rangle\langle j| = \sum_{ij}\hbar\omega_j|i\rangle\delta_{ij}\langle j| = \sum_j \hbar\omega_j\sigma_{jj}, \tag{3.27}$$

and

$$\mathbf{p} = \sum_i |i\rangle\langle i|\mathbf{p}\sum_j |j\rangle\langle j| = \sum_{ij}\mathbf{p}_{ij}\sigma_{ij}, \tag{3.28}$$

where $\mathbf{p}_{ij} = \langle i|\mathbf{p}|j\rangle$. The atomic dyadic operators obey the following commutation relation:

$$[\sigma_{jm}, \sigma_{ln}] = \delta_{ml}\sigma_{jn} - \delta_{jn}\sigma_{ml}. \tag{3.29}$$

3.1.3 Interaction Hamiltonian

The term $e^2(2m)^{-1}\mathbf{A}^2$ in Eq. (3.4) does not enter in the processes of concern here and can be omitted. The interaction term of the Hamiltonian can thus be expressed as

$$\mathcal{V} = \hbar \sum_{j,n,\lambda} \sigma_{jn} \left(g_\lambda^{(j,n)} a_\lambda + g_\lambda^{(j,n)*} a_\lambda^\dagger \right), \tag{3.30}$$

where the indexes j, n and λ refer to atomic states and radiation modes respectively, while

$$g_\lambda^{(j,n)} = -\frac{e}{m}\sqrt{\frac{1}{2\hbar\epsilon_0\omega_\lambda}}\langle j|\mathbf{u}_\lambda(\mathbf{r})\mathbf{p}|n\rangle, \tag{3.31}$$

or, in coordinate representation,

$$g_\lambda^{(j,n)} = -\frac{e}{m}\sqrt{\frac{1}{2\hbar\epsilon_0\omega_\lambda}}\int \phi_j^*(\mathbf{r})\left[\mathbf{u}_\lambda(\mathbf{r})\mathbf{p}\right]\phi_n(\mathbf{r})d^3\mathbf{r}, \tag{3.32}$$

with $\phi_l(\mathbf{r}) \equiv \langle \mathbf{r}|l\rangle$.

Electric-Dipole Approximation: If we are interested in photons of wavelength much larger than the atomic size, the mode-function $\mathbf{u}_\lambda(\mathbf{r})$ is slowly varying compared to the electronic wavefunctions and we can thus take it outside the integral (3.32) and replace it by its value at the atomic position [2]. Furthermore, it can be shown that

$$-\frac{e}{m}\int \phi_j^*\mathbf{p}\phi_n d^3\mathbf{r} = -i\omega_{jn}\int \phi_j^*\mathbf{d}\phi_n d^3\mathbf{r} \equiv -i\omega_{jn}\mathbf{d}_{jn}, \tag{3.33}$$

where $\mathbf{d} = e\mathbf{r}$ is the dipole moment and $\omega_{jn} = \omega_j - \omega_n$. We thus have,

$$g_\lambda^{(j,n)} = -i\sqrt{\frac{1}{2\hbar\epsilon_0\omega_\lambda}}\omega_{jn}\mathbf{u}_\lambda(\mathbf{R}_A)\cdot\mathbf{d}_{jn}, \tag{3.34}$$

where $\mathbf{R}_A$ is the atomic position.

Alternatively, as the interaction Hamiltonian, one may adopt that of an electric dipole interacting with the electric field,

$$\mathcal{V} = -e\mathbf{E}(\mathbf{r})\cdot\mathbf{r}, \tag{3.35}$$

[2] Since the atomic diameter $r \approx 1$Å, this approximation is valid at optical wavelengths, where $\lambda_{photon} = 10^3$Å, or even in microwave regime.

while in the electric-dipole approximation, the electric field is evaluated at the atomic position. Let us compare the electric field interaction with that of an electron subject to the vector potential $\mathbf{A}(\mathbf{R}_A)$:

$$i\hbar\frac{\partial}{\partial t}\psi(\mathbf{r},t) = \left[\frac{1}{2m}\left(\mathbf{p} - e\mathbf{A}(\mathbf{R}_A)\right)^2 + \Phi(r)\right]\psi(\mathbf{r},t), \tag{3.36}$$

where $\psi(\mathbf{r},t)$ is the electronic wavefunction. If we set

$$\psi(\mathbf{r},t) = exp\left[\frac{ie}{\hbar}\mathbf{A}(\mathbf{R}_A)\cdot\mathbf{r}\right]\phi(\mathbf{r}), \tag{3.37}$$

where $\phi(\mathbf{r},t)$ is a new wavefunction, Eq. (3.36) yields

$$i\hbar\frac{\partial}{\partial t}\phi(\mathbf{r},t) = \left(\mathcal{H}^0 - e\mathbf{E}(\mathbf{R}_A)\cdot\mathbf{r}\right)\phi(\mathbf{r},t), \tag{3.38}$$

where $\mathcal{H}^0 = \mathcal{H}_A + \mathcal{H}_R$ is the unperturbed Hamiltonian. Instead of the velocity gauge $(-em^{-1}\mathbf{A}\cdot\mathbf{p})$ one can thus work in length gauge $(-e\mathbf{E}\cdot\mathbf{r})$ where any expectation values are calculated through $\phi(\mathbf{r},t)$. The difference is that in this case, the coupling constant reads

$$g_\lambda^{(j,n)} = -i\sqrt{\frac{\omega_\lambda}{2\hbar\epsilon_0}}\mathbf{u}_\lambda(\mathbf{R}_A)\cdot\mathbf{d}_{jn}. \tag{3.39}$$

3.2 Density Operator

Consider a quantum system and let $\{|s\rangle\}$ be a basis set. An arbitrary wavefunction of the system then can be written in the form

$$|\psi(t)\rangle = \sum_s C_s(t)|s\rangle. \tag{3.40}$$

This is a pure state since it is a superposition of eigenstates. In many cases, however, the system is in a statistical mixture of pure states. Such a mixed state can be written as

$$|\Psi(t)\rangle = \sum_j a_j|\psi_j\rangle \tag{3.41}$$

where $\sum_j$ is a sum over all pure states entering the statistical mixture with probabilities $|a_j|^2$ and $\sum_j |a_j|^2 = 1$.

In quantum mechanics, physical quantities are associated with linear operators. Let $\mathcal{O}$ be such an operator, whose expectation value is given by

$$\langle\mathcal{O}\rangle = \langle\Psi(t)|\mathcal{O}|\Psi(t)\rangle. \tag{3.42}$$

Using the completeness of the eigenstates $|s\rangle$, the expectation value of the operator can be written as,

$$\langle\mathcal{O}\rangle = \sum_s\langle s|\rho\mathcal{O}|s\rangle \equiv Tr(\rho\mathcal{O}), \tag{3.43}$$

where we have introduced the total **density operator** [21, 75]

$$\rho \equiv \sum_j |a_j|^2 |\psi_j\rangle\langle\psi_j|. \tag{3.44}$$

The density operator contains all the information about the system as well as its time evolution.

Using Eq. (3.40), Eq. (3.44) yields

$$\rho = \sum_{s,s'} \rho_{ss'} |s\rangle\langle s'|, \tag{3.45}$$

where the matrix representation of the density operator is defined by,

$$\rho_{ss'} = \sum_j |a_j|^2 C_s^{(j)} C_{s'}^{(j)*}. \tag{3.46}$$

The diagonal matrix element ρ_{ss} gives the population in state $|s\rangle$ while the off-diagonal $\rho_{ss'}$ is the so-called ss'-coherence. In a pure state we always have non-vanishing diagonal elements, whereas in incoherent statistical mixtures no coherence exists. We finally note that the density matrix is Hermitian ($\rho_{ss'} = \rho_{s's}$) and has unit trace, $Tr(\rho) \equiv \sum_s \rho_{ss} = 1$.

The evolution of the system is governed by Schrödinger equation:

$$i\hbar \frac{\partial}{\partial t} |\psi_j(t)\rangle = \mathcal{H} |\psi_j(t)\rangle, \tag{3.47}$$

from which we may obtain the following equation of motion for the density operator

$$i\hbar \frac{\partial \rho}{\partial t} = [\mathcal{H}, \rho], \tag{3.48}$$

where $\mathcal{H}$ is the total Hamiltonian of the system.

3.3 The Quantum Optical Master Equation

In this section we focus on the interaction of a "small" atomic system (few quantal degrees of freedom), with a "large" radiation reservoir (many quantal degrees of freedom) [1, 19, 21, 33]. Let $t = 0$ be the time at which the atomic system (A) and the radiation field (R) are brought into interaction, and let $\mathcal{H}_A$ and $\mathcal{H}_R$ be the corresponding unperturbed Hamiltonians given by Eqs. (3.27) and (3.6), respectively. The states of the combined system satisfy the following eigenvalue problem

$$\mathcal{H}^0 |s\rangle \equiv (\mathcal{H}_A + \mathcal{H}_R) |s\rangle = \hbar\omega_s |s\rangle, \tag{3.49}$$

and they are of the form $|s\rangle \equiv |j\rangle|\{n_\lambda\}\rangle \equiv |j; \{n_\lambda\}\rangle$, where by $|j\rangle$ and $|\{n_\lambda\}\rangle$ we denote the eigenstates of $\mathcal{H}_A$ and $\mathcal{H}_R$, respectively. The corresponding

eigenvalues are $\hbar\omega_s = \hbar\omega_j + \sum_\lambda \hbar\omega_\lambda n_\lambda$. These states are orthogonal and the set is complete, as is determined by Eqs. (3.17) and (3.25) and thus they form a basis.

In analogy to the previews section, we may define the density operator of the combined system w_{tot}, which satisfies the following equation of motion in the interaction picture

$$\dot{w}_{tot}(t) = -\frac{i}{\hbar}\left[\mathcal{V}(t), w_{tot}(t)\right], \tag{3.50}$$

where $\mathcal{V}$ is the interaction between the reservoir and the atomic system. We are usually interested in the dynamics of the latter which are given by the *reduced density operator* $\rho_A(t) = Tr_R(w_{tot})$, where Tr_R denotes a trace over all reservoir variables. Let's assume that the atomic system and the reservoir are initially uncorrelated, so that the total density operator factorizes as $w_{tot}(0) = \rho_A(0) \otimes \rho_R$, where ρ_R is a stationary reduced density operator for the reservoir.

Integration of Eq. (3.50) from 0 to t yields,

$$w_{tot}(t) = w_{tot}(0) - \frac{i}{\hbar}\int_0^t dt' \left[\mathcal{V}(t'), w_{tot}(t')\right]. \tag{3.51}$$

Iteration of this solution, tracing over all reservoir variables and subsequent differentiation with respect to t yield the following integro-differential equation for the reduced density operator

$$\frac{\partial \rho_A}{\partial t} = \mathcal{Q}(\rho_A, t), \tag{3.52}$$

where $\mathcal{Q}(\rho_A, t) \equiv \sum_m U_m$ and for instance

$$U_1 = -\frac{i}{\hbar} Tr_R\{[\mathcal{V}(t), w_{tot}(0)]\}, \tag{3.53}$$

$$U_2 = \left(-\frac{i}{\hbar}\right)^2 Tr_R\{\int_0^t dt' \left[\mathcal{V}(t), [\mathcal{V}(t'), w_{tot}(t')]\right]\}. \tag{3.54}$$

Without loss of generality we assume that the interaction has no diagonal elements and the reservoir is in thermal equilibrium, i.e., $Tr_R(\mathcal{V}(t) w_{tot}(0)) = 0$, which implies that $U_1(t) = 0$. At this point we proceed by making two approximations which will result to a closed integro-differential equation for the reduced density operator.

• **Born Approximation:** Considering *weak interaction* between the atomic system and reservoir, we may apply *lowest non-vanishing order perturbation theory*, dropping terms of order higher than two, on the right-hand side of Eq. (3.52). We may additionally consider that the statistical properties of the large reservoir remain practically unaffected by this weak coupling and thus $w_{tot}(t') \approx \rho_R \otimes \rho_A(t')$.

• **Markov Approximation:** If the *correlation time of the reservoir* τ_R is smaller than the time scale over which $\rho_A(t)$ varies, we may set $\rho_A(t') \approx \rho_A(t)$. This means that the evolution of the atomic system is determined by the present and not its past since, any photon emitted into the radiation reservoir will never return back to the atom and thus the *atomic system does not develop any memory.* We may additionally extend the upper limit of the integration to infinity, as long as $t \gg \tau_R$.

Under all these approximations, the final form of the quantum optical master equation for the reduced density operator in Schrödinger picture is:

$$\frac{\partial \rho_A}{\partial t} = -\frac{i}{\hbar}[\mathcal{H}_A, \rho_A] - \frac{1}{\hbar^2}\int_0^\infty dt' Tr_R\{[\mathcal{V}(t), [\mathcal{V}(t'), \rho_R \otimes \rho_A(t)]]\}, \quad (3.55)$$

which is *valid to second order in the coupling constant* and for times such that $\tau_R \ll t \ll \gamma_a^{-1}$, where γ_a^{-1} is the decay rate of the atomic system. In other words the spectral bandwidth of the reservoir must be much larger than the atomic linewidth. This is the definition of a *flat radiation reservoir.*

3.4 A TLA Coupled to a Radiation Reservoir

Let's apply now the formalism we have developed above, in the case of a TLA coupled to a radiation reservoir [2]. Let $|e\rangle$ and $|g\rangle$ be the first excited and ground states of our model TLA, with respective energies $\hbar\omega_e$ and $\hbar\omega_g$. The atomic dyadic operators are then given by $\sigma_{eg} = |e\rangle\langle g| \equiv \sigma^+$ and $\sigma_{ge} = |g\rangle\langle e| \equiv \sigma^-$, while the inversion operator is defined as $\sigma_z = |e\rangle\langle e| - |g\rangle\langle g|$ and the population operators are $\sigma_{ee} = |e\rangle\langle e|$ and $\sigma_{gg} = |g\rangle\langle g|$. Let us also adopt the notation $\hbar\omega_o = \hbar\omega_e - \hbar\omega_g$ for the energy difference between the two atomic levels and unless otherwise specified, we shall take $\hbar = 1$ in our equations.

3.4.1 Open Space

The standard situation in QED is that of open space [100, 110]. In this case, we may use plane-wave mode-functions, which for a cubical volume of side L are of the form

$$\mathbf{u}_\lambda(\mathbf{r}) = \frac{1}{\sqrt{V}}\mathbf{e}_\lambda^{(\sigma)} e^{i\mathbf{k}_\lambda \cdot \mathbf{r}}, \quad (3.56)$$

where $V = L^3$ while $\mathbf{e}_\lambda^{(\sigma)}$ is the polarization vector such that $\mathbf{e}_\lambda^{(\sigma)} \cdot \mathbf{e}_\lambda^{(\sigma')} = \delta_{\sigma\sigma'}$ and $\mathbf{e}_\lambda^{(\sigma)} \cdot \mathbf{k}_\lambda = 0$.

The total unperturbed Hamiltonian is

$$\mathcal{H}^0 = \omega_o \sigma_z + \sum_\lambda \omega_\lambda a_\lambda^\dagger a_\lambda, \quad (3.57)$$

while, following the notation of the previous section, the states of the combined system are of the form $|s\rangle \equiv |j; \{n_\lambda\}\rangle$, where $j \in \{e, g\}$, and are

eigenstates of $\mathcal{H}^0$ with eigenvalues $\omega_s = \omega_j + \sum_\lambda \omega_\lambda n_\lambda$. For the study of spontaneous emission, we consider the atom initially excited and the field in its vacuum state (in thermal equilibrium at $T = 0$), i.e., $|\psi(0)\rangle = |e; \{0_\lambda\rangle\} \equiv |I\rangle$ with corresponding energy $\omega_I = \omega_o$. The interaction between the TLA and the infinitely many oscillators of the radiation field in the electric-dipole approximation can now be expressed as

$$\begin{aligned} \mathcal{V} &= \sum_\lambda g_\lambda(\sigma_{eg} + \sigma_{ge})(a_\lambda^\dagger + a_\lambda) \\ &= \sum_\lambda g_\lambda(\sigma_{eg} a_\lambda^\dagger + \sigma_{ge} a_\lambda^\dagger + \sigma_{eg} a_\lambda + \sigma_{ge} a_\lambda), \end{aligned} \tag{3.58}$$

where the coupling constant is given by Eq. (3.34) with $j = e$, $n = g$, while we have set $g_\lambda^{(e,g)} \to g_\lambda$, and the phase of $\mathbf{u}_\lambda(\mathbf{R}_A)$ has been chosen such that g_λ is real.

Rotating-Wave Approximation (RWA): The terms $\sigma_{eg} a_\lambda^\dagger$ and $\sigma_{ge} a_\lambda$ in Eq. (3.58) correspond to highly non-energy-conserving processes, namely, the excitation of the atom accompanied by the emission of a photon and de-excitation of the atom accompanied by the absorption of a photon, respectively. We may neglect these terms in favor of the other two energy-conserving terms, obtaining thus

$$\mathcal{V} = \sum_\lambda g_\lambda(\sigma_{eg} a_\lambda + \sigma_{ge} a_\lambda^\dagger). \tag{3.59}$$

Note that the interaction is linear in the field operators $a_\lambda^\dagger$ and a_λ and thus, the only states that give a non-vanishing matrix element of $\mathcal{V}$ with the initial state $|I\rangle$ are of the form $|F\rangle \equiv |g; 1_\lambda\rangle$, i.e., the atom in the ground state and one photon present in an arbitrary mode λ of the reservoir. Accordingly, the wavefunction of the system at an arbitrary time t can be written in the form

$$|\psi(t)\rangle = a_0(t)|e; \{0_\lambda\}\rangle + \sum_\lambda b_\lambda(t)|g; 1_\lambda\rangle. \tag{3.60}$$

In order to obtain a master equation for the problem at hand, we substitute both the unperturbed and the interaction part of the Hamiltonian (Eqs. 3.57 and 3.59), into (3.55). For the evaluation of the integrand in Eq. (3.55), we may let $V \to \infty$ (or equivalently $L \to \infty$) taking thus the *open-space limit*. In other words, the variables k_x/L, k_y/L, k_z/L, become continuous and thus, the sum over λ can be turned into an integral in $k-$space or, by means of the DOS $\rho(\omega)$, in $\omega-$space:

$$\frac{1}{V}\sum_\lambda \longrightarrow \frac{1}{(2\pi)^3}\sum_\sigma \int d\Omega \int k^2 dk \longrightarrow \frac{1}{(2\pi)^3}\sum_\sigma \int d\Omega \int \rho(\omega) d\omega. \tag{3.61}$$

For an arbitrary reservoir, we introduce the *spectral response* $\mathcal{D}(\omega)$, given by the following angular integral

$$\mathcal{D}(\omega) = \frac{V}{(2\pi)^3} \sum_{\sigma} \int d\Omega \rho(\omega) |g(\omega)|^2, \tag{3.62}$$

with the sum running over all polarizations. For the continuum under consideration, the DOS is of the well known form $\rho_o(\omega) = \omega^2/c^3$. Substituting $\rho_o(\omega)$ into Eq. (3.62) and performing the angular integration we have

$$\mathcal{D}_o(\omega) = \frac{\omega_o^2 |\mathbf{d}_{eg}|^2 \omega}{6\pi^2 \epsilon_0 c^3}. \tag{3.63}$$

This is a smoothly varying function around $\omega \approx \omega_o$ while for optical wavelengths, $\omega_o \sim 10^{15} sec^{-1}$. Hence, we are dealing with a flat (broad-band) continuum and Born and Markov approximations are valid.

Skipping over many steps of calculations which can be found in most books on quantum optics [1, 19, 21, 79, 121], we present the master equation for the reduced density operator of the atom

$$\frac{\partial \rho_A}{\partial t} = -i(\omega_o + S_a) [\sigma_z, \rho_A] + \frac{\gamma_a}{2} \left(2\sigma^- \rho_A \sigma^+ - \sigma^+ \sigma^- \rho_A - \rho_A \sigma^+ \sigma^- \right), \tag{3.64}$$

where γ_a is the atomic decay rate given by

$$\gamma_a = 2\pi \mathcal{D}_o(\omega = \omega_o). \tag{3.65}$$

The quantity S_a represents one contribution to the vacuum shift (Lamb shift) of the state $|e\rangle$, due to the coupling to the reservoir [100]. To obtain the complete expression for the vacuum shift we must include in our calculation the non-energy-conserving terms we dropped in RWA as well as all atomic states $|f\rangle$ for which $\mathbf{d}_{ef} \neq 0$. In our theoretical description we have adopted a rather simplified model, namely, TLA and RWA and as a result we have obtained the correct atomic linewidth (as long as $|e\rangle$ is the first excited state) but only part of the shift due to the reservoir.

The probability for the atom remaining excited at time t is given by the matrix element $\langle e|\rho_A|e\rangle \equiv \rho_{ee}$ and satisfies the following differential equation:

$$\frac{d\rho_{ee}}{dt} = -\gamma_a \rho_{ee}, \tag{3.66}$$

with solution $\rho_{ee} = e^{-\gamma_a t}$. The spectrum of the emitted light is associated with the Fourier transform of the two-time correlation function $\langle \sigma^+(t) \sigma^-(t') \rangle$ and has the well known Lorentzian form with width at half maximum equal to γ_a.

3.4.2 Cavity QED: Jaynes Cummings Model

There are many cases in quantum optics, where the dimensions of the environment into which the atom is embedded, are much larger than the wavelength of the atomic transition. One may thus work with the quantized electromagnetic field and let $V \to \infty$ after the calculations are complete, obtaining thus a continuous mode-structure with DOS that of open space. A closed cavity is the simplest departure from this limit and a standard by now situation in quantum optics. The volume is finite and the boundary conditions imposed to electromagnetic field lead to a discrete set of modes, whose spacing is inversely proportional to the length of the cavity. Furthermore, unlike open space, in the context of quantization one needs stationary-wave mode-functions and not plane-wave. For instance, the mode-function corresponding to TEM_{00} mode in a cylindrical cavity, is of the form $u_{00}(\mathbf{r}) \propto \sin(k_z z) e^{-(x^2+y^2)/w_0^2}$, where w_0 is a constant, and z is the axis of the cylinder. A harmonic oscillator can be associated with each one of the cavity-modes and thus the problem of spontaneous emission in a cavity can be approached by means of the formalism we have outlined in previous sections.

Consider a TLA placed in a perfect closed cavity whose geometric characteristics are such that only one cavity-mode interacts with the atom (single-mode cavity). The Hamiltonian describing the dynamics of the system in RWA is then of the form,

$$\mathcal{H} = \omega_o \sigma_z + \omega_c a^\dagger a + g(\mathbf{R}_A)(\sigma_{eg} a + \sigma_{ge} a^\dagger), \tag{3.67}$$

where ω_c and $a(a^\dagger)$ are the frequency and the annihilation(creation) operator corresponding to the cavity-mode. The coupling constant $g(\mathbf{R}_A)$ is given by Eq. (3.34). Considering the atom at rest, we may take the coupling approximately constant, i.e., $g(\mathbf{R}_A) = g$. Even for atoms flying through a cavity there are situations where the mode-function is approximately constant along the atomic trajectory and thus this assumption is still valid. The Hamiltonian (3.67) describes the simplest form of atom−field interaction, and is known as *Jaynes-Cummings model* [79, 110, 111].

Let's consider now a somewhat more general initial condition for the system, namely, the atom initially excited and the cavity-mode prepared in a pure Fock state $|n\rangle$, i.e., $|I\rangle = |e; n\rangle$. Accordingly, the final states that give non-zero matrix element of the interaction part of the Hamiltonian (3.67) are of the form $|F\rangle = |g; n+1\rangle$.

Dressed Photon−Atom States: The field−atom interaction $\mathcal{V}$, mixes these two basis states. The resulting states are eigenstates of the total Hamiltonian $\mathcal{H}$ and are the *dressed-states* of the combined field+atom system [110]. If the atomic transition is near-resonant with the cavity-mode, $|e; n\rangle$ and $|g; n+1\rangle$ are nearly degenerate. Diagonalizing the Hamiltonian $\mathcal{H}$ in the basis formed by $|I\rangle$ and $|F\rangle$ we obtain a new set of eigenstates $|\pm\rangle$ with

corresponding eigenvalues $\omega_{\pm}$. In some sense, the coupling of the atom to the cavity-mode splits the otherwise common resonance of the cavity and the atom, into two peaks. This splitting is referred to as *Rabi splitting*. In the case of resonance ($\omega_o = \omega_c$) the dressed states are $|\pm\rangle = (|e;n\rangle \pm |g;n+1\rangle)/\sqrt{2}$ with corresponding eigenenergies $\omega_{\pm} = \pm\Omega_n$, respectively, with $\Omega_n = g\sqrt{n+1}$ being the *Rabi frequency*. The probability P_{II} of finding the system in its initial state after time t is

$$P_{II} = \cos^2(\Omega_n t), \tag{3.68}$$

which reflects a periodic exchange of energy (*Rabi oscillations*) between the atom and the cavity-mode. *Vacuum Rabi oscillations* appear even for an initially empty cavity ($n = 0$), which is in contrast to the irreversible atomic decay in open space. From another point of view, the combined system (atom + cavity-mode) oscillates between the two stable dressed states.

As long as no loss mechanism has been taken into account in our theoretical model, Rabi oscillations will persist for ever. In any experimental test, however, there are mainly two mechanisms of dissipation that affect the "atom + mode" dynamics and lead to damped Rabi oscillations. The first is spontaneous atomic decay at rate γ_a into continuum modes other than those supported by the cavity, and the second involves losses through the imperfect walls and mirrors of the cavity at a rate γ_c. Both spontaneous emission and cavity-dissipation can be incorporated in our treatment as a coupling of the atom and the cavity-mode itself to a large radiation reservoir (the external world), into which they dissipate their energy. We thus obtain the following master equation for the reduced density matrix of the small combined system:

$$\begin{aligned} \frac{\partial \rho}{\partial t} &= -i\left[\mathcal{H}^0, \rho\right] + \frac{\gamma_a}{2}\left(2\sigma^- \rho \sigma^+ - \sigma^+\sigma^-\rho - \rho\sigma^+\sigma^-\right) \\ &\quad + \frac{\gamma_c}{2}\left(2a\rho a^\dagger - a^\dagger a\rho - \rho a^\dagger a\right). \end{aligned} \tag{3.69}$$

where $\mathcal{H}^0 = \omega_o\sigma_z + \omega_c a^\dagger a$. This master equation, supplemented with the idea of pumping via the transit of the excited atom through the cavity, forms the basis of the theory of the micromaser as well as a model for the laser [101, 107].

Considering a closed cavity ($\gamma_a \to 0$) and weak atom–mode coupling ($\gamma_c >> g$), we have exponential decay of the initially excited atom as in open space. In this case, the damping of the energy in the cavity is so fast, compared to the rate with which it is deposited by the atom, that it is as if the atom were radiating directly into open space. On the contrary, in the *strong-coupling regime* ($\gamma_c << g$) the losses to the outside environment are comparatively slow. The emitted photon survives sufficiently long to be reabsorbed causing thus vacuum Rabi oscillations and the *spontaneous*

de-excitation of the atom ceases being *irreversible*. The strong-coupling regime is characterized not only by g and γ_c, but also by the open-space atomic linewidth γ_a and the transit time τ of light through the cavity. It has been found that spontaneous emission can be affected by the size of the cavity [38]. This stems from the fact that an initially excited atom "learns" about its surrounding world by simply emitting wave-packets during the time interval determined by its linewidth. For short times, spontaneous decay takes place, as if the atom was in open space. The initially emitted wave-packet returns back to the atom after having propagated along the cavity and been reflected by the walls of the cavity. It carries the "information" about the environment, i.e., the presence of mirrors. For sufficiently long cavities ($\tau >> \gamma_a^{-1}$), the atom has completely decayed by the time the initially emitted wave-packet returns back to it and thus any memory is lost (Markovian problem). On the contrary, if $\tau << \gamma_a^{-1}$ the atom has not decayed, and thus a constructive interference between the reflected wave-packet and the one that is instantly emitted by the atom takes place. Clearly, the "atom + cavity" dynamics in the latter case are non-Markovian. It is possible, however, to overcome this difficulty by choosing atom + cavity be the small system which is coupled to a flat reservoir, whose dynamics are purely Markovian.

Alternatively, one may focus on the atom, while treating both cavity and external fields as a reservoir. This choice yields a Lorentzian spectral response for the reservoir [98, 107],

$$\mathcal{D}_c(\omega) = \frac{\gamma_a}{2\pi} \frac{\gamma_c}{(\omega - \omega_c)^2 + (\gamma_c/2)^2}. \tag{3.70}$$

In general, a cavity involves more than one modes. Nevertheless, if they are separated in frequency by much more than their widths (in other words assuming high-quality (Q) and high-finesse cavity), we can meaningfully examine the behaviour of the atom when is on(off) resonance with one cavity-mode, as we have done up to now. In general, the Fourier transform of the spectral response gives the *memory-kernel* of the reservoir we are dealing with. For the continuum under consideration we have

$$G_c(t - t') \propto e^{-\gamma_c |t - t'|}, \tag{3.71}$$

which indicates the *non-Markovian* nature of the interaction between the atom and the cavity. Note that for open space $G_o(t - t') \propto \delta(t - t')$ which reflects the instant loss of memory, whenever a photon is emitted.

Although up to now we have concentrated on the case of exact resonance, the situation differs quantitatively, but not qualitatively, for $\omega_o \neq \omega_c$. If the atom is detuned from the cavity-mode, it is protected somewhat against decay, due to the low DOS available to the emitted photon. The essential point, however, is that in the long-time limit, no matter how far the atom

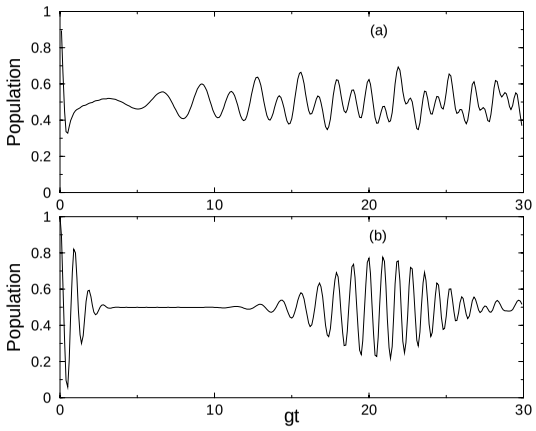

Fig. 3.1: Collapses and revivals. The population in the upper state of a two-level atom driven by (a) thermal and (b) coherent field, is plotted as function of the dimensionless time gt. In both cases $\bar{n} = 10$, $\omega_o = \omega_c$.

is detuned from the cavity-mode, it will eventually end up in the ground state. This is because of the Lorentzian profile of DOS, whose wings extend to infinity, which should be kept in mind in order to be compared with the case of PCs in the following chapter.

Quantum Collapses and Revivals [107, 110, 111]**:** With an uncertain number of photons in the cavity-mode, Eq. (3.68) reads

$$P_{II} = \sum_{n=0}^{\infty} \mathcal{P}(n) \cos^2(\Omega_n t), \tag{3.72}$$

where $\mathcal{P}(n)$ is the probability of having n photons. For a thermally-excited mode, $\mathcal{P}(n) = \mathcal{P}_t(n)$, whereas for a coherent field $\mathcal{P}(n) = \mathcal{P}_c(n)$, with $\mathcal{P}_c(n)$ and $\mathcal{P}_t(n)$ given by Eqs. (3.20) and (3.22) respectively. As one expects, such superpositions of periodic solutions result to damped oscillations, the so called *collapses* [Fig. 3.1(a)]. What is remarkable is that for a coherent field the Rabi oscillations revive after time $t_R \sim g^{-1}\sqrt{\bar{n}}$ [Fig. 3.1(b)]. These *revivals* (which mathematically stem from the discreteness of the sum in Eq. (3.72)), have been observed experimentally [14, 97], and reflect the phase relation between successive terms in the expansion of a coherent state in terms of Fock states.

3.5 Resonance Fluorescence

Resonance fluorescence is a classic problem in quantum optics and has been shown to be associated with many quantum mechanical effects, such as photon antibunching, squeezing, etc [21, 121]. In its simplest form the problem

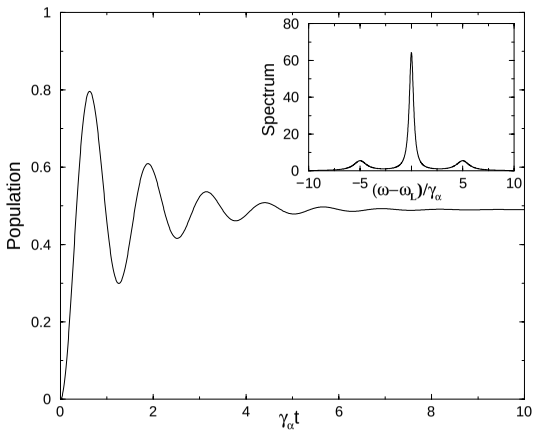

Fig. 3.2: Resonance fluorescence in open space. The population in the upper state of a two-level atom, driven by a classical field is plotted as function of the dimensionless time $\gamma_a t$. The inset shows the spectrum of the emitted radiation (Mollow triplet). Parameters: $\Omega = 5\gamma_a$, $\Delta_L = 0$.

consists of a TLA situated in open space and driven by a single coherent mode of the radiation field, for instance a laser (L), while simultaneously it can decay into the vacuum modes of the electromagnetic field. The Hamiltonian describing the system is $\mathcal{H} = \mathcal{H}^0 + \mathcal{V}_{A-L} + \mathcal{V}_{A-R}$, where $\mathcal{H}^0$ is the unperturbed Hamiltonian and $\mathcal{V}_{A-R}$ is the atom–reservoir interaction as given by Eq. (3.59). Treating the coherent driving classically, $\mathcal{V}_{A-L}$ reads

$$\mathcal{V}_{A-L} = \frac{\Omega}{2}(\sigma^+ e^{-i\omega_L t} + \sigma^- e^{i\omega_L t}), \tag{3.73}$$

where Ω is the Rabi frequency and ω_L the frequency of the laser. Clearly, in resonance fluorescence dissipation takes place simultaneously with the coherent driving and thus, the master equation formalism is necessary for its treatment. The master equation for the reduced density operator of the atom has an incoherent part which refers to spontaneous emission into the flat continuum and a coherent one which describes the driving of the atom by the laser. Specifically, in an interaction picture rotating at ω_L we have

$$\begin{aligned} \frac{\partial \rho_A}{\partial t} &= -i\Delta_L \left[\sigma_z, \rho_A\right] - i\frac{\Omega}{2}\left[\sigma^+ + \sigma^-, \rho_A\right] \\ &+ \frac{\gamma_a}{2}\left(2\sigma^-\rho_A\sigma^+ - \sigma^+\sigma^-\rho_A - \rho_A\sigma^+\sigma^-\right), \end{aligned} \tag{3.74}$$

where $\Delta_L = \omega_o - \omega_L$. The population in the excited atomic state is then given by $\langle\sigma_z\rangle \equiv Tr(\rho_A\sigma_z)$. For weak driving, the atomic population varies monotonically with time and in the long-time limit the atom relaxes in its ground state. On the contrary, for strong laser fields an oscillatory behavior

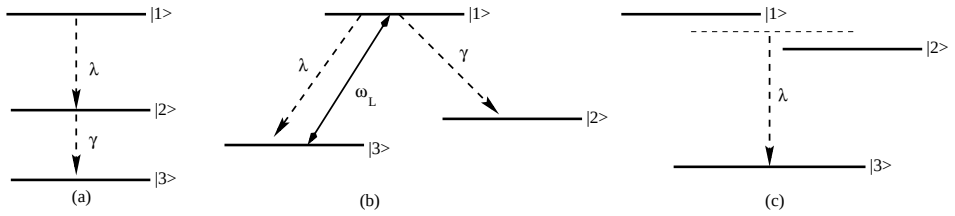

Fig. 3.3: Three-level atomic systems.

is obtained till the atom becomes saturated with equal probability of being found in the upper and lower levels, respectively (Fig. 3.2). We finally note that the spectrum of the fluorescent light into the vacuum modes of the electromagnetic field is known as *Mollow triplet* since it exhibits three peaks at frequencies ω_L and $\omega_L \pm \Omega$ respectively. Its mathematical treatment is highly non-trivial with a number of subtleties.

3.6 Three-level Atoms

For a number of reasons, three-level atomic models of the ladder (Ξ), lambda (Λ) or V configuration (see Fig. 3.3) are of interest in quantum optics [107, 110]. All three of these three-level arrangements involve two in general different transition frequencies. In this section we present a brief overview of radiative processes associated with each one of these three-level configurations.

3.6.1 Cascade Decay

In a three-level atom of Ξ configuration [Fig. 3.3(a)], the upper and lower levels have the same parity and thus, considering the atom initially in upper state, a cascade is the only way of de-excitation. If both atomic transitions are coupled to open space, an exponential decay takes place and two photons are emitted as the atom cascades down to the ground state. The spontaneous-emission spectrum for the upper transition is, to a very good approximation, a Lorentzian of width equal to the sum of the linewidths of the upper and intermediate states. On the other hand, the spectrum for the lower transition is a Lorentzian too, but its width is equal to the linewidth of the intermediate state. Measurements involving angular correlation between the two spontaneously emitted photons, are of particular interest in tests of the validity of Bell's inequality in connection with the possible existence of hidden variables. In spectroscopic studies through double optical resonance, one or both transitions of the ladder system are driven by external fields.

3.6.2 Branching Decay

In a Λ-system, the two lower levels have the same parity. Considering the atom initially prepared in the upper level [see Fig.3.3(b)], we have two decay channels, namely, $|1\rangle \rightarrow |2\rangle$ and $|1\rangle \rightarrow |3\rangle$. If both transitions are coupled to open space the total decay rate out of the upper state is $\gamma_1 = \gamma_{12} + \gamma_{13}$, where γ_{12} and γ_{13} are the decay rates for $|1\rangle \rightarrow |2\rangle$ and $|1\rangle \rightarrow |3\rangle$ transitions respectively. The spectrum of the emitted photon exhibits two Lorentzian peaks centered at the frequencies of the two possible transitions and with equal widths. When both transitions are driven by external fields, the system may exhibit coherent population trapping (even when the upper state decays), while the adiabatic population transfer from one to the other of the lower states, through a Raman transition, without loss from the upper state is also feasible. The coherent population trapping and the formation of the so-called dark state plays a decisive role in laser cooling of atomic motion, where the three levels correspond to quantized states of the center of mass motion.

3.6.3 Quantum Interference in Spontaneous Decay

Consider a V-system [Fig. 3.3(c)] initially prepared in a superposition of the upper levels, and both transitions being coupled to open space. It has been found that if the separation of the two upper levels is small compared to their decay rates the evolution of the system is oscillatory and not exponential. This is due to quantum interference between the two possible decay paths. Additionally, the spontaneous-emission spectrum may exhibit spectral narrowing and dark lines. The V-system, with one of the transitions driven by an external field, is essential in studies of quantum jumps.

3.7 Decay of Interacting Atoms

So far, we have considered the interaction of an isolated few-level atom with the radiation field. In this section, we briefly discuss the dynamics of a collection of atoms confined in a volume small compared to the wavelength corresponding to the atomic transition frequency. All atoms, identical or not, are simultaneously coupled to the same radiation reservoir. The evolution of such an atomic system and the spectrum of the emitted photons can be significantly different from that of a single atom.

Consider an ensemble of N TLAs identified by the subscripts $1, 2, \ldots, N$, and let $|e_l(g_l)\rangle$, ω_l be the atomic levels and atomic transition frequency for atom l, with $l \in \{1, 2, \ldots, N\}$. The unperturbed Hamiltonian of the system is then the sum of the unperturbed Hamiltonians for the atoms and the

radiation field, i.e.,

$$\mathcal{H}^0 = \sum_{l=1}^{N} \omega_l \sigma_z^l + \sum_{\lambda} \omega_\lambda a_\lambda^\dagger a_\lambda, \tag{3.75}$$

while the position of the center of mass of the atoms must also be included in the coupling to the radiation, which now reads

$$\mathcal{V} = \sum_{l=1}^{N} \sum_{\lambda} \left[g_\lambda^{(l)} a_\lambda \sigma_l^+ + g_\lambda^{(l)*} a_\lambda^\dagger \sigma_l^- \right], \tag{3.76}$$

with

$$g_\lambda^{(l)} = -i\sqrt{\frac{1}{2\epsilon_0 \omega_\lambda}} \omega_l \mathbf{u}_\lambda(\mathbf{R}_l) \cdot \mathbf{d}_{eg}^{(l)}, \tag{3.77}$$

where $\mathbf{d}_{eg}^{(l)}$ denotes the electric dipole matrix element for atom l, while the corresponding atomic dyadic operators are $|e_l\rangle\langle g_l| \equiv \sigma_l^+$ and $|g_l\rangle\langle e_l| \equiv \sigma_l^-$.

3.7.1 Dipole-Dipole Interaction

Let's consider the mutual interaction between two TLAs [80]. One of them is assumed to be initially in the upper state and the other in the lower. If we label the atoms by 1 and 2, the relevant states of the problem are:

$$|a\rangle = |e_1, g_2; 0\rangle, \tag{3.78}$$

$$|b\rangle = |g_1, e_2; 0\rangle, \tag{3.79}$$

$$|c\rangle = |g_1, g_2; 1_\lambda\rangle, \tag{3.80}$$

and $\mathcal{H}^0|j\rangle = \omega_j|j\rangle$ with $j \in \{a, b, c\}$. Thus an arbitrary wavefunction $|\psi(t)\rangle$ can be expressed as a superposition of these states, while its evolution is given by:

$$|\psi(t)\rangle = e^{-i\mathcal{H}t}|\psi(0)\rangle = e^{-i(\mathcal{H}^0+\mathcal{V})t}|\psi(0)\rangle \equiv \mathcal{U}(t)|\psi(0)\rangle, \tag{3.81}$$

where $|\psi(0)\rangle$ is the initial state of the combined system, while $\mathcal{U}(t)$ is the time-evolution operator. Introducing the Laplace transform $\int_0^\infty dt \mathcal{U}(t) e^{-st}$, changing the variable s to $-iz$ and denoting by $G(z)$ the Laplace transform in the complex z-plane (known as *Resolvent operator* [21, 42]), we have

$$G(z) = \frac{1}{z - \mathcal{H}}, \tag{3.82}$$

with $\mathcal{H}$ defined in Eqs. (3.75) and (3.76). Working in the basis formed by the states (3.78)-(3.80), we obtain the following equations for the matrix elements of $G(z)$:

$$(z - \omega_a) G_{aa} = 1 + \sum_c \mathcal{V}_{ac} G_{ca}, \tag{3.83}$$

$$(z - \omega_b) G_{ba} = \sum_c \mathcal{V}_{bc} G_{ca}, \tag{3.84}$$

$$(z - \omega_c) G_{ca} = \mathcal{V}_{ca} G_{aa} + \mathcal{V}_{cb} G_{ba}. \tag{3.85}$$

Eliminating the continuum amplitude G_{ca} we obtain

$$(z-\omega_a)G_{aa} = 1+\sum_c \frac{|\mathcal{V}_{ac}|^2}{z-\omega_c}G_{aa}+\sum_c \frac{\mathcal{V}_{ac}\mathcal{V}_{cb}}{z-\omega_c}G_{ba}, \quad (3.86)$$

$$(z-\omega_b)G_{ba} = \sum_c \frac{|\mathcal{V}_{bc}|^2}{z-\omega_c}G_{ba}+\sum_c \frac{\mathcal{V}_{bc}\mathcal{V}_{ca}}{z-\omega_c}G_{aa}. \quad (3.87)$$

We have two kinds of couplings which need to be calculated, namely,

$$V_{jc}(z)=\sum_c \frac{|\mathcal{V}_{jc}|^2}{z-\omega_c}, \quad (3.88)$$

and

$$M_{12}(z)=\sum_c \frac{\mathcal{V}_{ac}\mathcal{V}_{cb}}{z-\omega_c}=M_{21}^*(z). \quad (3.89)$$

The V_{jc} refers to the direct coupling of each individual atom to the continuum, whereas M_{12} describes the interatomic coupling through the continuum. The physical picture is that the photon emitted by the excited atom is absorbed by the unexcited one; hence the term *dipole-dipole interaction* (DDI) or *photon hopping*.

Assuming two *identical* atoms, interacting with a broadband (flat) reservoir, such as open space, Born and Markov approximations hold and thus $V_{jc}(z) \approx S_a - i\gamma_a$. The shift S_a can be assumed absorbed in the energy of the upper state and with the lower state energy set equal to zero, the relevant matrix elements of the resolvent obey the following equations in matrix form:

$$\begin{bmatrix} z-\tilde{\omega}_o+i\gamma_a & -M_{12} \\ -M_{12} & z-\tilde{\omega}_o+i\gamma_a \end{bmatrix}\begin{bmatrix} G_{aa} \\ G_{ba} \end{bmatrix}=\begin{bmatrix} 1 \\ 0 \end{bmatrix}, \quad (3.90)$$

where $\tilde{\omega}_o$ is the atomic transition frequency shifted by S_a. The quantity γ_a represents the spontaneous-decay width of each atom. The dipole-dipole matrix element M_{12} is in general complex and diverges as the interatomic distance approaches to zero. This is to be expected since in that limit a molecule is formed. For open space, M_{12} is turns out to be a z-independent quantity:

$$\begin{aligned} M_{12}\equiv V_{12}+i\Gamma_{12} &= \frac{3}{2}\gamma_a\left[\frac{cos(r_{12})}{r_{12}}-\frac{sin(r_{12})}{r_{12}^2}-\frac{sin(r_{12})}{r_{12}^3}\right] \\ &- \frac{3i}{2}\gamma_a\left[\frac{sin(r_{12})}{r_{12}}+\frac{cos(r_{12})}{r_{12}^2}-\frac{sin(r_{12})}{r_{12}^3}\right]. \end{aligned} \quad (3.91)$$

This expression has been obtained, as an example, for the two atomic dipoles parallel to each other but perpendicular to r_{12}, where r_{12} is the normalized

interatomic distance with respect to the wavevector $\mathbf{k}_o$ corresponding to the atomic transition frequency, i.e., $r_{12} \equiv \mathbf{k}_o \cdot |\mathbf{R}_1 - \mathbf{R}_2|$.

In general, the time-evolution operator $\mathcal{U}(t)$ is obtained from $G(z)$ through the inversion integral

$$\int_{\mathcal{C}} G(z) e^{-izt} dz, \tag{3.92}$$

integrated on the appropriate contour $\mathcal{C}$ which, upon examination of the poles of $G(z)$ on the z-plane, leads to the somewhat more convenient form

$$\mathcal{U}(t > 0) = \lim_{\eta \to 0} \int_{-\infty}^{+\infty} dx e^{-xt} G(x + i\eta), \tag{3.93}$$

which is valid as indicated only for $t > 0$ and x is a real variable. The eigenvalues and the corresponding eigenvectors of the matrix in Eq. (3.90) are

$$z_{\pm} = \tilde{\omega}_o - i\gamma_a \pm M_{12}, \tag{3.94}$$

and

$$|\psi_{\pm}\rangle = \frac{1}{\sqrt{2}} \left[|e_1, g_2\rangle \pm |g_1, e_2\rangle \right], \tag{3.95}$$

respectively, where by $(+)$ and $(-)$ we denote the symmetric and antisymmetric product states, respectively, which correspond to entanglement of the two atoms. In open space, the symmetric state is unstable, leading to superradiance (see also the following section). Substitution of the eigenvalues into the inversion integral, yields a damped sinusoidal behaviour in time. How strongly damped it is, depends on the atomic separation and strength of interaction in relation to the decay rate γ_a. In the long-time limit, however, the excited-state population in either atom will decay. The atoms may exchange excitation for a while, but they will eventually end up in the ground state.

The situation is basically similar if the atoms are inside a cavity on (or near) resonance with a mode [43]. The equations for the matrix elements of the resolvent are in this case a bit more complicated [4, 6]. As in the case of open space, however, in the long-time limit all excitation is lost. The evolution in time is more involved because not only can the photon hop from one atom to the other, but as we have seen in Sec. 3.4.2, it can be reabsorbed by the same atom. But the end result is the same; the atoms in the ground state and the cavity empty.

3.7.2 Superradiance

When the collection of N identical TLAs is initially fully excited, a cooperative effect, known as superradiance occurs. The phenomenon was first

discussed by Dicke [24] in open space who showed that in a superradiant system, spontaneous emission takes place over a time scale inversely proportional to the number of radiated atoms, while the emission intensity is proportional to N^2. The superradiant behaviour is due to the induction of correlations between the dipole moments of the initially uncorrelated atoms, that interact via a common electromagnetic field [2, 3, 44]. The emitted radiation, on the other hand, is characterized by a well defined directionality, depending on the geometry of the sample.

Let us introduce at this point the *Dicke notation*, which is widely used in the literature on superradiance. At t=0, all atoms are excited and uncorrelated and thus $|\psi(0)\rangle = |e_1, e_2, \ldots, e_N\rangle$. For small times close to $t = 0$, superradiance is purely quantum mechanical, since the atoms interact with the vacuum field until dipole-dipole correlations arise. After this initial stage, however, the phenomenon becomes classical with a macroscopic collection of dipoles emitting radiation in a way analogous to that of classical antennas. Since the atoms are confined in a volume with dimensions smaller than the emission-wavelength, we can assume that the total dipole moment of the system is the sum over the dipole moments of individual atoms. Introducing the macroscopic atomic operators $J^+ = \sum_l |e_l\rangle\langle g_l|$, $J^- = \sum_l |g_l\rangle\langle e_l|$, $J_z = \sum_l (|e_l\rangle\langle e_l| - |g_l\rangle\langle g_l|)$ the Hamiltonian of the complete system in RWA can be written as

$$H = \omega_o J_z + \sum_\lambda \omega_\lambda a_\lambda^\dagger a_\lambda + \sum_\lambda g_\lambda (a_\lambda^\dagger J^- + a_\lambda J^+), \tag{3.96}$$

where ω_o is the atomic transition frequency for each individual atom, while we have dropped the index l, since the atoms are identical. The macroscopic operators obey the well known commutation relations:

$$[J_z, J^\pm] = \pm J^\pm, \quad [J^+, J^-] = 2J_z, \tag{3.97}$$

while we can define a complete set of orthogonal *Dicke states* $|j, m\rangle$ where $j = \frac{N}{2}$ and $m\epsilon[-j, j]$ which are eigenstates of J_z and J^2, with eigenvalues m and $j(j+1)$, respectively. The state $|j, m\rangle$ is the fully symmetrical atomic state where $j + m$ atoms are excited and $j - m$ are in the ground state and thus the corresponding energy is $m\omega_o$. For instance, for a system of two TLAs the relevant states are: $|1, 1\rangle \equiv |e_1, e_2\rangle$, $|1, 0\rangle \equiv (|e_1, g_2\rangle + |g_1, e_2\rangle)/\sqrt{2}$ and $|1, -1\rangle \equiv |g_1, g_2\rangle$, with corresponding energies: ω_o , 0 , $-\omega_o$, respectively. In the language of the Dicke states, the system is initially $(t = 0)$ prepared in state $|\psi(0)\rangle = |j, j\rangle$ and cascades down a ladder of $N + 1$ equidistant levels.

There are mainly two ways of studying superradiance problems and both have been employed in the literature. The first is the derivation of a Markovian master equation for the reduced density operator of the atomic system. Alternatively, one may work with the Heisenberg equations of motion for

the atomic and field operators. In the Heisenberg picture, the equation of motion for an operator $\mathcal{O}$ reads $\dot{\mathcal{O}} \equiv -i[\mathcal{O}, \mathcal{H}]$. Following this definition and using Eq. (3.96), one obtains the equations of motion for the field operators, the atomic inversion J_z and the atomic polarization J^-:

$$\frac{da_\lambda}{dt} = -i\omega_\lambda a_\lambda - ig_\lambda J^-, \tag{3.98}$$

$$\frac{dJ_z}{dt} = i\sum_\lambda g_\lambda a_\lambda^+ J^- + H.c, \tag{3.99}$$

$$\frac{dJ^-}{dt} = -i\omega_o J^- + 2i\sum_\lambda g_\lambda a_\lambda J_z, \tag{3.100}$$

and after eliminating the field operators by formal integration, we have

$$\frac{d\langle J_z\rangle}{dt} = -\left\{\int_0^t dt' G(t-t')\langle J^+(t)J^-(t')\rangle - i\langle\xi(t)J^+(t)\rangle\right\} + H.c, \tag{3.101}$$

$$\frac{d\langle J^-\rangle}{dt} = 2\int_0^t dt' G(t-t')\langle J_z(t)J^-(t')\rangle + 2i\langle\xi(t)J_z(t)\rangle, \tag{3.102}$$

where we have transformed to an interaction picture rotating at the atomic transition frequency ω_o, i.e., $\delta_\lambda = \omega_\lambda - \omega_o$. We have in addition introduced the *quantum-noise operator*

$$\xi(t) = \sum_\lambda g_\lambda a_\lambda(0) e^{-i\delta_\lambda t}, \tag{3.103}$$

while $G(t-t') \equiv \langle\xi(t)\xi(t')\rangle$ is the memory-kernel (correlation) function of the reservoir.

As we can see, the equations of motion (3.101) and (3.102), do not constitute a closed set of differential equations. On the contrary, they lead to other expectation values of higher order correlations, i.e., $\langle J^+J^-\rangle$ and $\langle J_zJ^-\rangle$. The resulting hierarchy of equations can not be solved, unless it is somehow truncated. This truncation involves a decorrelation scheme and is an approximation to the exact solution. There is no unique decorrelation approach, but the simplest is the direct decorrelation of the products, i.e., $\langle J_zJ^-\rangle = \langle J_z\rangle\langle J^-\rangle$. Following this approach, (3.101) and (3.102) read

$$\frac{d\langle J_z\rangle}{dt} = -2\Re\left\{\langle J^+(t)\rangle\int_0^t dt' G(t-t')\langle J^-(t')\rangle\right\}, \tag{3.104}$$

$$\frac{d\langle J^-\rangle}{dt} = 2\langle J_z(t)\rangle\int_0^t dt' G(t-t')\langle J^-(t')\rangle, \tag{3.105}$$

where the average over the quantum noise has been set to zero ($\langle\xi(t)\rangle = 0$) and $\Re\{\cdot\}$ denotes the real part of the expression in curly braces. From now on, we refer to these equations as *mean-field* (MF) *equations*.

It is well-known that in open space the memory-kernel is a delta function which leads to an exponential behavior of the system, while in the long-time limit, all atoms are in the ground state, and thus there is no inversion or polarization. On the contrary, if the superradiant system is placed in a cavity, we have an oscillatory evolution for both inversion and polarization reflecting the exchange of energy between the atomic system and the cavity-mode(s). Both cavity-field and atomic system, however, will eventually end up in their ground states.

As long as the coupling of each atom to the radiation field is invariant under any atomic permutation, the evolution of the collection is restricted to the Hilbert subspace involving only the symmetric atomic states of the system. In general, the DDI, is not symmetric under all atomic permutations. As a consequence, it tends to destroy the correlation between various couples of dipoles (*Van-der-Waals dephasing* or *symmetry-breaking effect*), weakening thus the cooperative character of superradiance. There are atomic arrangements, however, in which the interatomic coupling is invariant under any atomic permutation and thus its net effect is to shift the symmetric states which become non-equidistant. This gives rise to the emission of photons with different energies and the time-dependent shift of the superradiant emission, the so-called *frequency chirping effect.*

3.8 Stochastic Quantum Trajectories

Consider a quantum system with N (states) degrees of freedom. The master equation treatment then, requires the solution of $N \times N$ differential equations. There are quantum-optical systems involving a large number of states and as such, they are intractable using the density-operator approach. One can, however, obtain the result that would correspond to the solution of the master equation by simulating the stochastic evolution of a wavefunction for the system in Hilbert space of dimension N [33, 35, 94]. As a result, the evolution of the system can be obtained through the solution of no more than N differential equations. In this section we present two ways to *unravel* a Markovian master equation of the *Lindbland* form:

$$\frac{\partial \rho}{\partial t} = -i\left[\mathcal{H}_s, \rho\right] + \frac{1}{2}\sum_m \left(2L_m \rho L_m^\dagger - L_m^\dagger L_m \rho - \rho L_m^\dagger L_m\right), \tag{3.106}$$

into *stochastic quantum trajectories.* The *Lindbland operators* $L_m^\dagger$ (L_m) represent the interaction of the system with the environment, while $\mathcal{H}_s$ is the Hamiltonian of the system.

3.8.1 Quantum Monte-Carlo (QMC) Method

In the context of QMC approach [23, 28, 34, 81] the time evolution of the open system is governed by a non-Hermitian Hamiltonian,

$$\mathcal{H}_u = \mathcal{H}_s - \frac{i}{2}\sum_m L_m^\dagger L_m, \tag{3.107}$$

and thus, if $|\psi(t)\rangle$ is the state-vector of the system at t, at time $t + dt$ we have

$$|\psi(t+dt)\rangle = e^{-i\mathcal{H}_u t}|\psi(t)\rangle. \tag{3.108}$$

The coherent evolution of the system at each time-step dt may be interrupted by an instantaneous *quantum jump* which is related to a *gedanken measurement* of the number of photons in the radiation reservoir. After each measurement, the wavefunction of the system is projected on its zero- or one-photon component and the photon in the latter case is annihilated by the detector. Note that, since $\mathcal{H}_u$ is non-Hermitian, the norm is not preserved and thus $|\psi(t+dt)\rangle$ has to be renormalized at each time-step.

3.8.2 Quantum State-Diffusion (QSD) Method

The unraveling we have just presented is definitely not unique. Another kind of quantum trajectory is the so-called QSD method [39, 40, 41]. Gisin and Percival have provided a natural symmetry condition which leads to the derivation of a unique diffusion-equation for master equations of the form (3.106), namely,

$$\begin{aligned} |\psi(t+dt)\rangle &= -i(\mathcal{H}_s - iL_m^\dagger L_m)|\psi(t)\rangle dt \\ &+ \sum_m (2\langle L_m^\dagger\rangle L_m - \langle L_m^\dagger\rangle\langle L_m\rangle)|\psi(t)\rangle dt \\ &+ \sum_m (L_m - \langle L_m\rangle)|\psi(t)\rangle d\xi_m. \end{aligned} \tag{3.109}$$

The first sum represents the "drift" of the state-vector while the second one the random fluctuations resulting from the coupling of the system to its environment. The $d\xi_m$ represent complex normalized Wiener processes. In appendix A, we illustrate the application of both QMC and QSD methods in the problem of resonance fluorescence.

Chapter 4

Quantum Optical Phenomena in Photonic Crystals

In this chapter we extent the problems we have discussed in the previous chapter to environments provided by PBG structures [64]. To this end, we need a suitable DOS, incorporating the essential physical features associated with such materials.

4.1 Models of DOS for PBGs

4.1.1 Isotropic Model

In 1990, John and Wang proposed an isotropic model assuming that a propagating photon in a PC, experiences the same periodic potential, irrespective of its polarization or direction of propagation [59, 60]. The propagation of an electromagnetic wave in such an ideal structure, can thus be described by a scalar wave-equation in one dimension:

$$-\nabla^2\psi(x) + \Phi(x)\psi(x) = \frac{\omega^2}{c^2}\psi(x), \tag{4.1}$$

where ω is the frequency of the wave and $\Phi(x)$ is a periodic "potential" associated with the modulation of the dielectric constant.

In appendix B, we present a full description of this hypothetical model and we derive the corresponding dispersion relation which, for a particular choice of parameters, reads:

$$\omega_k = \frac{c}{4na} arccos\left[\frac{4ncos(2ka(1+n)) + (1-n)^2}{(1+n)^2}\right], \tag{4.2}$$

and relates the frequency to the propagation vector k, where a is the size of the dielectric scatterers (with refractive index n) periodically arranged. This dispersion relation leads to gaps at $k = \frac{m\pi}{2(n+1)a}$ for odd integer values

of m. The lowest gap is centered at the frequency $\omega_{gap} = \pi c(4na)^{-1}$ and for $n = 1.082$, its width is $\Delta\omega = 0.05\omega_{gap}$. Hence, no radiation of frequency $\omega \in \left[\omega_{gap} - \frac{1}{2}\Delta\omega, \omega_{gap} + \frac{1}{2}\Delta\omega\right]$ can propagate inside the crystal.

We shall be interested in the behaviour of small atomic systems with transition frequencies around the edge. Assuming thus, a large gap compared to the atomic linewidth, we may restrict ourselves to frequencies close to the upper band-edge frequency $\omega_e = \omega_{gap} + \frac{1}{2}\Delta\omega$, and Eq. (4.2) yields

$$\omega_k = \omega_e + A(k - k_e)^2, \tag{4.3}$$

where A is a material specific constant and k_e is the wave-vector corresponding to the band-edge frequency. In the context of quantization of the electromagnetic field in such periodic structures one may consider plane-wave mode-functions. For the dispersion relation (4.3), the corresponding DOS reads

$$\rho_I(\omega) = \frac{k_e^2}{2\sqrt{A}} \frac{\Theta(\omega - \omega_e)}{\sqrt{\omega - \omega_e}} \tag{4.4}$$

where $\Theta(\omega - \omega_e)$ is the usual step function, indicating that there is a gap below ω_e. In a finite one-dimensional PC, however, the singular behavior is always smoothed [9, 32]. This effect can be incorporated in our model, by introducing a smoothing parameter ϵ and rewriting Eq. (4.4) in the form [62, 68]

$$\rho_S(\omega) = \frac{k_e^2}{2\sqrt{A}} \frac{\sqrt{\omega - \omega_e}}{\omega - \omega_e + \epsilon} \Theta(\omega - \omega_e). \tag{4.5}$$

Neglecting the vectorial nature of electromagnetic waves we have thus obtained a simple isotropic model. Band-structure studies have shown that the vectorial nature of electromagnetic waves has to be taken into account in order to achieve good agreement with experiments. Quantum optical phenomena, however, are expected to be dependent on the local DOS (LDOS), i.e., the DOS in the neighborhood of the atomic system, rather than total DOS. Furthermore, according to band-structure calculations, even if a PC does not possess a complete PBG, its LDOS may exhibit pseudogaps as well as Van-Hove singularities, where the isotropic DOS is a good local approximation [15, 112]. Nevertheless, what should be always kept in mind is that the isotropic dispersion relation [Eq. (4.3)], is valid for atomic transition frequencies close to the upper band-edge and for relatively large gaps. As a consequence, it may lead to unrealistic predictions if carried beyond its range of reasonable validity. Closing, this section it is worth noting that even for an ideal waveguide, close to its fundamental frequency, the DOS has been shown to exhibit a highly peaked behavior analogous to that in Eq. (4.4) [61].

4.1.2 Anisotropic Model

Besides the isotropic model, John and Wang have proposed an anisotropic one which is still valid for frequencies close to the upper band-edge but the vectorial nature of electromagnetic waves is preserved [60]. The corresponding dispersion relation reads

$$\omega_k = \omega_e + A(\mathbf{k} - \mathbf{k}_e)^2, \tag{4.6}$$

while the DOS differs from Eq. (4.4), with the square-root factor appearing in the numerator rather than the denominator, i.e.,

$$\rho_A(\omega) \sim \sqrt{\omega - \omega_e}\Theta(\omega - \omega_e). \tag{4.7}$$

Although the anisotropic model, is closer to a real 3D PC, it is mainly the isotropic one that has been used in quantum-optics problems. Much of our discussion in the following sections, will thus be in the context of the isotropic model but differences between the two models will be discussed wherever necessary.

4.1.3 Gap with a Lorentzian Profile of the DOS

As long as both isotropic and anisotropic models are valid for frequencies around the band-edge, they do not exhibit the correct behavior for relatively large frequencies. Specifically, one would expect the DOS for both models to approach the open-space value for $\omega \gg \omega_e$. It is obvious, however, that in this limit, on the one hand the isotropic model goes to zero and on the other, the anisotropic model diverges.

The essential point therefore is that, an appropriate model of DOS for the description of a PBG continuum must exhibit a dip over a range of frequencies and also tend to the open-space DOS as the frequency becomes much larger or smaller than the mid-gap frequency. In our work, we have also adopted as a model of such a DOS an inverted Lorentzian of higher order given by the expression

$$\rho_L(\omega) = \rho_o(\omega)\left[1 - \frac{\Gamma^p}{(\omega - \omega_c)^p + \Gamma^p}\right], \tag{4.8}$$

where $\rho_o(\omega)$ is the open-space DOS (see Sec. 3.4.1) which is a smooth function of ω and thus we may set $\rho_o(\omega) = \rho_o(\omega_o) \equiv \rho_o$ where ω_o is the atomic transition frequency.

First of all, note that the DOS (4.8) approaches the open-space value ρ_o for $|\omega - \omega_c| >> \Gamma$. Second, it does not exhibit a divergence at the edge. In fact, the "edge" is not infinitely steep, but does rise more steeply, as we increase the order of the Lorentzian. It could be thus argued that this DOS does not exhibit a clear edge and possesses a zero only at one point. It should

be kept in mind, however, that in a realistic PBG material, the gap does not necessarily mean a true zero but a range of frequencies over which the DOS is several orders of magnitude smaller than that of open space. Taking p sufficiently large in Eq. (4.8), one can obtain a range of frequencies over which $\rho_L(\omega)/\rho_o$ is smaller than a desired value. For $p = 6$, for example, $\rho_L(\omega)/\rho_o \leq 10^{-6}$ for $\omega \in [\omega_c - 0.1\Gamma, \omega_c + 0.1\Gamma]$. One can further combine the inverted Lorentzian with step functions in order to simulate a true zero over a range of ω, if so desired. The shape of the DOS given by Eq. (4.8), can be viewed as a compromise between the isotropic and the anisotropic models and has been used in the literature for $p = 2$ [8, 36, 37, 68, 85].

4.2 Spontaneous Emission at the Edge of a PBG

We return once more to the excited TLA assuming now that it can somehow be placed in a material exhibiting gaps in the spectrum of the electromagnetic field it supports [6, 53, 62, 130]. Following the notation we have developed in Sec. 3.4, the Hamiltonian of the system in RWA is given by Eqs. (3.57) and (3.59). Adopting the isotropic model for the description of the PBG continuum, the corresponding spectral response is

$$\mathcal{D}_I(\omega) = \frac{C}{\pi} \frac{\Theta(\omega - \omega_e)}{\sqrt{\omega - \omega_e}}, \tag{4.9}$$

where C represents the strength of the coupling of the atomic transition to the reservoir and is given by

$$C = \frac{|\mathbf{d}_{eg}|^2 k_e^2 \omega_e}{12\pi\epsilon_0\sqrt{A}}. \tag{4.10}$$

For the anisotropic model, one would have a spectral response of the form $\mathcal{D}_A(\omega) \sim \Theta(\omega - \omega_e)\sqrt{\omega - \omega_e}$, with the corresponding coupling constant being different from that in Eq. (4.10).

Clearly, for atomic transitions around the edge ($\omega_o \sim \omega_e$), in both cases we have an unconventional spectral response and thus the Born and Markov approximations are not valid. The corresponding memory kernels reflect long-range correlations between the atomic system and the reservoir and are of the form

$$G_I(t - t') \sim \frac{1}{\sqrt{t - t'}}, \quad G_A(t - t') \sim \frac{1}{(t - t')^{3/2}}, \tag{4.11}$$

with $t > t'$ [118]. Nevertheless, as long as the problem under consideration involves a single excitation in the structured reservoir (emission of one photon), the atomic dynamics can be obtained in terms of the Laplace transforms (see Sec. 3.7) of the time-dependent coefficients of the total wavefunction expanded in terms of the relevant states [see Eq. (3.60)].

Focusing on the isotropic model for the time being, the matrix element of the resolvent operator $G(z)$ associated with the upper atomic state reads

$$G_{ee}(z) = \frac{z(z+\delta_e) - iC\sqrt{z+\delta_e}}{z^2(z+\delta_e) + C^2}, \tag{4.12}$$

where we have changed the Laplace variable z to $z + \omega_o$ and we have introduced the detuning $\delta_e = \omega_o - \omega_e$ of the atomic transition frequency ω_o from the band-edge [6]. The expression for $G_{ee}(z)$ has now three poles. If they are complex or real, will be determined by the value of the detuning δ_e. For instance, for exact resonance ($\delta_e = 0$) of the atomic transition with the edge, the three roots are $z_1 = -C^{2/3}$, $z_2 = e^{i\pi/3}C^{2/3}$, $z_3 = e^{-i\pi/3}C^{2/3}$. Since the atomic dynamics in the time domain are obtained by substitution of the poles into the inversion integral (3.93), in the long-time limit only real roots contribute. Thus, for $\delta_e = 0$, the atomic population in the excited state, in this limit is,

$$|U_{ee}(t)|^2_{t\to\infty} = \left| \frac{z_1^2 - iC\sqrt{z_1}}{(z_1 - z_2)(z_1 - z_3)} \right|^2 = \frac{4}{9}, \tag{4.13}$$

which indicates that a substantial fraction of the initial excitation (about 45%) remains trapped at the atom even at $t \to \infty$. This is in contrast with open space as well as cavities where at $t \to \infty$ the atom has completely decayed.

In Fig. 4.1, we show the atomic population as a function of time, for various detunings from the band-edge frequency, i.e, from atomic transitions well inside the gap ($\delta_e < 0$) to outside the gap ($\delta_e > 0$). As was expected, for atomic transitions well inside the gap ($\delta_e = -10C^{2/3}$), the atom remains in the excited state forever. The periodically modulated dielectric host prevents the atom from getting rid of its energy and thus a significant part of the emitted *radiation*, remains *localized at* the site of *the atom*. In contrast to cavities, such localized photonic states may extent over many wavelengths (*localization length*) around the atom [60]. The strong interaction between the atom and its own localized radiation is reflected in the oscillations in the atomic population for $\delta_e < 0$ and the formation of a *"photon + atom" bound state* in the long-time limit, which is associated with a non-zero steady-state atomic population. This bound state consists of an excited-state component, a ground-state component as well as electromagnetic field which can not propagate in the dielectric structure, while its formation has been predicted in the early '70s by Bykov [17]. For atomic transitions sufficiently outside the gap ($\delta_e = 10C^{2/3}$), the Born and Markov approximations are valid, leading thus to an exponential decay of the initially excited atom. The corresponding decay rate, however, depends on the atomic detuning from the band-edge ($\sim C/\sqrt{\delta_e}$), since the isotropic DOS does not a pproach its open-space value for $\delta_e \gg 0$.

In the language of dressed states, the coupling of the atom to the strongly modified radiation reservoir causes a strong vacuum Rabi splitting which is reflected by the vacuum Rabi oscillations in the atomic populations. One of the two components of the doublet created by the splitting is pushed inside the gap, where it is protected against dissipation, while the other is pushed outside where it decays. Depending on the magnitude and the sign of δ_e, the relative magnitude of the two components changes, which determines what fraction of the initial excitation remains trapped at the atom, in the long-time limit. Recall that in the case of an atom in a cavity, both components of the doublet decay since the DOS, although not flat, does not exhibit any gap.

For the isotropic model, the atom exhibits non-zero steady state population, even for positive detunings ($\delta_e = C^{2/3}$). It has been shown, however, that this is an artifact of the divergent isotropic DOS. For the anisotropic model, as well as the Lorentzian profile of DOS, the component of the doublet outside the gap, decays much faster and thus, even for small positive detunings (see Chap. 5), the "photon + atom" bound state will decay, while the oscillations in the atomic excitation are not so pronounced.

In contrast to the decay rate, the Lamb shift of the excited atomic state is not expected to be affected by the unconventional radiation reservoirs provided by PCs, since it is associated with virtual photons of frequencies lying in the allowed part of continuum [69]. Calculations in the context of both the isotropic and anisotropic models, however, are expected to predict strong modification of the Lamb shift (compared to its open-space value), since none of these models is valid for frequencies sufficiently away from the band-edge [60, 135].

4.3 Three-level Atoms at the Edge of a PBG

If the TLA with a transition frequency around the edge of a PBG exhibits unusual behaviour, it is to be expected with certainty that three-level models will also share this behaviour [124]. The variety of the questions that can now be asked increases, as there are different combinations to be made with the position of each transition frequency with respect to the edge.

4.3.1 Spontaneous Decay

Consider the ladder system first, with the atomic levels being denoted by $|1\rangle$, $|2\rangle$ and $|3\rangle$ as in Fig. 3.3(a) and let one of the atomic transitions be coupled to a PBG continuum, while the other is sufficiently far from the edge [5]. For the latter transition we can use the DOS for open space and proceed with the Born and Markov approximations. Considering first the case of the lower transition coupled to the edge, we have the upper state $|1\rangle$ which decays spontaneously but ends up in an intermediate state that exhibits

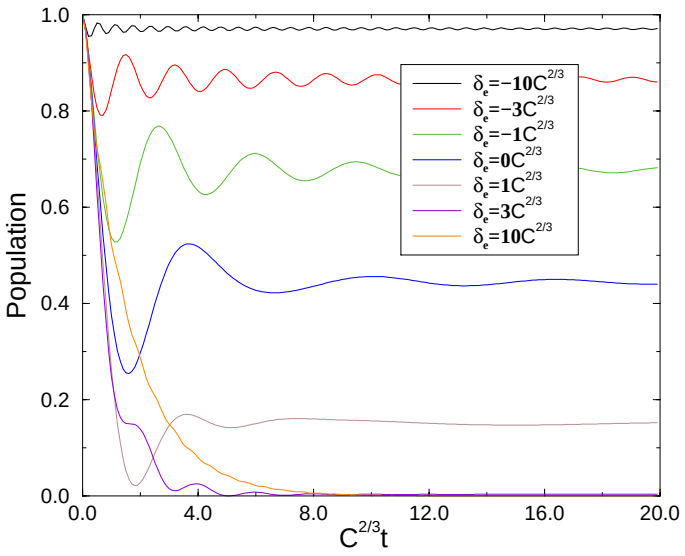

Fig. 4.1: Spontaneous decay at the edge of an isotropic PBG continuum. The population in the upper state of a two-level atom is plotted as function of the dimensionless time $C^{2/3}t$ and for various detunings (δ_e) from the band-edge frequency.

unusual behaviour in time since it is coupled to the PBG reservoir. The photon emitted in the upper transition can be observed since its frequency lies far outside the gap and its spectrum, for various values of the detuning ($\delta_{23} = \omega_{23} - \omega_e$) of the lower transition frequency from the edge, is presented in Fig. 4.2.

For δ_{23} positive and relatively large, the spectrum is Lorentzian as in open space. It is also, for all practical purposes Lorentzian, but narrower than the open-space line, for δ_{23} well inside the gap ($\delta_{23} = -10$). In analogy with the atom in a cavity, the spectrum exhibits a doublet structure for δ_{23} around the edge. The magnitude of the splitting is a measure of the strength of the coupling of the lower atomic transition to the structured reservoir.

We may also analyze the case in which the upper transition is coupled to the PBG and the lower one lies outside the gap. The expected behaviour should be identical to that of a Λ-system [Fig. 3.3(b)] initially in the upper state ($|1\rangle$), having one of its transitions inside the gap and the other outside [53]. In both cases we have the formation of a "photon + atom" bound state which, however, becomes metastable due to the fact that the other atomic transition is coupled to open space. The effect of metastability on the population of the upper state of a ladder system, is presented in Fig. 4.3. For a non-zero value of the decay rate into open space, the vacuum Rabi oscillations are damped and the atom ends up in the lower state of the transition outside the gap. Furthermore, as depicted in Fig. 4.4, the

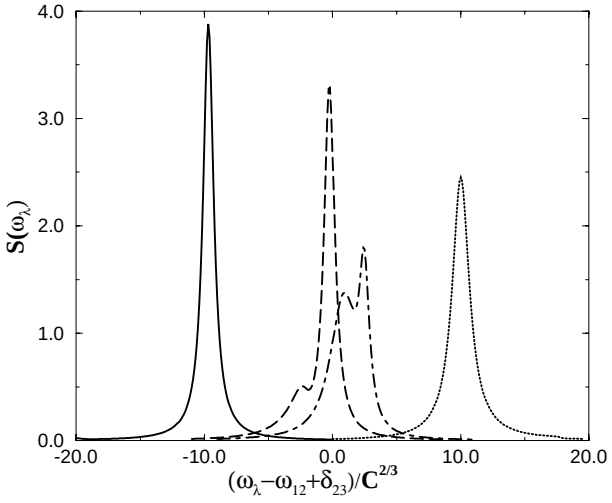

Fig. 4.2: Spectrum for the photon emitted in the upper transition of a ladder system for various detunings of the lower transition from the band-edge frequency $\delta_{23} = \omega_{23} - \omega_e$: $\delta_{23} = -10C^{2/3}$ (solid line), $\delta_{23} = -1C^{2/3}$ (dashed line), $\delta_{23} = 1C^{2/3}$ (dot-dashed line), $\delta_{23} = 10C^{2/3}$ (dotted line). The linewidth of state $|1\rangle$ is $\gamma_1 = C^{2/3}$.

spectrum of the photon emitted in the upper transition, is strongly non-Lorentzian.

Atomic systems of V configuration [Fig. 3.3(c)] have been analyzed by Zhu and co-workers [131, 134] in the context of PBG continua. They have focused on the behaviour of the de-excitation of an initial coherent superposition of the upper two atomic states, when at least one of the transitions is strongly coupled to the edge of a PBG. As in open space, their calculations predict quantum beats with enhanced amplitude due to the coherent driving of the system by the vacuum Rabi oscillations.

4.3.2 Externally Driven Three-level Atoms

Let us focus now our discussion on the Λ-system with one of the transitions, let's say $|1\rangle \rightarrow |2\rangle$, coupled to a PBG continuum. The other atomic transition is assumed to be coupled to open space and thus can be driven resonantly or near-resonantly, by an external laser field. As has been shown by Bay and co-workers [7], this problem can be solved by combining the resolvent with a QMC approach, circumventing thus the lack of a master equation. Specifically, the decay of the upper state into open space can be handled through an effective Hamiltonian (analogous to that in Sec. 3.8), which can be afterwards combined with the resolvent. Quang and co-workers

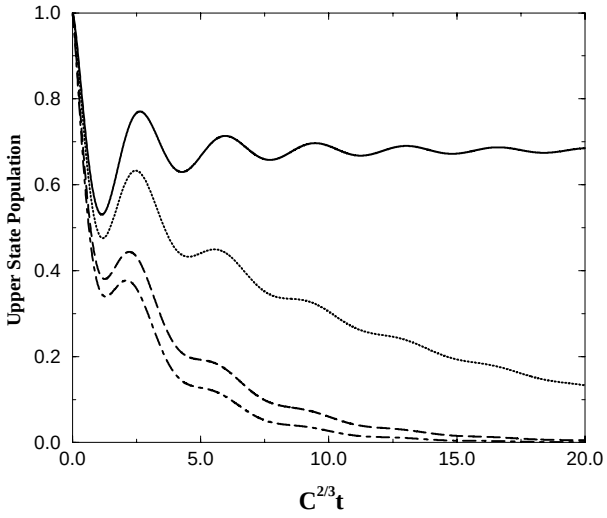

Fig. 4.3: The population in the upper state of a ladder system with the upper transition coupled near-resonantly to the edge of the gap, versus dimensionless time $C^{2/3}t$ for $\delta_{12} = \omega_{12} - \omega_e = -1C^{2/3}$ and various decay rates of the excited state $|2\rangle$: $\gamma_2 = 0$ (solid line), $\gamma_2 = 0.1C^{2/3}$ (dotted line), $\gamma_2 = 0.3C^{2/3}$ (dashed line), $\gamma_2 = 0.5C^{2/3}$, (dot-dashed line).

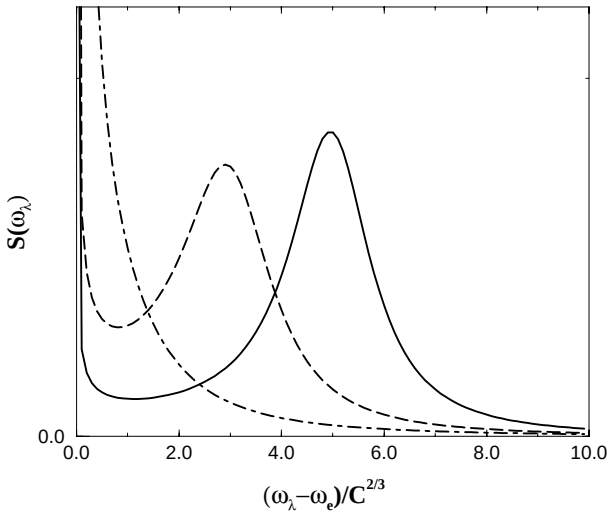

Fig. 4.4: Spectrum for the photon emitted in the upper transition of a ladder system for various detunings of its frequency from the band-edge, $\delta_{12} = \omega_{12} - \omega_e$: $\delta_{12} = 5C^{2/3}$ (solid line), $\delta_{12} = 1C^{2/3}$ (dashed line), $\delta_{12} = 0$ (dot-dashed line). The linewidth of state $|2\rangle$ is $\gamma_2 = C^{2/3}$.

have analyzed the case of a Λ-system where the driven transition lies well inside the gap [96]. For this purpose, a defect must exist in the material, associated with a mode, whose frequency falls in the gap and coincides with the atomic transition. This assumption allowed them to neglect spontaneous emission in the PBG continuum, avoiding thus an *open problem*, namely *multiple fluorescence by an externally driven TLA, at the edge of the gap* (see Sec. 4.5).

4.4 Atom–Atom Interaction

For atomic transitions well inside the gap, spontaneous emission is absent, and thus DDI is expected to be the dominant process in a collection of closely-spaced atoms [60, 63]. This is due to the fact that the phenomenon involves virtual photons with frequencies lying far outside the gap. On the contrary, for atomic transition frequencies close to the edge of a PBG, an interplay between the DDI and atom–continuum coupling is expected [6].

Let us consider for example, two identical closely-spaced atoms, one of which is initially excited and the other in its ground state. Following the notation of Sec. 3.7.1 and adopting the isotropic model of the DOS, it turns out that the matrix elements of the resolvent operator obey the following equations in matrix form [6]:

$$\begin{bmatrix} z - V_{1c}(z) & -M_{12}(z) \\ -M_{12}(z) & z - V_{2c}(z) \end{bmatrix} \begin{bmatrix} G_{aa} \\ G_{ba} \end{bmatrix} = \begin{bmatrix} 1 \\ 0 \end{bmatrix}, \tag{4.14}$$

with the relative couplings being obtained by Eqs. (3.88) and (3.89)

$$V_{jc}(z) = -\frac{iC}{\sqrt{z-\omega_e}}, \quad M_{12}(z) = V_{12} - \frac{iC_M}{\sqrt{z-\omega_e}}, \tag{4.15}$$

where $j = 1, 2$. For the two atomic dipoles parallel to each other and perpendicular to the interatomic distance we have:

$$\begin{aligned} V_{12} &= \frac{3}{2} C^{2/3} \left[\frac{cos(r_{12})}{r_{12}} - \frac{sin(r_{12})}{r_{12}^2} - \frac{sin(r_{12})}{r_{12}^3} \right], \\ C_M &= \frac{3}{2} C \left[\frac{sin(r_{12})}{r_{12}} + \frac{cos(r_{12})}{r_{12}^2} - \frac{sin(r_{12})}{r_{12}^3} \right], \end{aligned} \tag{4.16}$$

where r_{12} is now the normalized interatomic separation with respect to the wave-vector corresponding to the band-edge frequency. Note that, in the derivation of the above expressions for the couplings, no approximation has been introduced at any stage, while the shift term has been omitted, assuming that it will be incorporated in the energy of the upper states. Clearly, for atomic transitions outside the gap, i.e., $z > \omega_e$ the term involving C_M gives an imaginary part to $M_{12}(z)$ while for $z < \omega_e$, $M_{12}(z)$ is real. Thus,

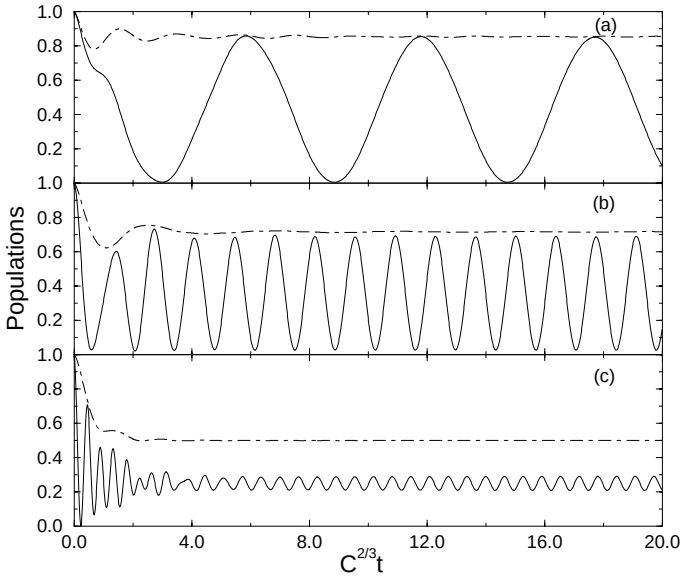

Fig. 4.5: The population in the upper state of the initially excited atom (solid line) and the total excitation in both atoms (dot-dashed line) are plotted as functions of time for $\delta_e = -3C^{2/3}$, $C_M = 0.8C$ and for various values of V_{12}: (a) $V_{12} = 1C^{2/3}$, (b) $V_{12} = 3C^{2/3}$, (c) $V_{12} = 7C^{2/3}$.

as expected, for frequencies inside the gap the atom–atom interaction is dominated by the exchange of virtual photons, whereas for frequencies outside the gap, $M_{12}(z)$ contains a dissipative part, which is different from the dissipative term involved in the coupling of each atom directly to the reservoir.

As we have discussed in Sec. 3.7.1, the eigenstates of the matrix in Eq. (4.14) are the so-called symmetric and antisymmetric product states, with the former one being unstable in open space, leading to superradiance. In the PBG reservoir, however, it can be shown that we may have population trapping even in the symmetric state (see Chap. 8). The real part V_{12} of $M_{12}(z)$, becomes dominant for small interatomic separations. Typical results, illustrating the behaviour in this regime, are shown in Figs. 4.5 and 4.6.

For atomic detunings sufficiently far inside the gap and relatively small V_{12}, there is almost complete population trapping [Fig. 4.5(a)], whereas for detunings outside the gap [Fig. 4.6(a)], the system decays completely. The population trapping in both cases can be altered by increasing the magnitude of V_{12}. This is due to the fact that the interatomic coupling V_{12} causes a splitting which, pushes one part of the atomic levels towards the gap and the other into the allowed part of the continuum. Thus, as V_{12} becomes

comparable to the atomic detuning from the edge, the partial population trapping is increased (decreased) for positive (negative) detunings. What is worth keeping in mind is that, in contrast to the situation in open space, DDI may have a stabilizing effect, even when the atomic frequency is outside the gap.

The photon hopping in a collection of N identical TLAs with transition frequency far inside the gap, has been studied by John and Quang [54]. In their studies, spontaneous emission was neglected and thus the only interaction term in their Hamiltonian was that of the DDI between neighbouring atoms. For an ordered system and for large values of N, the excited atom does not transfer any excitation to the others. On the contrary, in a disordered system only a fraction of the initial excitation (proportional to N^{-1}) can be transfered from the initially excited atom to each unexcited one, with a rate of transfer proportional to $\sqrt{N}$. The same authors have also studied the case of initially unexcited atoms which are near-resonantly coupled to a defect-mode with single excitation. They showed that transfer of energy from the defect-mode to the atoms occurs only for a disordered system. Furthermore, considering the defect-mode driven by an external laser, they analyzed phenomena such as, optical bistability, phase transitions and collective atomic steady states [54, 55, 57, 58].

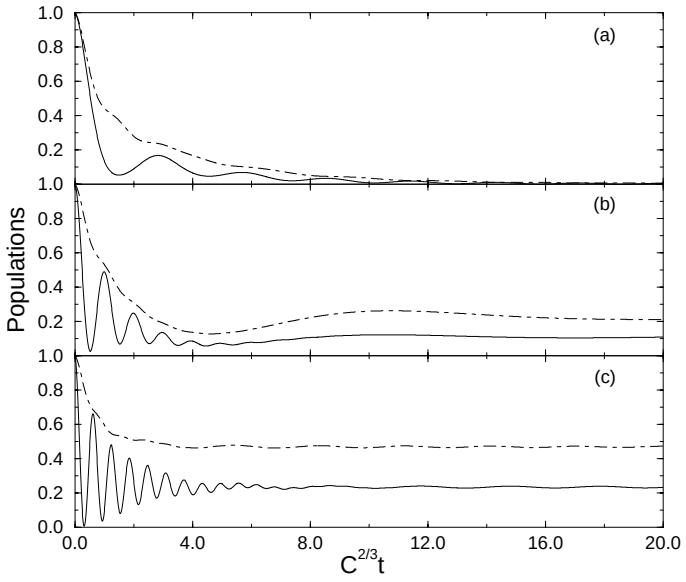

Fig. 4.6: The population in the upper state of the initally excited atom (solid line) and the total excitation in both atoms (dot-dashed line) are plotted as functions of time for $\delta_e = 3C^{2/3}$, $C_M = 0.8C$ and for various values of V_{12}: (a) $V_{12} = 1C^{2/3}$, (b) $V_{12} = 3C^{2/3}$, (c) $V_{12} = 5C^{2/3}$.

4.5 Research Question

The problems we have discussed so-far involve single excitation in the PBG continuum and as such can be handled through the direct solution of the respective time-dependent Schrödinger equation. The direct extension of this approach to situations involving more than one photon in the reservoir demands multiple integrations over photonic continua and thus does not seem tractable. On the other hand, the unconventional DOS associated with PBG structures invalidates Born and Markov approximations, essential in obtaining a master equation.

The QMC approach, as has been developed in its Markovian formulation, can not describe the localization of photons at the site of the atoms. Recall that, whenever a jump occurs it is related to a gedanken measurement of the number of photons in the radiation reservoir and after each measurement any detected photon is annihilated. In PBG materials, however, a significant part of the emitted radiation, remains localized at the site of the atom(s), leading thus to subsequent atomic re-excitation and population in higher sectors of the Hilbert space of the system (2-photon, 3-photon, etc.). Only photons with energy outside the gap can be subject of such a gedanken measurement.

Despite the lack of theoretical tools capable of providing solution to problems involving multiple excitations at the edge of a PBG continuum, many authors have addressed such problems. Specifically, resonance fluorescence has been mainly discussed in the context of a master equation applying only the Born approximation [4, 62, 67, 82, 109]. On the other hand, working in a dressed-states picture, John and Quang have addressed the same problem by means of a purely Markovian master equation [58]. The argument for such a Markovian description is the assumption that the DOS, while singular at one frequency, varies smoothly around the dressed-state resonant frequencies. The discontinuity in the DOS can thus be incorporated as strongly different decay rates of the two sidebands in the Mollow triplet.

The problem of superradiance in the context of PCs, has been addressed by John and co-workers [56, 118], using mean-field Heisenberg equations of motion for the atomic operators [see Eqs. (3.104) and (3.105)]. In open space and cavities it is well-known that, in the long-time limit, all atoms are in the ground state and thus the ensemble does not exhibit any inversion or polarization. On the contrary, at the edge of the gap the ensemble has been shown to exhibit the main features of the single atom behaviour. Specifically, the localization of the emitted radiation at the site of the atoms leads to an oscillatory behavior in both inversion and polarization, while in the long-time limit the system exhibits fractional steady-state inversion and macroscopic polarization. Additionally, for the ensemble, the radiative lifetime is shortened by $N^{2/3}$ in the isotropic model and by N^2 in the anisotropic, where N is the number of atoms. Recall that for open space the

decay rate is proportional to N and the radiated intensity, is proportional to N^2. This means that the superradiance phenomenon at the edge of the gap for the anisotropic model is much faster and more intense than in open space, while the opposite is true for the isotropic model.

All of the above approaches are approximations (reasonably good ones) to the real problem; namely the **description of non-Markovian and non-Born dynamics of an atomic system interacting with a structured radiation reservoir**. First of all, recall that both Born and Markov approximations are valid to second order in the coupling constant between atom and reservoir and consequently not applying one of them in the derivation of a master equation, is not expected to improve things significantly. On the other hand, the semiclassical approach followed by John and co-workers, is valid for the description of the superradiance in large atomic collections, after the early stage, where dipole correlations have already been established and thus the evolution of the ensemble is purely classical. This stems from the fact that the mean-field equations fail to recapture the influence of the vacuum (noise) at the early stage of the phenomenon, where the evolution is purely quantum mechanical. This aspect of the semiclassical equations is of course well known in laser theory [107, 121].

The question has been attracting increasing interest as non-Markovian (non-Born) problems keep emerging in different contexts of physics, from PBG materials to semiconductors [18, 122] and from molecules [95] to atom lasers [83, 84]. As a result, many authors have focused their efforts on the development of new techniques applicable to strongly interacting dissipative systems. Imamoglu and Garraway have proposed an extension of the well known QMC approach to the strong-coupling regime [36, 47, 113]. The memory effects associated with non-Markovian dynamics can be described by expanding the initial system using a large number of fictitious harmonic-oscillator modes (*pseudomodes*). Each pseudomode interacts with the original system as well as a flat reservoir. The dynamics of the enlarged system "atom + pseudomodes", are then purely Markovian and as such can be described by the standard techniques. Alternatively, Diosi and coworkers have derived an exact QSD equation, which may describe the time evolution of an open quantum system beyond Born and Markov approximations [25, 114, 133]. Other authors have proposed extensions of the QMC method based on the continuous measurement interpretation of the stochastic unraveling [48] or the time-convolutionless projection operator technique [13].

Although at first sight all of these approaches seem applicable to reservoirs of any DOS, up to now mathematical and computational difficulties have limited their application to relatively tractable problems involving weakly non-Markovian systems (intermediate-coupling regime) and standard Lorentzian spectral responses. In the following chapters, we develop an approach that can at least partially overcome this stumbling block. Hav-

ing introduced such an approach, we then proceed to the investigation of problems involving multiple excitations in structured radiation reservoirs, associated with PCs.

Part II

Beyond Single-Photon Localization at the Edge of a Photonic Band-Gap

Chapter 5

Discretization of Photonic Continua

The basic idea of discretization relies on the replacement of the continuum, near the atomic transition frequency, by a finite (but large) number of discrete modes. The couplings and frequencies corresponding to each of these discrete modes, are chosen so as to model the effect of the structured continuum to the desired accuracy. The judicious choice of this parameterization is of critical importance to the success of this idea. In the following sections, we formulate the discretization and we discuss its application and validity in the context of reservoirs of various DOS.

5.1 Formalism

Consider an atomic system with transitions $l = 1, 2, \ldots$ and let at least one of them, be coupled to a structured reservoir for which Born and Markov approximations are not valid. In the spirit of discretization, the near-resonant part of the continuum is replaced by a number of discrete modes. To this end, we choose an upper (ω_{up}) and a lower (ω_{low}) limit for the discretization such that $\omega_{low} < \omega_l < \omega_{up}$, where ω_l is the frequency corresponding to the atomic transition l.

Starting from the definition of the DOS for the reservoir, that is number of photonic states (ΔN) per unit frequency interval ($\Delta\omega$), we have

$$\Delta N = \rho(\omega)\Delta\omega. \tag{5.1}$$

For $\Delta N = 1$ and introducing a discrete index, we find $\Delta\omega_j = 1/\rho(\omega_j)$ and thus

$$\omega_{j+1} = \omega_j + \Delta\omega_j = \omega_j + 1/\rho(\omega_j). \tag{5.2}$$

This recurrence relation determines the frequencies of the discrete modes while an alternative form can be obtained if we choose $\rho(\omega_j)$ as $\rho(\omega_j) =$

$2(\omega_{j+1} - \omega_{j-1})^{-1}$:

$$\omega_{j+1} = \omega_{j-1} + \Delta\omega_j = \omega_{j-1} + 2/\rho(\omega_j). \tag{5.3}$$

Introducing N discrete modes in our implementation, the following relation must be satisfied

$$\int_{\omega_{low}}^{\omega_{up}} d\omega\rho(\omega) = N, \tag{5.4}$$

which determines any constants in our model and furthermore the spacing between the discrete modes.

The coupling $\mathcal{G}_j^{(l)}$ of the atomic transition l to the j discrete mode, can be chosen frequency-independent as determined by

$$\sum_{j=1}^{N} \left(\mathcal{G}_j^{(l)}\right)^2 \approx \int_{\omega_{low}}^{\omega_{up}} d\omega\mathcal{D}^{(l)}(\omega), \tag{5.5}$$

where the integral on the right hand side is over the spectral response $\mathcal{D}^{(l)}(\omega)$ of the continuum for transition l.

The discretization we have just presented is not unique. One may for example consider an alternative discretization scheme involving a number (N) of equally spaced modes, distributed between ω_{low} and ω_{up}. In this case, the mode-spacing is uniform and thus the frequency for the mode j reads

$$\omega_j = \omega_{low} + j\delta\omega, \quad \delta\omega = \frac{|\omega_{up} - \omega_{low}|}{N}. \tag{5.6}$$

The corresponding coupling of the atomic transition l, is now frequency-dependent and is determined by the spectral response of the continuum as follows,

$$\left(\mathcal{G}_j^{(l)}\right)^2 = \mathcal{D}^{(l)}(\omega_j)\delta\omega. \tag{5.7}$$

By way of comparison illustrating the philosophy of the discretization technique, note that in the latter scheme, all information about the structure of the reservoir is included in the coupling of the atom to each of the discrete modes [Eq. (5.7)], whereas the mode spacing is uniform [Eq. (5.6)]. On the contrary, in the former scheme it is the distribution of the modes that carries this information [Eqs. (5.2) and (5.3)], while the coupling constant is frequency-independent [Eq. (5.5)]. Both discretization schemes should in general work with any form of DOS. There are situations, however, where the one or the other scheme might be preferable.

5.2 Application and Validity

Having discretized the strongly-varying near-resonant part of the continuum, the system "atom + discrete modes" can be handled through differential

equations governing the evolution of the amplitudes entering the Schrödinger equation. In order to demonstrate the discretization approach and test its validity, consider the problem pertaining to the decay of an initially excited TLA coupled to a structured radiation reservoir. Replacing the DOS for frequencies around the atomic transition frequency ω_o, by N discrete modes, the Hamiltonian of the system within the RWA reads

$$\begin{aligned}\mathcal{H} &= \sum_{j=1}^{N}\Delta_j a_j^\dagger a_j + \sum_\lambda \Delta_\lambda a_\lambda^\dagger a_\lambda \\ &+ \sum_{j=1}^{N}\mathcal{G}_j(a_j\sigma^+ + a_j^\dagger\sigma^-) + \sum_\lambda g_\lambda(a_\lambda\sigma^+ + a_\lambda^\dagger\sigma^-),\end{aligned} \tag{5.8}$$

where $\Delta_{j,\lambda} = \omega_{j,\lambda} - \omega_o$, while we have dropped the index l, since we have only one atomic transition. The atomic raising and lowering operators are denoted by $\sigma^+ = |e\rangle\langle g|$ and $\sigma^- = |g\rangle\langle e|$, respectively. The corresponding wavefunction can be written as

$$|\psi(t)\rangle = a_0|e;\{0_\lambda\}\rangle + \sum_{j=1}^{N} b_j|g;1_j\rangle + \sum_\lambda b_\lambda|g;1_\lambda\rangle. \tag{5.9}$$

The label j in the Hamiltonian and the wavefunction refers to the discrete modes ($\omega_{low} < \omega_j < \omega_{up}$), while the label λ refers to the modes with frequency $\omega_\lambda > \omega_{up}$ and $\omega_\lambda < \omega_{low}$.

The time-evolution of the amplitudes is governed by the Schrödinger equation from which we obtain

$$\dot{a}_0 = \frac{1}{i}\sum_{j=1}^{N}\mathcal{G}_j b_j + \frac{1}{i}\sum_\lambda g_\lambda b_\lambda, \tag{5.10}$$

$$\dot{b}_j = \frac{1}{i}\Delta_j b_j + \frac{1}{i}\mathcal{G}_j a_0, \tag{5.11}$$

$$\dot{b}_\lambda = \frac{1}{i}\Delta_\lambda b_\lambda + \frac{1}{i}g_\lambda a_0. \tag{5.12}$$

Formal integration of Eq. (5.12) gives

$$b_\lambda(t) - b_\lambda(t_0)e^{\Delta_\lambda(t-t_0)/i} = \frac{g_\lambda}{i}\int_{t_0}^{t} dt' a_0(t')e^{\Delta_\lambda(t-t')/i}. \tag{5.13}$$

The modes λ are far off-resonant ($\Delta_\lambda \gg g_\lambda$) and as such can be treated perturbatively, i.e., they can be eliminated adiabatically. Furthermore, $a_0(t')$ remains almost constant for short times and thus can be replaced by $a_0(t)$ in Eq. (5.13). The remaining integral over the exponential is easily performed with the result

$$b_\lambda(t) \simeq -\frac{g_\lambda}{\Delta_\lambda}a_0(t). \tag{5.14}$$

Substituting Eq. (5.14) into Eq. (5.10) we have

$$\dot{a}_0 = \frac{1}{i}\sum_{j=1}^{N}\mathcal{G}_j b_j - \sum_{\lambda}\frac{g_\lambda^2}{i\Delta_\lambda}a_0, \tag{5.15}$$

$$\dot{b}_j = \frac{1}{i}\Delta_j b_j + \frac{1}{i}\mathcal{G}_j a_0. \tag{5.16}$$

The effect of the off-resonant part of the modes is thus to add a vacuum shift term to the equation of motion for the upper state amplitude. This approximation leads to a significantly reduced number of differential equations and the remaining amplitudes are distributed over a much narrower frequency interval.

Converting the mode sum over λ into an integral for $\omega > \omega_{up}$ and $\omega < \omega_{low}$ and using the spectral response of the photonic continuum under consideration, we obtain

$$\dot{a}_0 = -\frac{S}{i}a_0 + \frac{1}{i}\sum_{j=1}^{N}\mathcal{G}_j b_j, \tag{5.17}$$

$$\dot{b}_j = \frac{1}{i}\Delta_j b_j + \frac{1}{i}\mathcal{G}_j a_0, \tag{5.18}$$

where the shift term is given by

$$S = \int_{-\infty}^{\omega_{low}} d\omega \frac{\mathcal{D}(\omega)}{\omega - \omega_o} + \int_{\omega_{up}}^{\infty} d\omega \frac{\mathcal{D}(\omega)}{\omega - \omega_o}. \tag{5.19}$$

In the context of discretization, we may thus define the following effective Hamiltonian for the system, which reproduces Eqs. (5.17) and (5.18), in the basis formed by $|e;\{0_j\}\rangle$ and $|g;1_j\rangle$:

$$\mathcal{H} = -S\sigma^+\sigma^- + \sum_{j=1}^{N}\Delta_j a_j^\dagger a_j + \sum_{j=1}^{N}\mathcal{G}_j(a_j\sigma^+ + a_j^\dagger\sigma^-). \tag{5.20}$$

In order to proceed further, we need to consider a particular form of spectral response. Let us for example start with a standard cavity reservoir, where the corresponding spectral response is Lorentzian as determined by Eq. (3.70). Taking full advantage of the symmetry of $\mathcal{D}_c(\omega)$ one may choose ω_{up} and ω_{low} symmetrically placed around ω_c, which yields a vanishing shift term. Any of the two discretization schemes can be followed. In Fig. 5.1, for instance, we compare the exact known solution (solid line) with that obtained by a uniform discretization. Clearly, the discretization converges relatively fast and a good agreement with the exact solution can be obtained by using a small number of modes. This is definitely not the case for all radiation reservoirs. In the following sections, we discuss the discretization technique in the context of PBG continua which have been shown to be associated with more complicated DOS.

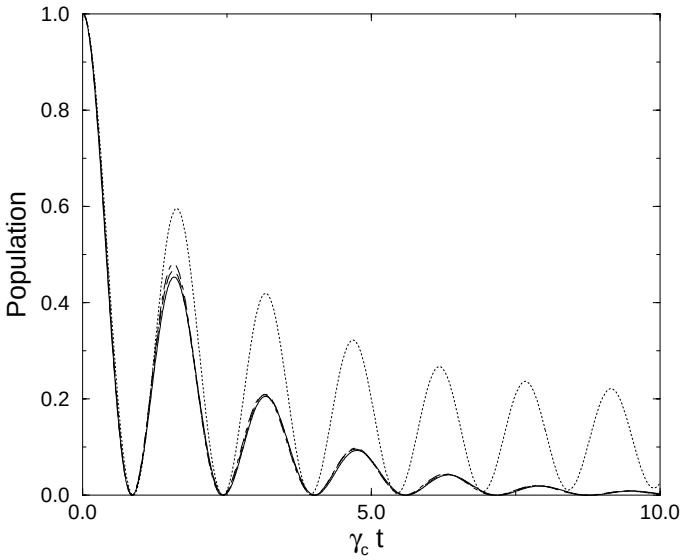

Fig. 5.1: The population in the upper state of a two-level atom coupled to a cavity reservoir, is plotted as function of the dimensionless time $\gamma_c t$. The solid line is the solutions obtained using pseudomodes for $\omega_o = \omega_c$ and $\gamma_a = 4\gamma_c$. The corresponding discretization solutions are: (a) dotted line: $N = 20$ and $\omega_{up} = -\omega_{low} = 2\gamma_c$; (b) dot-dashed line: $N = 20$ and $\omega_{up} = -\omega_{low} = 3.5\gamma_c$; (c) dashed line: $N = 30$ and $\omega_{up} = -\omega_{low} = 4\gamma_c$.

5.2.1 Isotropic Model

Let us adopt the singular isotropic DOS, [Eq. (4.4)] and the corresponding spectral response (4.9). Applying the first discretization scheme we presented in the previous section, we replace the density of modes in the vicinity of the edge-frequency, by a collection of discrete harmonic oscillators. Apparently, for the DOS under consideration, $\omega_{low} = \omega_e$, since for $\omega < \omega_e$ DOS is zero, as dictated by the Heaviside function on the right hand side of Eq. (4.4).

The frequencies of the modes can be obtained by Eq. (5.3), which now can be simplified to

$$\omega_j = \omega_e + j^2 \delta\omega, \tag{5.21}$$

where $\delta\omega$ is determined by the upper-limit condition,

$$\omega_{up} = \omega_e + N^2 \delta\omega. \tag{5.22}$$

The atomic coupling to each of the discrete modes is given by

$$\sum_{j=1}^{N} \mathcal{G}_j^2 \approx \frac{C}{\pi} \int_{\omega_e}^{\omega_{up}} d\omega \frac{1}{\sqrt{\omega - \omega_e}}, \tag{5.23}$$

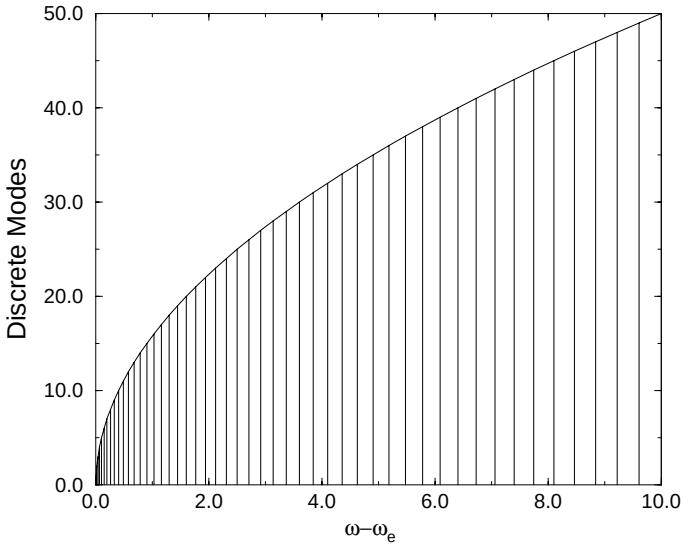

Fig. 5.2: The discrete modes in relation to the simulated number of states.

with C being the effective coupling of the atom to the PBG structure [see Eq. (4.10)], and since $\mathcal{G}_j$ is the same for all discrete modes, we have

$$\mathcal{G}_j \equiv \mathcal{G} \approx \sqrt{\frac{2C}{N\pi}\sqrt{\omega_{up}-\omega_e}}. \tag{5.24}$$

Using Eq. (5.22), the coupling constant may be further simplified to

$$\mathcal{G} \approx \sqrt{\frac{2C}{\pi}\sqrt{\delta\omega}}. \tag{5.25}$$

In Fig. 5.2, we show the discrete modes, in relation to the simulated number of states ($\sim \sqrt{\omega-\omega_e}$). As one would expect, for the DOS given by Eq. (4.4) the distribution of the discrete modes becomes more dense for frequencies close to the edge, as determined by Eq. (5.21). The equations of motion for the amplitudes corresponding to the excited atomic state and the discrete modes are given by Eqs. (5.17) and (5.18), and after evaluating the shift through Eq. (5.19), we obtain

$$\dot{a}_0 = \frac{1}{i}\left(\delta_e - \frac{\mathcal{G}^2 N}{\omega_{up}-\omega_e}\right) a_0 + \frac{1}{i}\sum_{j=1}^{N}\mathcal{G}_j b_j, \tag{5.26}$$

$$\dot{b}_j = \frac{1}{i}\delta_j b_j + \frac{1}{i}\mathcal{G}_j a_0, \tag{5.27}$$

where for later convenience we have transformed to an interaction picture rotating at ω_e with $\delta_e = \omega_o - \omega_e$ and $\delta_j = \omega_j - \omega_e$ while $\mathcal{G}_j = \mathcal{G}$ as is given by

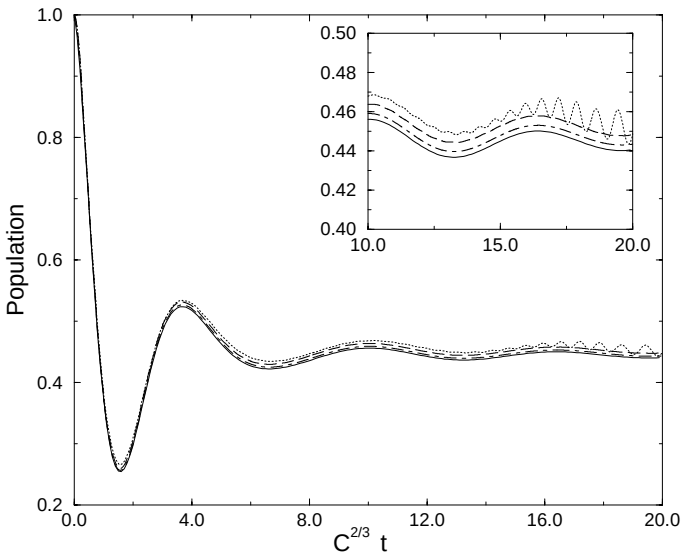

Fig. 5.3: The population in the upper state of a two-level atom is plotted as function of the dimensionless time $C^{2/3}t$. The solid line is the exact solution for $\delta_e = 0$. The corresponding discretization solutions are: (a) dotted line: $N = 50$ and $\omega_{up} = 10C^{2/3}$; (b) dashed line: $N = 150$ and $\omega_{up} = 10C^{2/3}$; (c) dot-dashed line: $N = 500$ and $\omega_{up} = 111C^{2/3}$. The insert shows a close-up of the long-time behavior.

Eq. (5.25). Note that, due to the far off-resonant modes, the upper atomic level, is shifted towards the gap where it is protected against dissipation.

In Fig. 5.3, we present the results obtained by propagation of Eqs. (5.26) and (5.27) for various discretization parameters. For comparison, we also plot the exact known solution (see Sec. 4.2). The calculation involving not sufficiently dense discretization (dotted line), exhibits revivals for longer times. These revivals are artificial without any physical meaning and stem from the discretization of the continuum. As the discretization becomes more dense, the revivals appear at later and later times (dashed and dot-dashed line). We may thus argue that, the number of modes in our calculation determines the time-scale on which the propagation is free of revivals, while $|\omega_{up} - \omega_{low}|$ determines the proximity of the envelope to the correct result. This implies considerable flexibility in the method; in the sense that the size of the calculation can be tailored to the time scale, over which the behavior of the system is sought and the desired accuracy. For instance, as one would expect, for atomic detunings far inside the gap, the discretization calculation converges much faster, since in this case only for modes with frequencies close to the edge the atom−field interaction is strong. Thus, a narrower part of the continuum near ω_e needs to be dis-

cretized. Furthermore, it is worth noting that ω_{up} and ω_{low} determine the allowed atomic transition frequencies. For example, for the case under consideration, a calculation for $\delta_e > \omega_{up} - \omega_e$ would be meaningless leading to unphysical results, since the corresponding part of the continuum has been eliminated.

5.2.2 PBG with Lorentzian Profile of DOS

One of the strengths of the discretization technique is that it can be implemented with essentially any DOS. In fact, the expression of the DOS we adopt as a model for the description of a continuum, is of great importance to the choice of the manner of discretization, which should be adapted to the demands of the particular form. For the models we discussed in the previous sections, both discretization schemes are valid. There are situations, however, where mathematical difficulties prevent us from following the one or the other scheme. To become more specific, let us consider a PBG with a Lorentzian profile of DOS and with spectral response given by

$$\mathcal{D}_L(\omega) = \frac{\gamma_a}{2\pi}\left[1 - \frac{\Gamma^p}{(\omega-\omega_c)^p + \Gamma^p}\right], \tag{5.28}$$

where γ_a is the open-space decay rate of the excited atomic state [Eq. (3.65)].

Before proceeding to the discretization of this particular form of continuum, it should be noted that the analyticity of Lorentzian profiles [see Eq. (3.70)] and the lack of any branch cuts, make them amenable to the approach of the pseudomodes. These pseudomodes are intimately connected to the poles of the DOS in the lower half plane and as we have discussed in Sec. 4.5 their decay may lead to a Markovian master equation. Such master equations have been derived only for DOS involving up to two pseudomodes, in the context of the decay of a TLA [37]. For higher order Lorentzians or other non-normalizable DOS [see Eq. (5.28)], however, such a derivation seems to be cumbersome if not impossible. In this case, a pathological Schrödinger equation may describe correctly only the dynamics of the upper state of the atomic system. As a result, if the atomic system involves more than two states, the method fails to describe the atomic dynamics correctly.

The existence of the Heaviside step function on the right-hand side of Eqs. (4.4) and (4.5), ensures a full gap for frequencies $\omega < \omega_e$ and a clear edge at $\omega = \omega_e$. As a consequence, only part of the continuum ($\omega > \omega_e$) needs to be discretized. On the contrary, for the Lorentzian profile (5.28) the situation is substantially different. Specifically, the DOS is zero only for $\omega = \omega_c$, while there is a range of frequencies around ω_c over which $\mathcal{D}_L(\omega)\gamma_a^{-1} \ll 1$. Thus, we have to discretize the continuum, even for frequencies around the mid-gap frequency ω_c. Any attempt at applying the discretization approach given by Eqs. (5.2) and (5.3) will lead to serious computational problems as the factor $1/\rho_L(\omega_j)$ diverges for $\omega_j \to \omega_c$. On

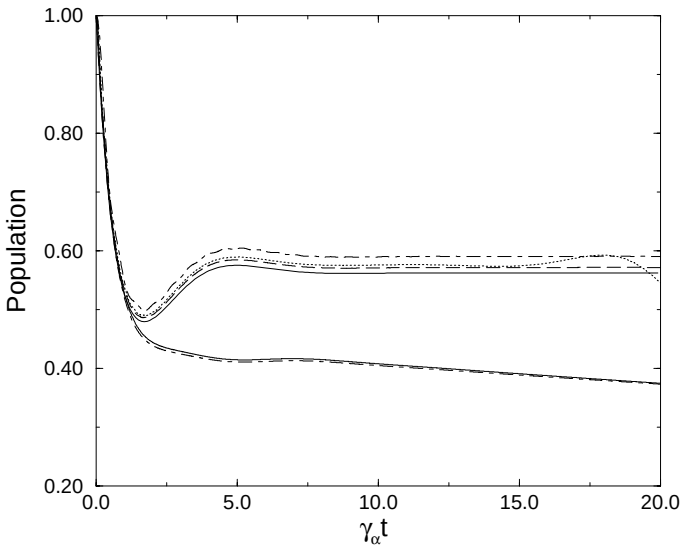

Fig. 5.4: The population in the upper state of a two-level atom is plotted as function of the dimensionless time $\gamma_a t$. The solid lines are the solutions obtained using pseudomodes for $\delta_c = 0$ (thick line) and $\delta_c = \frac{2}{3}\gamma_a$ (thin line), respectively. The corresponding discretization solutions are: (a) dot-dashed line: $N = 100$ and $\omega_{up} = -\omega_{low} = 10\gamma_a$; (b) dotted line: $N = 150$ and $\omega_{up} = -\omega_{low} = 20\gamma_a$; (c) dashed line: $N = 300$ and $\omega_{up} = -\omega_{low} = 30\gamma_a$. Parameters: $\Gamma = \gamma_a$, $p = 6$.

the other hand, the discretization given by Eqs. (5.6) and (5.7) seems to be appropriate for the model under consideration.

Choosing an upper (ω_{up}) and a lower (ω_{low}) frequency, we substitute the DOS by N equidistant discrete modes, symmetrically placed around ω_c. The coupling of the atom to each of these modes is given by

$$\mathcal{G}(\omega_j) = \sqrt{\frac{\gamma_a}{2\pi}\left[1 - \frac{\Gamma^p}{(\omega_j - \omega_c)^p + \Gamma^p}\right]\delta\omega}, \tag{5.29}$$

where $\delta\omega = |\omega_{up} - \omega_{low}|N^{-1}$. For the sake of simplicity, let us define all detunings with respect to the central frequency ω_c. The part of the continuum involving frequencies for $\omega < \omega_{low}$ and $\omega > \omega_{up}$ can be treated perturbatively as before, but, only the Lorentzian part of Eq. (5.28) contributes. In Fig. 5.4, we present results pertaining to a sixth order Lorentzian profile ($p = 6$), for two different atomic detunings from the mid-gap frequency ($\delta_c = \omega_o - \omega_c$). We also plot the solutions obtained using the pseudomode approach and we find a very good agreement for sufficiently dense discretization.

A further issue needs to be brought up here, in connection with the time scale of the persistence of any "photon + atom" bound state. As long as the model for the DOS involves an exact zero over some frequency range,

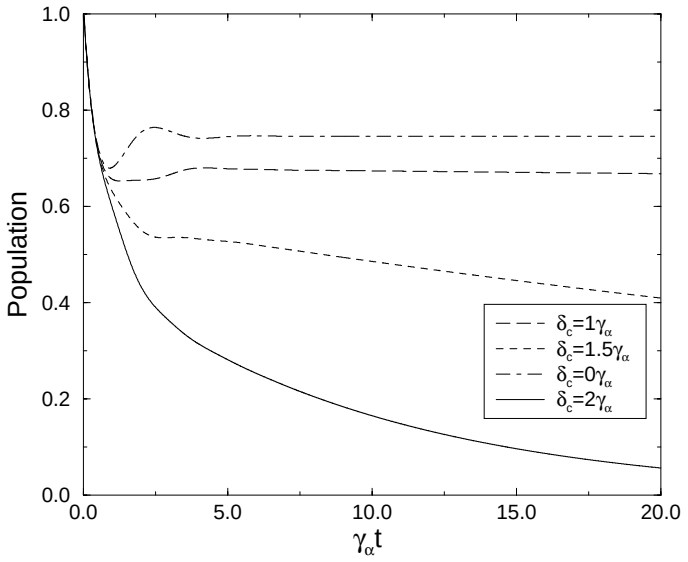

Fig. 5.5: The population in the upper state of a two-level atom is plotted as function of the dimensionless time $\gamma_a t$, for various detunings of the atomic transition from the mid-gap frequency. Parameters: $p = 8$, $\Gamma = 2\gamma_a$. Discretization parameters: $N = 1000$ and $\omega_{up} = -\omega_{low} = 100\gamma_a$.

the "photon + atom" bound state may live for ever, which mathematically implies a non-zero fractional population trapping in the limit $t \to \infty$. In reality, however, the DOS, more often than not, will not involve an exact zero but a deep minimum, as already mentioned in the beginning of this section. As a result, the life-time of the "photon + atom" bound state, is determined by the local DOS in the vicinity of the atomic transition frequency, and it may be long on some time scale but not necessarily for $t \to \infty$ in the mathematical sense. For instance, it is this finiteness of the lifetime of the "photon + atom" bound state that would cause the atomic population for $\delta_c = \frac{2}{3}\gamma_a$, in Fig. 5.4 to decay to zero, if the calculation were extended to sufficiently long times. This behavior is even more clear in Fig. 5.5, where the atomic population is plotted for various detunings from the mid-gap frequency.

In Fig. 5.6(a) we plot the excited-state population of a TLA, resonant with the mid-gap frequency of a Lorentzian DOS, for various widths of the gap. Note that, in analogy to CQED (see discussion in Sec. 3.4.2), for short times the atom decays as if it were in open space, regardless of the value of the ratio γ_a/Γ. This behavior is even more clear in the logarithmic plot of the excited-state population in Fig. 5.6(b). We may thus say that at the beginning the atom emits without feeling the modal density. The initially emitted wave-packet propagates in the crystal and is eventually Bragg-reflected back

to the atom, carrying the information about the periodic structure of the environment. In fact, the part of the population which is lost in the long-time limit is determined by the ratio γ_a/Γ. This can be understood by viewing the atomic resonance as a Lorentzian of width γ_a, centered around ω_o. The part of the wings of this Lorentzian spectrum that lies in the allowed part of the continuum will be emitted. Accordingly, as is depicted in Fig. 5.6(a), the population trapping in the long-time limit increases, as we increase the width of the gap in relation to the atomic linewidth.

The discretization approach has given us the opportunity to study the problem of spontaneous emission in the context of various DOS, in a fast and really effective way. Although some of these models are nothing more than mathematical imitation of a real PBG continuum, we have been able to draw some general conclusions about the parameters that affect the atomic dynamics significantly, for atomic transitions inside the gap or close to the edge. We have already discussed the life-time of the "photon + atom" bound state and the atomic behavior for short times. We additionally, may argue with certainty that *the dynamics of an atom coupled to a PBG continuum depend mainly on the width of the gap and on the "band-edge behavior" of the continuum.* On the contrary, they *slightly depend on* the particular *profile of the DOS* model we adopt. Finally, DOS models that do not exhibit any peak close to the edge seem to be more effective in trapping the light, since the vacuum Rabi splitting is relatively small and thus any phenomena associated with it (such as losses through the component of the doublet lying outside the gap, vacuum Rabi oscillations, etc) are suppressed.

5.2.3 Anisotropic Model

The discretization approach in the context of the anisotropic model presents a difficulty, in the sense that the corresponding DOS increases as we move away from the edge. As a result, the atomic coupling to far off-resonant modes is significant and accordingly the discretization approach is rather sensitive to the choice of the upper limit. One can, however, circumvent this difficulty by introducing the following DOS

$$\rho(\omega) = \rho_o \frac{\sqrt{\omega - \omega_e}}{\sqrt{\omega - \omega_e} + 1}, \tag{5.30}$$

which does approach the open-space value ρ_o for $\omega \gg \omega_e$, whereas it has the anisotropic behavior for frequencies close to the edge. Even in this case, however, the convergence of the discretization is relatively slow.

5.3 Summary

We have developed the discretization technique, which is applicable to photonic reservoirs of any DOS. Having tested the validity of the method, in

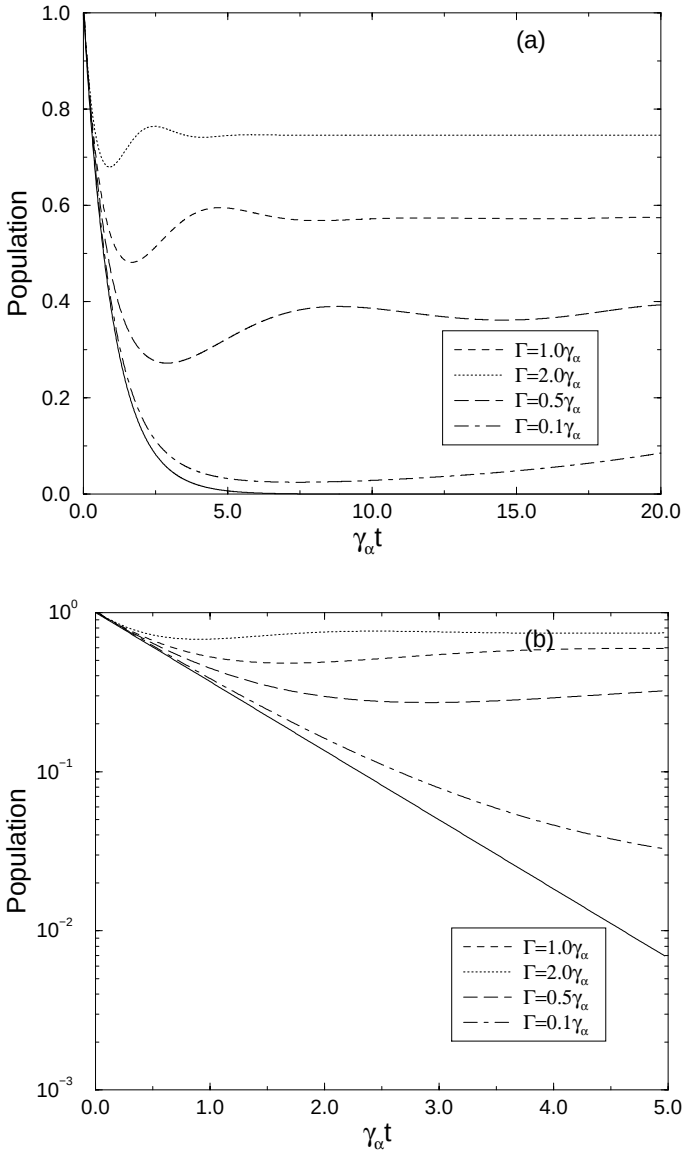

Fig. 5.6: (a) The population in the upper state of a two-level atom is plotted as function of the dimensionless time $\gamma_a t$ for $\delta_c = 0$, $p = 8$ and various widths of the Lorentzian gap. (b) The logarithmic plot of the population. The solid line corresponds to the open-space behavior. Discretization parameters: $N = 500$ and $\omega_{up} = -\omega_{low} = 50\gamma_a$.

contexts amenable to exact solutions, we may proceed to address problems involving more than one photon in structured radiation reservoirs. In the following chapters we focus on continua associated with PBG materials. As we show, the discretization approach is capable of providing solutions to a class of problems which can only be treated approximately through other techniques. What should be always kept in mind, however, is the danger of artificial oscillations and thus the convergence of our results has to be tested in terms of all discretization parameters.

Chapter 6

Cascade of Two Photons at the Edge of a PBG

In this chapter, we have chosen to present results on a ladder atomic system which in open space involves a cascade of two photon-emissions (see Sec. 3.6). As we show in the following sections, allowing both atomic transitions to be strongly coupled to a PBG reservoir we obtain what should be called *"two-photon + atom" bound state* [87]. The formation of such a state is then found to be associated with a *counterintuitive coherent evolution* of the three atomic states. Although the problem is mainly discussed in the context of the isotropic model we do, examine the persistence of our predictions in the context of a Lorentzian profile of DOS.

6.1 The System

Consider a three level atom in a cascade (Ξ) configuration, with atomic levels $|1\rangle, |2\rangle, |3\rangle$ and energies $\omega_1, \omega_2, 0$ respectively, where $(\omega_1 > \omega_2)$ [Fig. 6.1(a)]. Both atomic transitions ($l = 1, 2$) are considered to be coupled near-resonantly to the edge of a PBG and are thus strongly modified.

Neglecting the zero-point energies of the field modes and adopting the RWA, the Hamiltonian of the system in the interaction picture is written as

$$\mathcal{V} = i\sum_{\mu} g_{\mu}^{(1)}(a_{\mu}^{\dagger}\sigma_{21}e^{-i\delta_{\mu}^{1}t} - a_{\mu}\sigma_{12}e^{i\delta_{\mu}^{1}t}) + i\sum_{\lambda} g_{\lambda}^{(2)}(a_{\lambda}^{\dagger}\sigma_{32}e^{-i\delta_{\lambda}^{2}t} - a_{\lambda}\sigma_{23}e^{i\delta_{\lambda}^{2}t}), \tag{6.1}$$

where σ_{kn} denote the atomic dyadic operators with $k, n \in \{1, 2, 3\}$; $\delta_{\mu}^{1} = (\omega_1 - \omega_2) - \omega_{\mu}$, $\delta_{\lambda}^{2} = (\omega_2 - \omega_3) - \omega_{\lambda}$, while $a_{\mu}, a_{\mu}^{\dagger}(a_{\lambda}, a_{\lambda}^{\dagger})$ are the creation and annihilation operators of the structured continuum, which is coupled to the atomic transitions, via the respective coupling constants $g_{\mu}^{(1)}, g_{\lambda}^{(2)}$.

Let us denote by $|3; 1_{\lambda}, 1_{\mu}\rangle$, a state of the combined system (atom+field), where the atom is in state $|3\rangle$ and two photons have been emitted into the structured reservoir, populating the modes λ and μ respectively. Following

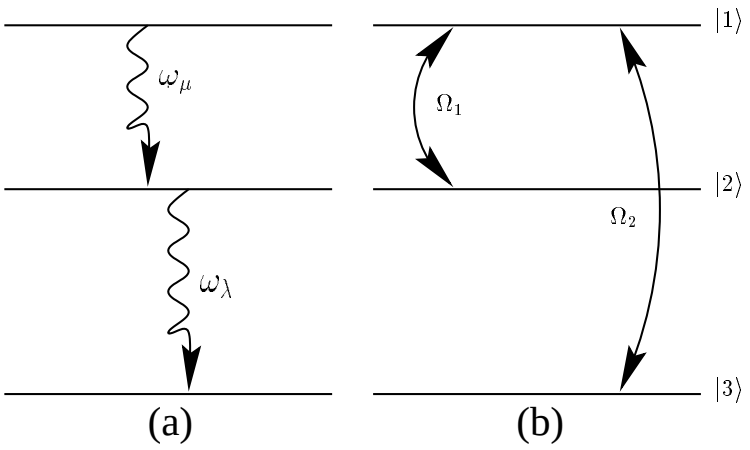

Fig. 6.1: (a) Schematic representation of the atomic system and the possible transitions. (b) The upper state simultaneously coupled to the intermediate state and the ground state via a single- and two-photon process respectively.

this pattern of notation, and discretizing the near resonant part of continuum ($\omega_{low} < \omega_l < \omega_{up}$), the wavefunction of the complete system reads

$$|\psi(t)\rangle = a|1;0\rangle + \sum_j b_j|2;1_j\rangle + \sum_{\substack{j,m \\ (j\geq m)}} C_{jm}|3;1_j,1_m\rangle + \sum_\mu b_\mu|2;1_\mu\rangle + \sum_{\substack{\lambda,\mu \\ (\lambda\geq\mu)}} C_{\lambda\mu}|3;1_\lambda,1_\mu\rangle. \tag{6.2}$$

where j, m are indices over all discrete modes while λ, μ correspond to modes with frequency $\omega_{\lambda,\mu} > \omega_{up}$ and $\omega_{\lambda,\mu} < \omega_{low}$. Furthermore, due to the fact that $|1_\lambda, 1_\mu\rangle \equiv |1_\mu, 1_\lambda\rangle$, we have $C_{\lambda\mu} = C_{\mu\lambda}$.

The time dependence of the amplitudes entering the wavefunction, is governed by the Schrödinger equation and after eliminating the off-resonant modes (see Sec. 5.2), we find

$$\dot{a} = -iS^{(1)}a - \sum_{j=1}^{N} \mathcal{G}_j^{(1)} b_j e^{i\delta_j^1 t}, \tag{6.3}$$

$$\dot{b_j} = -iS^{(2)}b_j - \sum_{\substack{m=1 \\ (m\neq j)}}^{N} \mathcal{G}_m^{(2)} C_{jm} e^{i\delta_m^2 t} - \sqrt{2}\mathcal{G}_j^{(2)} C_{jj} e^{i\delta_j^2 t} + \mathcal{G}_j^{(1)} a e^{-i\delta_j^1 t}, \tag{6.4}$$

$$\dot{C}_{jm} = \mathcal{G}_m^{(2)} b_j e^{-i\delta_m^2 t} + \mathcal{G}_j^{(2)} b_m e^{-i\delta_j^2 t}, \tag{6.5}$$

$$\dot{C}_{jj} = \sqrt{2}\mathcal{G}_j^{(2)} b_j e^{-i\delta_j^2 t}, \tag{6.6}$$

where by $\mathcal{G}_k^{(l)}$ we denote the coupling of the atomic transition l to the k discrete mode. The shift terms in the equations of motion for the two upper levels are given

$$S^{(l)} = \int_{-\infty}^{\omega_{low}} d\omega \frac{\mathcal{D}^{(l)}(\omega)}{\omega_l - \omega} + \int_{\omega_{up}}^{\infty} d\omega \frac{\mathcal{D}^{(l)}(\omega)}{\omega_l - \omega}. \tag{6.7}$$

6.2 Time-Evolution of the System

Isotropic Model: Adopting the isotropic model for the description of the PBG continuum, the spectral response for transition l, is given by

$$\mathcal{D}_I^{(l)}(\omega) = \frac{C_l}{\pi} \frac{\Theta(\omega - \omega_e)}{\sqrt{\omega - \omega_e}}, \tag{6.8}$$

where C_l is the effective coupling to the structured continuum.

Following the discretization approach we have developed in the previous chapter, the continuum for $\omega \leq \omega_e + 10C_1^{2/3}$, is replaced by 150 discrete modes. The frequency of the j discrete mode, is then obtained through Eq. (5.21) with $\delta\omega$ being chosen sufficiently small ($\delta\omega \approx 4.4 \times 10^{-4} C_1^{2/3}$), while the corresponding coupling $\mathcal{G}_j^{(l)}$ for transition l is frequency-independent and is given by

$$\mathcal{G}_j^{(l)} \equiv \mathcal{G}^{(l)} \approx \sqrt{\frac{2C_l}{\pi}\sqrt{\delta\omega}}. \tag{6.9}$$

In general, the dipole moments $\langle 1|\mathbf{d}|2\rangle$ and $\langle 2|\mathbf{d}|3\rangle$ are different and thus for the rest of this chapter we let the couplings C_1 and C_2 be different.

The set of Eqs. (6.3) – (6.6) is solved numerically and the results are presented in Figs. 6.2 – 6.6. We plot the population in the upper level (solid line), the intermediate level (dashed line) and the lower level (dot-dashed line), for various detunings of the upper ($\delta_{12} = \omega_1 - \omega_2 - \omega_e$) and lower ($\delta_{23} = \omega_2 - \omega_3 - \omega_e$) transitions from the band-edge frequency.

In all figures, we can identify a "transient regime", on a short time scale of the order of $C_1^{2/3}$, when part of the atomic population is lost. On a longer time scale ("dynamic regime"), the populations in the atomic levels undergo oscillations, strongly dependent on the relative detunings from the band-edge, reflecting the emission and reabsorption of the photon(s). The localization at the atom of the photon emitted in the first transition, is accompanied by emission of a photon in the lower transition, which will be also localized at the atom. In analogy with the case of one photon in a TLA, two photons are now backscattered to the atom after tunneling a characteristic distance and reexcite it.

As is known from the coupling of a TLA to the PBG reservoir, the dressing of the atom by its own localized radiation causes splitting of the atomic levels. This splitting is sufficiently strong to push one level of the

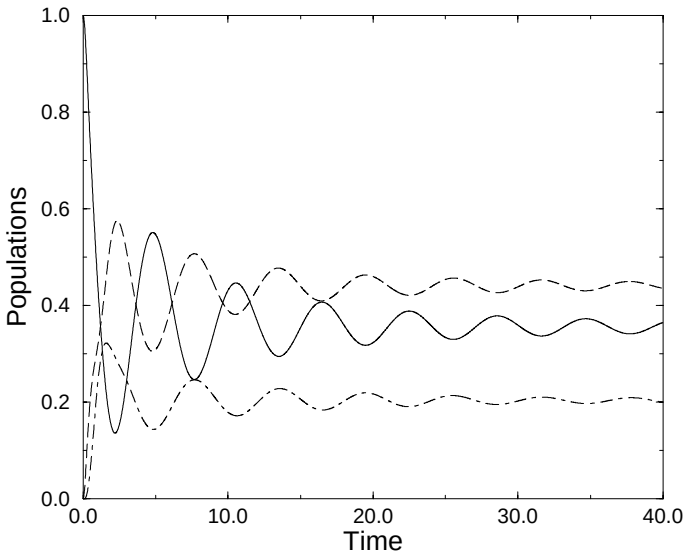

Fig. 6.2: The population in the atomic states as function of time. The solid line is for $|1\rangle$, the dashed line for $|2\rangle$ and the dot-dashed line for $|3\rangle$. Parameters: $C_2 = 1.5C_1$, $\delta_{12} = -C_2^{2/3}$ and $\delta_{23} = 0$. The time is in units of $C_1^{2/3}$.

doublets outside the gap and the other inside. The dressed state outside the gap looses all its population in the long-time limit, while the one inside the gap is protected from dissipation and thus is stable. The number of stable localized states, is intimately connected to the behavior of the system in the long-time limit. One such state gives rise to steady state population in the excited level, while two of them lead to an undamped beating of the system between the two non-decaying states [6, 62].

For our three-level atom, two transitions are at the edge, and thus more than one stable localized state can be found in the gap. In analogy to the "single-photon + atom" bound state, we have the formation of a *"two-photon + atom" bound state*, which exhibits population trapping in both excited states, in the long-time limit. Thus, the atom is finally excited, in a superposition of the upper states (Fig. 6.2). This is a novel behavior, due to the fact that both transitions and not only one, are coupled to the same structured continuum. Note that, even in the case that only the ($|2\rangle \rightarrow |3\rangle$) transition is at the edge of the gap, it is the intermediate level that exhibits non-zero steady-state population but not the upper level [5, 53].

In the language of dressed states, the oscillations in the populations of the atomic levels reflect the interference between the dressed states of the atom. We additionally note that the oscillations in the populations of the intermediate and lower level are "in phase". This is a rather surprising result, since one would expect the population in the intermediate state to

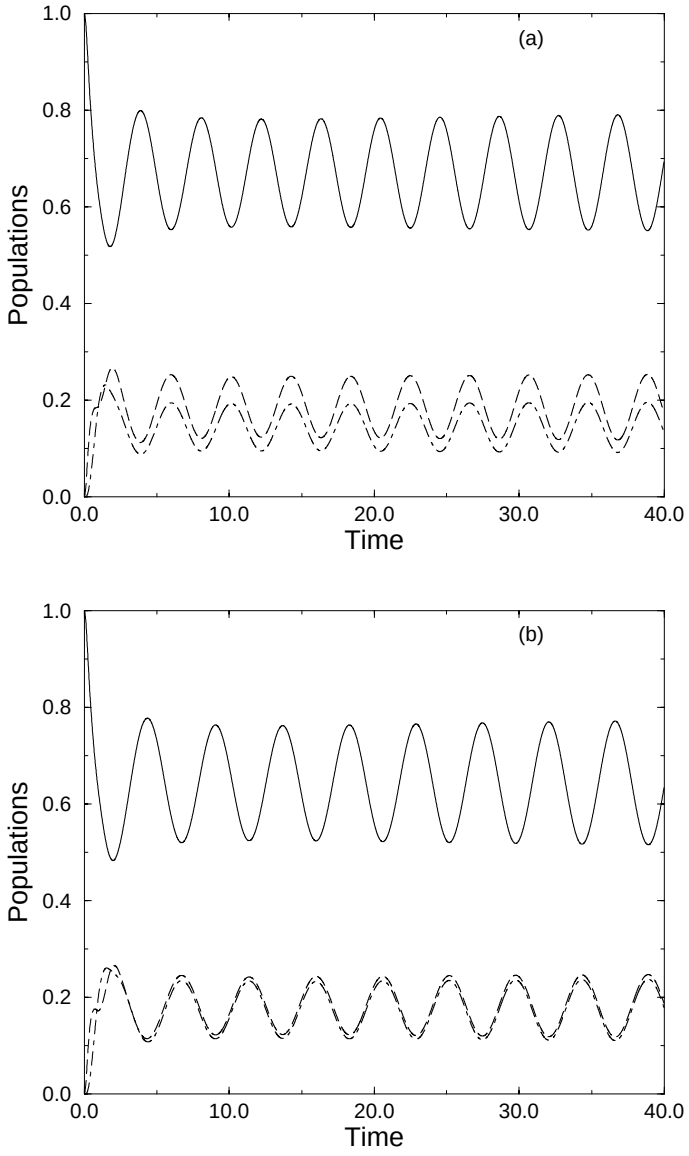

Fig. 6.3: The population in the atomic states as function of time. The solid line is for $|1\rangle$, the dashed line for $|2\rangle$ and the dot-dashed line for $|3\rangle$. Parameters: $C_2 = 1.5C_1$, (a) $\delta_{12} = -2C_2^{2/3}$ and $\delta_{23} = 1C_1^{2/3}$; (b) $\delta_{12} = -2C_2^{2/3}$ and $\delta_{23} = 1C_2^{2/3}$. The time is in units of $C_1^{2/3}$.

be maximum when the population in the lower state is minimum and vise-versa. The phenomenon is even more pronounced in Fig. 6.3. After an initial transient regime in which about 15% of the population is lost, the remaining population oscillates between the upper level and the two lower levels, in a non-dissipative way. The undamped oscillations imply the beating of the system, between more than two non-decaying dressed states.

The "in phase" oscillations, stem from the localization of both photons at the site of the atom. The system can make the transitions $|1\rangle \leftrightarrow |3\rangle$ either with a stepwise process ($|1\rangle \leftrightarrow |2\rangle \leftrightarrow |3\rangle$) or with a two-photon process ($|1\rangle \leftrightarrow |3\rangle$). Which of the two routes the system will follow to arrive at $|3\rangle$ depends on the detuning δ_{12}. Specifically, if the upper transition is outside the gap, irrespective of the detuning of the lower transition from the band-edge, it seems preferable for the system to "decay" via the stepwise process rather than the two-photon process indicated in Fig. 6.4. This is no different from the behaviour of a ladder system in open space. On the contrary, if the upper transition is inside the gap, the system evolves in time as if the upper state were coupled to the intermediate state via a single-photon process, and simultaneously to the ground state via a "direct" two-photon process, with respective frequencies Ω_1 and Ω_2. This can not be anticipated on the basis of the behaviour in open space and it is what we meant by counterintuitive in the introduction.

To gain further insight into this effect, we can adopt a simple three-level model without dissipation and assign a single-photon Rabi frequency Ω_1 between $|1\rangle$ and $|2\rangle$ and a two-photon Rabi frequency Ω_2 between $|1\rangle$ and $|3\rangle$ [Fig. 6.1(b)]. Denoting by P_n the population in state n and following an analysis of the system through standard rate equations, we obtain

$$P_1 = cos^2(\sqrt{\Omega_1^2 + \Omega_2^2}t), \tag{6.10}$$

$$P_2 = \frac{\Omega_1^2}{\Omega_1^2 + \Omega_2^2} sin^2(\sqrt{\Omega_1^2 + \Omega_2^2}t), \tag{6.11}$$

$$P_3 = \frac{\Omega_2^2}{\Omega_1^2 + \Omega_2^2} sin^2(\sqrt{\Omega_1^2 + \Omega_2^2}t). \tag{6.12}$$

Thus the populations of the atomic levels oscillate with the same frequency $\Omega = \sqrt{\Omega_1^2 + \Omega_2^2}$, with the oscillation of the two lower levels being in phase. Furthermore, the ratio of the amplitude of the oscillation of the intermediate level to that of the lower level is related to the ratio of the Rabi frequencies, i.e., Ω_1/Ω_2. In Fig. 6.3(b), representing the result of the numerical calculation for the system in the PBG reservoir, we note that the dashed and the dot-dashed lines, corresponding to the populations in the intermediate and ground levels, respectively, are indistinguishable. This implies that the corresponding effective Rabi frequencies Ω_1 and Ω_2 are practically equal. It is the combination of the coupling constants and detunings that conspire to produce that behaviour.

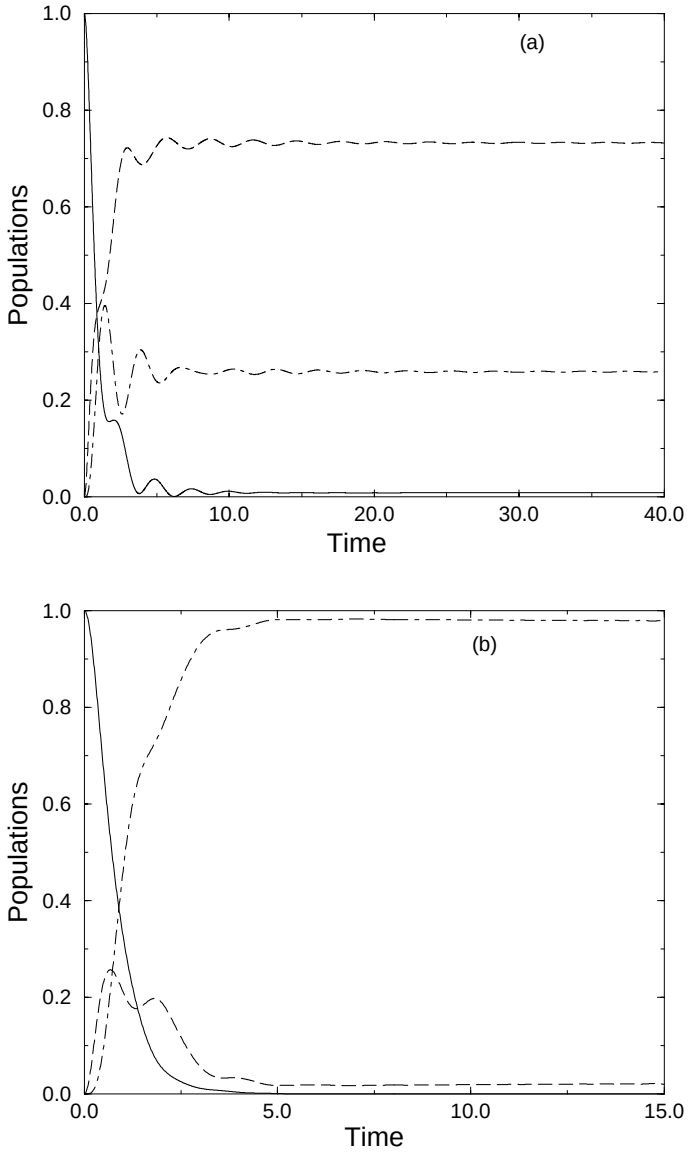

Fig. 6.4: The population in the atomic states as function of time. The solid line is for $|1\rangle$, the dashed line for $|2\rangle$ and the dot-dashed line for $|3\rangle$. Parameters: $C_2 = 1.5C_1$, (a) $\delta_{12} = 1C_2^{2/3}$ and $\delta_{23} = -1C_1^{2/3}$; (b) $\delta_{12} = 2C_2^{2/3}$ and $\delta_{23} = 3C_1^{2/3}$. The time is in units of $C_1^{2/3}$.

The effective detuning of the $|3\rangle \leftrightarrow |1\rangle$ transitions from the band-edge for the "direct" two-photon process is defined as $\Delta^{(2)} = \omega_1 - \omega_3 - 2\omega_e$. From the known dynamics of a TLA with transition frequency at the edge of the gap, depending on $\Delta^{(2)}$, we may expect suppression or inhibition of the "direct" two-photon process. Specifically, for detunings inside the gap ($\Delta^{(2)} < 0$), the "direct" two-photon emission should be totally or partially suppressed, while for detunings outside the gap and almost at the edge ($\Delta^{(2)} > 0$), it should be enhanced due to the high density of final available states.

For transitions symmetrically placed around the band-edge ($\delta_{12} = -\delta_{23}$), with the upper one being inside the gap ($\delta_{12} < 0$), the detuning for the "direct" two-photon transition is exactly at the edge ($\Delta^{(2)} = 0$) (Fig. 6.5). For the parameters used in Figs. 6.5 and without taking into account the "direct" two-photon process, the "single-photon + atom" bound state for the upper state should be metastable, in the sense that the main part of the population should be lost in the long-time limit. On the contrary, we find that this does not happen and the part of the population that has not been lost in the transient regime, oscillates between the upper and the ground state. These oscillations are not reflected in the intermediate level's population which remains almost constant with some oscillations of negligible amplitude. This behavior definitely indicates the coupling of the upper level to the ground level via a "direct" two-photon process as described above.

Note again the "in phase" oscillations for the two lower levels. Choosing δ_{23} such that $\Delta^{(2)} > 0$ (Fig. 6.6), the main part of the population is indeed lost in the long-time limit. The difference between Fig. 6.5(a) and Fig. 6.6 is the detuning of the lower transition from the band-edge. In both cases ($\delta_{23} = 2C_2^{2/3}$, $\delta_{23} = 4C_2^{2/3}$), the behavior of a TLA in the long-time limit is the same, i.e., the population is lost. For the ladder system, however, we note an oscillatory behavior where part of the population is trapped to the atom in the long-time limit for $\delta_{23} = 2C_2^{2/3}$ and complete decay for $\delta_{23} = 4C_2^{2/3}$. The "photon + atom" bound state formed due to the upper transition becomes therefore metastable (see Sec. 4.3) as soon as δ_{23} is chosen such that $\Delta^{(2)} > 0$. This is a conclusion that has been checked for various detunings of the atomic transitions from the band-edge but with the upper one always in the gap ($\delta_{12} \leq 0$).

Gap with a Lorentzian Profile of DOS: We proceed now to the exploration of the ladder system under the DOS (4.8) adopting the specific case of $p = 6$. The corresponding spectral response for transition l is of the form

$$\mathcal{D}_L^{(l)}(\omega) = \frac{\gamma_l}{2\pi}\left[1 - \frac{\Gamma^6}{(\omega - \omega_c)^6 + \Gamma^6}\right], \tag{6.13}$$

where γ_l is the decay rate for transition l in open space. Applying a uniform discretization, we substitute the continuum for $-20\gamma_2 < \omega - \omega_c < 20\gamma_2$,

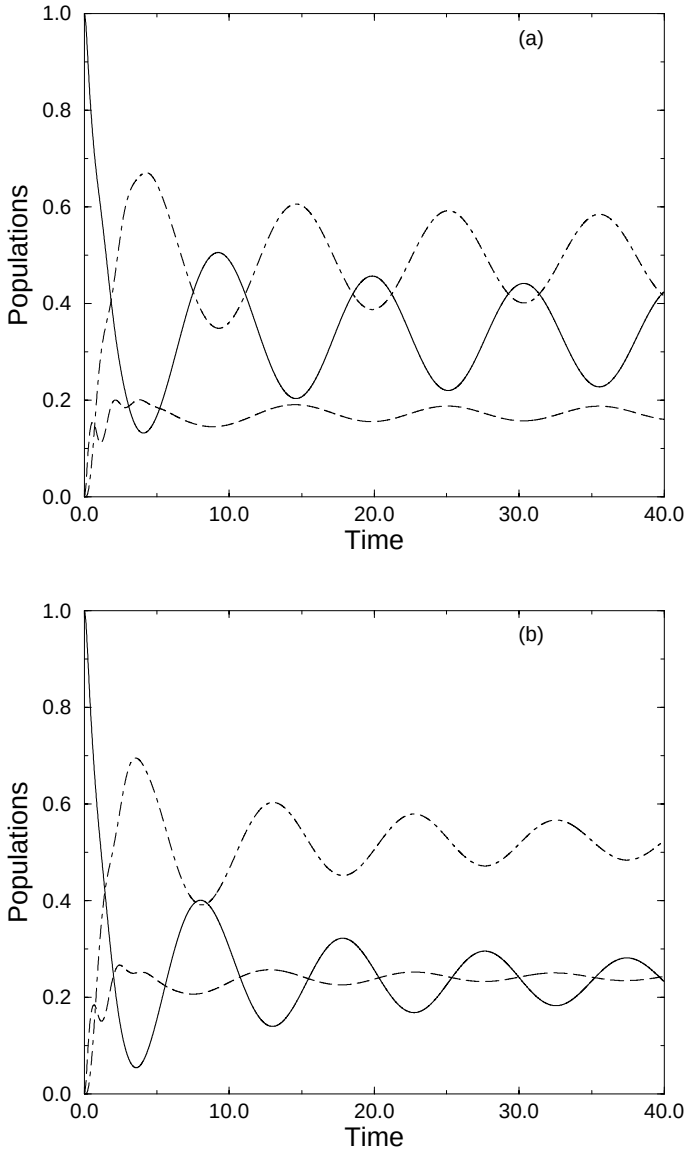

Fig. 6.5: The population in the atomic states as function of time. The solid line is for $|1\rangle$, the dashed line for $|2\rangle$ and the dot-dashed line for $|3\rangle$. Parameters: $C_2 = 1.5C_1$, (a) $\delta_{12} = -2C_2^{2/3}$ and $\delta_{23} = 2C_2^{2/3}$; (b) $\delta_{12} = -2C_1^{2/3}$ and $\delta_{23} = 2C_1^{2/3}$. The time is in units of $C_1^{2/3}$.

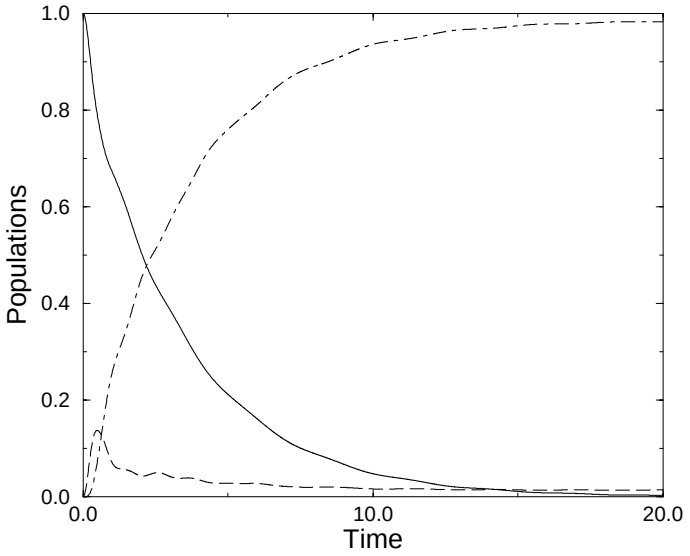

Fig. 6.6: The population in the atomic states as function of time. The solid line is for $|1\rangle$, the dashed line for $|2\rangle$ and the dot-dashed line for $|3\rangle$. Parameters: $C_2 = 1.5C_1$, $\delta_{12} = -2C_2^{2/3}$ and $\delta_{23} = 4C_2^{2/3}$. The time is in units of $C_1^{2/3}$.

by 150 discrete modes. The frequency ω_j corresponding to the j mode is obtained by Eq. (5.6) and the corresponding coupling to atomic transition l is

$$\mathcal{G}^{(l)}(\omega_j) = \sqrt{\frac{\gamma_l}{2\pi}} \sqrt{\left[1 - \frac{\Gamma^6}{(\omega_j - \omega_c)^6 + \Gamma^6}\right] \delta\omega}, \tag{6.14}$$

where $\delta\omega \approx 0.27\gamma_2$ is the spacing between two discrete modes.

The rest of the mode-density, for $\omega > \omega_c + 20\gamma_2$ and $\omega < \omega_c - 20\gamma_2$, can be treated perturbatively leading to a shift for the two upper levels. The relative positions of the upper and lower transition frequencies can now be defined with respect to the central frequency ω_c of the gap, in terms of the detunings: $\delta_{12} = \omega_1 - \omega_2 - \omega_c$ and $\delta_{23} = \omega_2 - \omega_3 - \omega_c$, respectively.

In Fig. 6.7, we present the evolution of the population in the states of the ladder system as a function of time, for a particular combination of detunings. As in the previous figures corresponding to the isotropic model, both upper and lower levels exhibit non-zero steady-state population, as a consequence of the "two-photon + atom" bound state. The oscillations, however, in the atomic populations, which can be interpreted as interference between the dressed states, are not present. It seems that this oscillatory behavior is strongly related to the isotropic model. For the Lorentzian profile, the part of the doublet that is pushed outside the gap, decays much faster than the isotropic model would predict. From this we conclude that in the isotropic

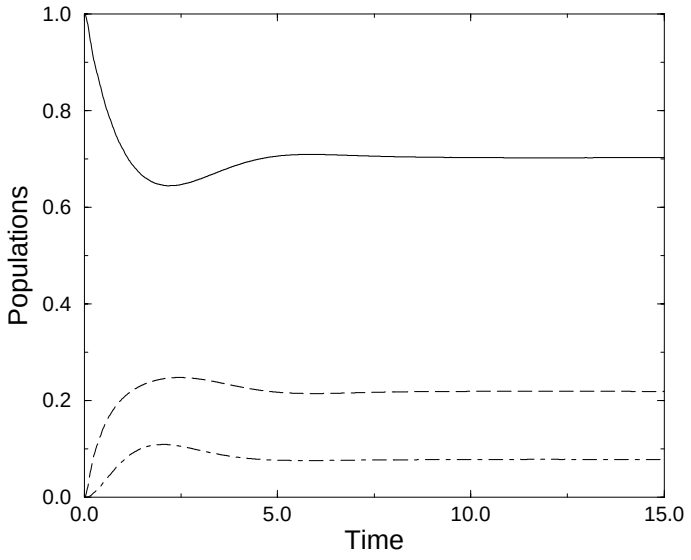

Fig. 6.7: The population in the atomic states as function of time. The solid line is for $|1\rangle$, the dashed line for $|2\rangle$ and the dot-dashed line for $|3\rangle$. Parameters: $\gamma_1 = 0.5\gamma_2$, $\Gamma = \gamma_2$, $\delta_{12} = 0.1\gamma_2$, $\delta_{23} = 0.3\gamma_2$ and $\omega_{up} = -\omega_{low} = 20\gamma_2$. The time is in units of γ_2.

model, the "dynamic regime" which follows the initial transient regime and is dominated by the emission and reabsorption of photons, or else the interference between the various dressed states, is much more pronounced than in the Lorentzian model, or we would argue any model that does not exhibit the highly peaked feature of the isotropic model. Without the concentration of the DOS around a peak, the notion of dressed states is diluted. Nevertheless, the coherent superposition of states and the "two-photon + atom" bound state persists even in this model. Atomic populations remain trapped for long times, long compared to $1/\gamma_2$.

6.3 Summary

We have investigated the dynamics of a ladder atomic system with both transitions coupled to the same structured reservoir. This has been possible through the discretization approach. We have found that this system supports a "two-photon + atom" bound state which leads to a fractional population trapping in both of the upper states and the atom can be in a superposition of the upper levels even in the long-time limit. In the presence of the two photons at the site of the atom, we have shown that the atom has two paths for the $|1\rangle \leftrightarrow |3\rangle$ transition, and found that a "direct" two-photon process coexists with a stepwise one. Which of the two dominates is deter-

mined mainly by the detuning of the upper transition from the band-edge. We have further explored the persistence of this effect under a much more relaxed forms of the DOS and shown that, although quantitatively modified, the basic effect remains.

Chapter 7

Resonance Fluorescence at the Edge of a PBG

In this chapter we elaborate on certain aspects of resonance fluorescence in the context of PBG continua, by means of the discretization approach. A TLA is driven by an initially populated near-resonant mode of the electromagnetic field, while simultaneously can decay into the other strongly modified modes which are initially unoccupied. For an atomic transition inside the gap, a defect-mode must exist with a frequency close to the atomic one. For the remainder of this chapter, we thus refer to the initially populated mode as defect-mode. Propagating the wavefunction of the system, we obtain results pertaining to the problem of two and three photons in the reservoir, for various states of the defect-field. We additionally explore the range of computational demands and applicability of the discretization. In that spirit, we discuss the scaling of computational requirements with increasing number of photons.

7.1 The System

We consider a TLA with ground ($|g\rangle$) and excited ($|e\rangle$) states whose energy difference is ω_o. The atom is coupled to a continuum exhibiting a gap, as well as an initially populated defect-mode of frequency ω_d. The Hamiltonian for this system in the RWA reads

$$\begin{aligned} \mathcal{H} &= \omega_o \sigma_{ee} + \omega_d a_d^\dagger a_d + \sum_\lambda \omega_\lambda a_\lambda^\dagger a_\lambda + g_d(a_d \sigma^+ + a_d^\dagger \sigma^-) \\ &+ \sum_{\substack{\lambda \\ (\lambda \neq d)}} g_\lambda (a_\lambda \sigma^+ + a_\lambda^\dagger \sigma^-), \end{aligned} \tag{7.1}$$

where $\sigma^\pm$ are the usual atomic raising and lowering operators and $\sigma_{ee} = \sigma^+\sigma^-$. The field operators $(a_d, a_d^\dagger)$ and $(a_\lambda, a_\lambda^\dagger)$ correspond to the defect-

mode and the PBG reservoir, respectively, which are coupled to the atom via the respective coupling constants g_d and g_λ.

The defect-field, can be either in a pure Fock state or in a mixture. In order to obtain the time-evolution of the system, we have to take into account states beyond the one-photon sector of the reservoir. As the simplest case, in the following section we consider the case of an initially excited TLA, interacting with a defect-mode prepared in a Fock state and no photons present in the PBG reservoir. We thus begin by considering the atom-field state-vector $|\psi(n,t)\rangle$ that evolves in time from an initial state with a fixed number of excitations in the system.

7.2 Defect-field in a Pure Fock State

7.2.1 One Fluorescent Decay

When only a single excitation is shared between the defect-mode and the atom, the wavefunction for the system can be written as

$$|\psi(0,t)\rangle = a_0|e;0_d,0\rangle + b_0|g;1_d,0\rangle + \sum_\mu b_\mu|g;0_d,1_\mu\rangle, \tag{7.2}$$

where the states involved are product states and, for instance, $|g;0_d,1_\mu\rangle = |g\rangle|0_d\rangle|1_\mu\rangle$ where $|0_d\rangle$ is the zero-photon state of the defect-mode and $|1_\mu\rangle$ is an one-photon state of the reservoir.

The initial state-vector of the system is $|\psi(0,0)\rangle = |e;0,0\rangle$ and its evolution can be obtained by the Schrödinger equation with the Hamiltonian given by Eq. (7.1). We thus have,

$$\dot{a}_0 = \frac{1}{i}\omega_o a_0 + \frac{1}{i}g_d b_0 + \frac{1}{i}\sum_\mu g_\mu b_\mu, \tag{7.3}$$

$$\dot{b}_0 = \frac{1}{i}\omega_d b_0 + \frac{1}{i}g_d a_0, \tag{7.4}$$

$$\dot{b}_\mu = \frac{1}{i}\omega_\mu b_\mu + \frac{1}{i}g_\mu a_0. \tag{7.5}$$

Since the calculation involves one photon, it is amenable to standard techniques such as the resolvent operator. Assuming, however, the defect-mode initially prepared in a photon-number state $|n_d\rangle$ with $n \neq 0$, several excitations of the structured continuum are involved, and the discretization approach is necessary for the investigation of the atomic dynamics.

7.2.2 Two and Three Fluorescent Decays

Considering the defect-mode initially prepared in the one-photon Fock state ($n = 1$) and the atom excited, we have a total of two excitations and thus,

the state-vector of the system reads,

$$\begin{aligned} |\psi(1,t)\rangle &= a_0|e;1_d,0\rangle + b_0|g;2_d,0\rangle + \sum_{\lambda} a_\lambda|e;0_d,1_\lambda\rangle \\ &\quad + \sum_{\lambda} b_\lambda|g;1_d,1_\lambda\rangle + \sum_{\substack{\lambda,\mu \\ (\lambda\geq\mu)}} b_{\lambda\mu}|g;0_d,1_\lambda,1_\mu\rangle, \end{aligned} \tag{7.6}$$

where $b_{\lambda\mu} = b_{\mu\lambda}$.

Let us first solve the problem in the context of the so-called isotropic model, for which the spectral response of the continuum for the atomic transition, is given by Eq. (4.9). Discretizing the near-resonant part of the continuum in the way we have shown in Sec. 5.2.1, and after eliminating the far off-resonant part, the equations of motion for the amplitudes entering the wavefunction (7.6) and are associated with the discrete modes read

$$\dot{a}_0 = \frac{1}{i}\left(\delta_e + \delta_d - S\right)a_0 + \frac{1}{i}\sqrt{2}g_d b_0 + \frac{1}{i}\sum_{j=1}^{N}\mathcal{G}_j b_j, \tag{7.7}$$

$$\dot{b}_0 = \frac{2}{i}\delta_d b_0 + \frac{1}{i}\sqrt{2}g_d a_0, \tag{7.8}$$

$$\dot{a}_j = \frac{1}{i}\left(\delta_e + \delta_j - S\right)a_j + \frac{1}{i}g_d b_j + \frac{1}{i}\sum_{\substack{k=1 \\ (k\neq j)}}^{N}\mathcal{G}_k b_{jk} + \frac{1}{i}\sqrt{2}\mathcal{G}_j b_{jj}, \tag{7.9}$$

$$\dot{b}_j = \frac{1}{i}(\delta_j + \delta_d)b_j + \frac{1}{i}\mathcal{G}_j a_0 + \frac{1}{i}g_d a_j, \tag{7.10}$$

$$\dot{b}_{jk} = \frac{1}{i}(\delta_k + \delta_j)b_{jk} + \frac{1}{i}\mathcal{G}_k a_j + \frac{1}{i}\mathcal{G}_j a_k, \tag{7.11}$$

$$\dot{b}_{jj} = \frac{2}{i}\delta_j b_{jj} + \frac{1}{i}\sqrt{2}\mathcal{G}_j a_j, \tag{7.12}$$

where j,k are indexes over all discrete modes and for the corresponding couplings we have $\mathcal{G}_j = \mathcal{G}_k = \mathcal{G}$, with $\mathcal{G}$ being defined in Eq. (5.25), while $\delta_{j(k)} = \omega_{j(k)} - \omega_e$ and $\delta_e = \omega_o - \omega_e$, $\delta_d = \omega_d - \omega_e$. Finally, the shift term S is the same with that in Eq. (5.26).

Solving this set of equations numerically, we may obtain the time-evolution of the system. In Fig. 7.1, we plot the atomic population (dotted line), the mean number of photons in the defect-mode (solid line) and the populations in the one-photon sector (dot-dashed line) and the two-photon sector (dashed line) of the reservoir Hilbert space as functions of time, for various couplings of the atom to the defect-mode. Both atom and defect-mode are chosen to be slightly detuned from the band-edge frequency. Clearly, we have an initial dynamic regime where the atom exchanges energy with both the defect-mode and the PBG continuum. In this regime, part of the total initial excitation is lost. On a longer time-scale, although the atom is not fully excited, it seems to become transparent to the defect-field. Specifically,

we see an exchange of energy (oscillation) between the defect-mode and the one-photon sector of the reservoir. This oscillation must involve the atom, since the defect-mode is not directly coupled to the reservoir, but is not reflected in the atomic inversion. As is evident in Fig. 7.1, although photons are exchanged between the defect-mode and the reservoir through the atom, after some initial time, the atomic population remains practically constant; a rather surprising effect. Furthermore, a change in the magnitude of g_d in relation to $C^{2/3}$ does not seem to affect the atomic oscillations for larger times, but it does affect the relative oscillations of the excitations in the defect-mode and the reservoir, which are smoothed out with increasing g_d.

The results we have just presented, have of course been tested for convergence in terms of the number of discrete modes and limits of discretization. In Fig. 7.2, for example, we plot the atomic population for various discretization parameters. Specifically, the dotted line is for a calculation with 50 modes ($\omega_{up} = 10C^{2/3}$), the solid line is for 150 modes ($\omega_{up} = 10C^{2/3}$) and the dashed line is for 300 modes ($\omega_{up} = 40C^{2/3}$). As we can see, the three lines are almost indistinguishable, while as we expected, in the long-time limit the calculation for 50 modes exhibits revivals. One could easily, however, have used 50 discrete modes, for a calculation tailored to a shorter time scale, without loosing accuracy.

When the frequencies of both the atom and the defect-mode are pushed further inside the gap, the atom does not become transparent to the defect-field. As is depicted in Fig. 7.3(a), for couplings of the same order of magnitude with the atomic detuning, the atom (solid line) exchanges energy with the defect-mode (dot-dashed line) and the PBG continuum, even for larger times. Note also that a significant part of the total initial excitation (dashed line) remains trapped to the atom and the defect-mode. As the coupling constant g_d increases, however, the oscillations at larger times are suppressed and we find less excitation trapping in the long-time limit.

In the language of dressed states, the coupling of the atom to the defect-mode, as well as the interaction with its own localized radiation field, causes a splitting of the atomic levels. A part of the dressed states is pulled into the gap where it is protected from dissipation, while the other is pushed away from the gap, towards the allowed part of the continuum. Hence, any oscillations in the atomic population can be interpreted as interference between these dressed states. In the long-time limit, the component outside the gap will eventually decay. On the contrary, the stable dressed states inside the gap are associated with a non-zero steady-state atomic population. The coupling of the atom to the defect-mode determines the magnitude of the splitting and thus the portion of the total initial excitation which remains trapped to the atom and the defect-mode in the long-time limit.

The reverse case is depicted in Fig. 7.4, where the atomic and the defect-excitations are plotted as functions of time for $\delta_e = \delta_d = 3.0C^{2/3}$ and various values of g_d. For this particular choice of parameters, the defect-mode lies

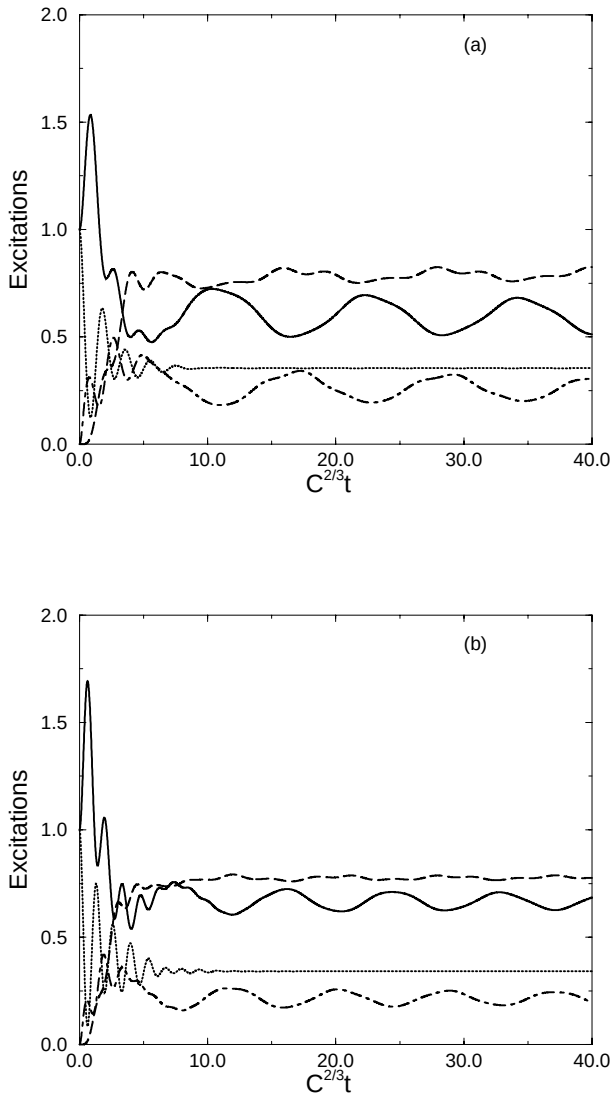

Fig. 7.1: The evolution of the system (atom + defect-mode + continuum) is plotted as a function of time. The dotted line is the population in the upper atomic state. The solid line is the mean number of photons in the defect-mode, the dot-dashed line is the population in the one-photon sector of the reservoir Hilbert space and the dashed curve is the population in the two-photon sector of the reservoir Hilbert space. Parameters: $N = 150$, $\omega_{up} = 10C^{2/3}$, $\delta_e = \delta_d = -0.1C^{2/3}$; (a) $g_d = 1.0C^{2/3}$, (b) $g_d = 1.5C^{2/3}$.

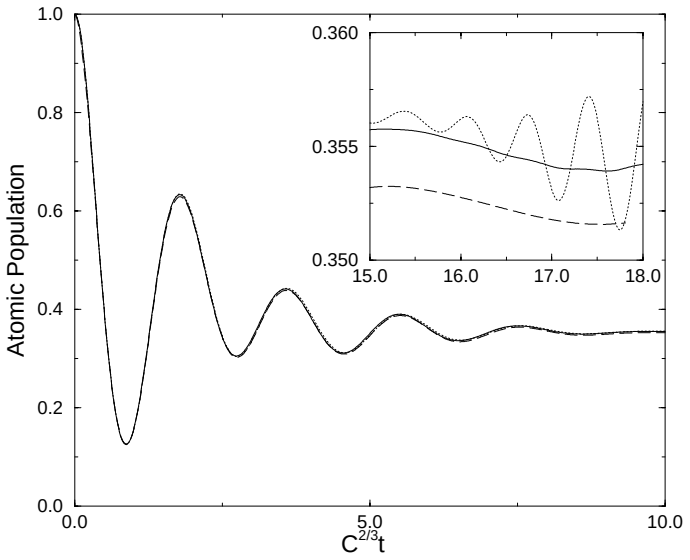

Fig. 7.2: The population in the excited atomic state is plotted as a function of time. The solid line is the solution for $N = 150$, the dotted line is for $N = 50$ and the long-dashed line is for $N = 300$. The insert shows a close-up of the long-time behavior. Parameters: $\delta_e = \delta_d = -0.1C^{2/3}$ and $g_d = 1.5C^{2/3}$.

within the allowed band of the continuum. For relatively weak values of g_d [Fig. 7.4(a)], the excitation is lost in the long-time limit. As g_d, however, becomes comparable to the atomic detuning from the band-edge frequency [Fig. 7.4(b)], the corresponding splitting is strong enough to push part of the dressed states inside the gap, leading thus to non-negligible population trapping. This behavior becomes more clear for even larger values of g_d [Fig. 7.4(c)], where about 25% of the total initial excitation remains trapped at the atom and the defect-mode, in the long-time limit.

It is well known that in the isotropic model, the band-edge is associated with an entire sphere, ($\mathbf{k} = |\mathbf{k}_e|$) rather than a point. This leads to an artificial divergence of the isotropic DOS for frequencies close to the band-edge, which is also reflected in the corresponding spectral response [Eq. (4.9)]. As we have seen, this sharp peak at the edge tends to exaggerate certain effects, such as the existence of "photon + atom" bound state for atomic transitions outside the gap. It is worth, therefore, investigating the persistence of the above mentioned effects in the context of the Lorentzian profile of DOS, with the corresponding spectral response given by Eq. (5.28). Accordingly, the frequencies and the couplings of the discrete modes are defined in Sec. 5.2.2, and the shift can be determined numerically.

In Fig. 7.5, we present results pertaining to an eighth order Lorentzian profile DOS ($p = 8$). The population in the excited state of the atom (solid

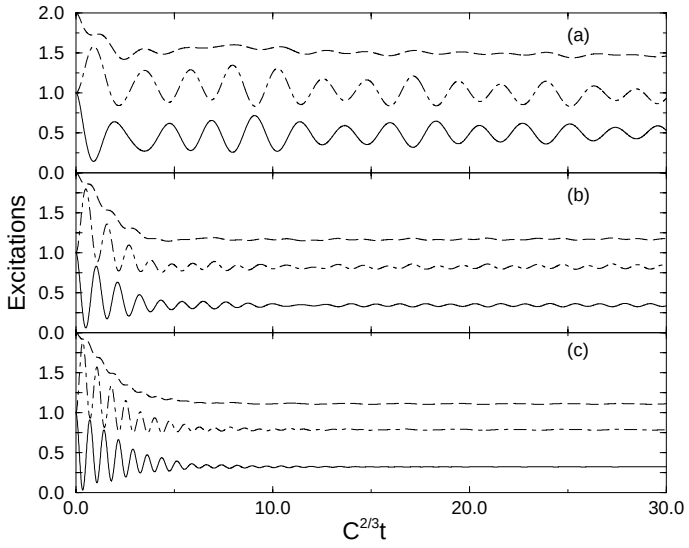

Fig. 7.3: The evolution of the system (atom + defect-mode + continuum) is plotted as a function of time. The solid line and the dot-dashed line are the atomic and the defect excitations respectively. The dashed line is the total excitation (atom + defect-mode). Parameters: $N = 150$, $\omega_{up} = 10C^{2/3}$, $\delta_e = \delta_d = -1.0C^{2/3}$; (a) $g_d = 1.0C^{2/3}$, (b) $g_d = 2.0C^{2/3}$, (c) $g_d = 3.0C^{2/3}$.

line), the defect-excitation (dot-dashed line) and the excitation in the PBG continuum (dashed line), are plotted as functions of time for $\delta_c = \omega_o - \omega_c = 0.5\gamma_a$, $\delta_d = \omega_d - \omega_c = 0.5\gamma_a$ and $g_d = 1.5\gamma_a$. In contrast with the isotropic model, the Lorentzian DOS is zero only for $\omega = \omega_c$. As a result the dressed states inside the gap do not persist for ever and the corresponding excitation will eventually be lost (Fig. 7.5). The time scale on which this decay takes place is determined by the width and the depth of the gap.

By means of the discretization approach, problems pertaining to more than two photons in a structured reservoir of any DOS can be treated in the same way. It should be noted, however, that the number of equations to propagate scales roughly as N^q, where N is the number of discrete modes and q is the number of excitations. Thus, the ultimate limitation of the approach is determined by computer memory and CPU time. The wave-function pertaining to a three-photon problem, for example, is of the form,

$$|\psi(2,t)\rangle = b_0|g;3_d,0\rangle + a_0|e;2_d,0\rangle + \sum_j b_j|g;2_d,1_j\rangle + \sum_j a_j|e;1_d,1_j\rangle + \sum_{\substack{j,k \\ (k\geq j)}} b_{jk}|g;1_d,1_j,1_k\rangle$$

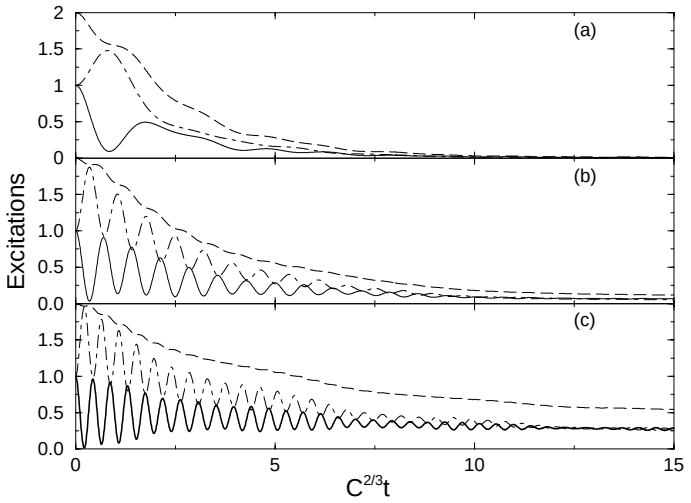

Fig. 7.4: The evolution of the system (atom + defect-mode + continuum) is plotted as a function of time. The solid line and the dot-dashed line are the atomic and the defect excitations respectively. The dashed line is the total excitation (atom + defect-mode). Parameters: $N = 150$, $\omega_{up} = 10C^{2/3}$, $\delta_e = \delta_d = 3.0C^{2/3}$; (a) $g_d = 1.0C^{2/3}$, (b) $g_d = 3.0C^{2/3}$, (c) $g_d = 5.0C^{2/3}$.

$$+ \sum_{\substack{j,k \\ (k \geq j)}} a_{jk}|e;0_d,1_j,1_k\rangle + \sum_{\substack{j,k,l \\ (l \geq k \geq j)}} b_{jkl}|g;0_d,1_j,1_k,1_l\rangle. \tag{7.13}$$

with the coefficients b_{jk}, a_{jk} and b_{jkl}, being invariant under any permutation of the indexes j,k,l. The Schödinger equation leads to a somehow enlarged and more complicated set of differential equations for the amplitudes:

$$\dot{a}_0 = \frac{1}{i}\left(\delta_e + 2\delta_d - S\right)a_0 + \frac{1}{i}\sqrt{3}g_d b_0 + \frac{1}{i}\sum_{j=1}^{N}\mathcal{G}_j b_j, \tag{7.14}$$

$$\dot{b}_0 = \frac{3}{i}\delta_d b_0 + \frac{1}{i}\sqrt{3}g_d a_0, \tag{7.15}$$

$$\dot{a}_j = \frac{1}{i}\left(\delta_e + \delta_d + \delta_j - S\right)a_j + \frac{1}{i}\sum_{\substack{k=1 \\ (k\neq j)}}^{N}\mathcal{G}_k b_{jk} + \frac{1}{i}\sqrt{2}g_d b_j + \frac{1}{i}\sqrt{2}\mathcal{G}_j b_{jj}, \tag{7.16}$$

$$\dot{b}_j = \frac{1}{i}(\delta_j + 2\delta_d)b_j + \frac{1}{i}\mathcal{G}_j a_0 + \frac{\sqrt{2}}{i}g_d a_j, \tag{7.17}$$

$$\dot{b}_{jk} = \frac{1}{i}(\delta_d + \delta_k + \delta_j)b_{jk} + \frac{1}{i}g_d a_{jk} + \frac{1}{i}\mathcal{G}_k a_j + \frac{1}{i}\mathcal{G}_j a_k \tag{7.18}$$

$$\dot{b}_{jj} = \frac{1}{i}(\delta_d + 2\delta_j)b_{jj} + \frac{1}{i}\sqrt{2}\mathcal{G}_j a_j + \frac{g_d}{i}a_{jj}, \tag{7.19}$$

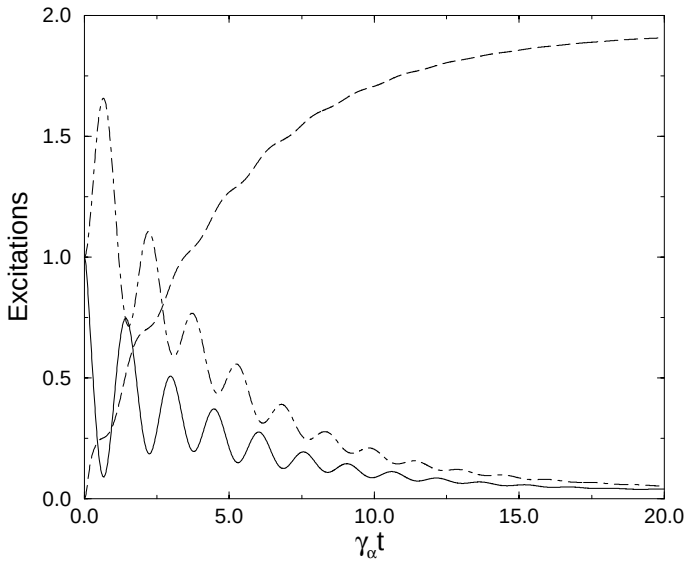

Fig. 7.5: The atomic excitation (solid line), the defect-excitation (dot-dashed line) and the total excitation in the PBG continuum (dashed line) as functions of time. Parameters: $p = 8$, $\Gamma = \gamma_a$, $\omega_{up} = -\omega_{low} = 20\gamma_a$, $N = 150$, $\delta_c = \delta_d = 0.5\gamma_a$, $g_d = 1.5\gamma_a$.

$$\dot{a}_{jk} = \frac{1}{i}\left(\delta_e + \delta_j + \delta_k - S\right) a_{jk} + \frac{1}{i} \sum_{\substack{m=1 \\ (m\neq j\neq k)}}^{N} \mathcal{G}_m b_{jkm} + \frac{1}{i} g_d b_{jk} + \frac{1}{i}\sqrt{2}\mathcal{G}_k b_{jkk} + \frac{1}{i}\sqrt{2}\mathcal{G}_j b_{jjk}, \tag{7.20}$$

$$\dot{a}_{jj} = \frac{1}{i}\left(\delta_e + 2\delta_j - S\right) a_{jj} + \frac{1}{i} \sum_{\substack{m=1 \\ (m\neq j)}}^{N} \mathcal{G}_m b_{jjm} + \frac{1}{i} g_d b_{jj} + \frac{1}{i}\sqrt{3}\mathcal{G}_j b_{jjj}, \tag{7.21}$$

$$\dot{b}_{jkl} = \frac{1}{i}(\delta_j + \delta_k + \delta_l) b_{jkl} + \frac{1}{i}\mathcal{G}_l a_{jk} + \frac{1}{i}\mathcal{G}_k a_{jl} + \frac{1}{i}\mathcal{G}_j a_{kl}, \tag{7.22}$$

$$\dot{b}_{jjk} = \frac{1}{i}(2\delta_j + \delta_k) b_{jjk} + \frac{1}{i}\mathcal{G}_k a_{jj} + \frac{\sqrt{2}}{i}\mathcal{G}_j a_{jk}, \tag{7.23}$$

$$\dot{b}_{jkk} = \frac{1}{i}(2\delta_k + \delta_j) b_{kkj} + \frac{1}{i}\mathcal{G}_j a_{kk} + \frac{\sqrt{2}}{i}\mathcal{G}_k a_{jk}, \tag{7.24}$$

$$\dot{b}_{jjj} = \frac{3}{i}\delta_j b_{jjj} + \frac{\sqrt{3}}{i}\mathcal{G}_j a_{jj}, \tag{7.25}$$

where j, k, l are mode indices over the discrete modes and $\delta_{j(k,l)} = \omega_{j(k,l)} - \omega_e$. Adopting the isotropic model for the description of the PBG continuum, the

time-evolution of the system is shown in Fig. 7.6, where we plot again the excitations for various couplings and detunings of the atom and the defect-mode from the band-edge. The dynamics resembles that of the two-photon problem, with the atom and the defect-mode exhibiting non-zero excitation trapping in the long-time limit, while the atom becomes transparent to the defect-field for detunings slightly inside the gap.

A further issue needs to be brought up here in connection with the steady-state population of an atom initially prepared in its ground state ($|\psi(n,0)\rangle = |g;n_d,0\rangle$). Specifically, although the basic effects we have discussed so far remain practically the same (Fig. 7.7), the atom may exhibit population inversion in the long-time limit. Such a case is depicted in Figs. 7.8(a) and (b) where the atomic inversion is plotted as a function of time, for a defect-mode initially prepared in a 2- and 3-photon Fock state, respectively. Clearly, although the defect-field is relatively weak, the atom can be found inverted in the long-time limit. Such an inversion can not be obtained in the context of resonance fluorescence in ordinary vacuum even for strong driving fields. This is due to the fact that all three bands of the Mollow triplet exhibit resonance fluorescence. For a PBG, however, one or more of them can be found inside the gap, exhibiting thus negligible decay and population trapping in the long-time limit. It is the combination of the coupling (g_d) and the atomic detuning that conspire to produce this behavior and consequently to lead the atomic system to a steady-state population inversion in both Figs. 7.8(a) and (b). As g_d increases in relation to δ_e, the main part of the atomic population is lost in the long-time limit [Fig. 7.8(c)].

7.3 Defect-field in a mixture of Fock states

Up to now, we have discussed problems with a well defined number of excitations in the system. It could be argued, however, that the assumption of a defect-mode initially prepared in a pure Fock state is somewhat restrictive. Although in recent years such initial conditions have become experimentally realizable, at least in the context of CQED [12, 14, 91, 117], a general and more usual condition would involve a defect-field with well defined statistical properties but not number of photons. In that spirit, the state of the defect-field may be a superposition of Fock states,

$$|F\rangle = \sum_{n=0}^{\infty} c_n |n_d\rangle, \tag{7.26}$$

where $|n_d\rangle$ is the $n-photon$ state, or even a mixture. Although the number of photons is then uncertain, the statistical properties of the field are well defined with mean number of photons $\bar{n}$ and the photon-number distribution $\mathcal{P}(n) = |c_n|^2$, i.e., the probability of observing n photons. If the defect-field

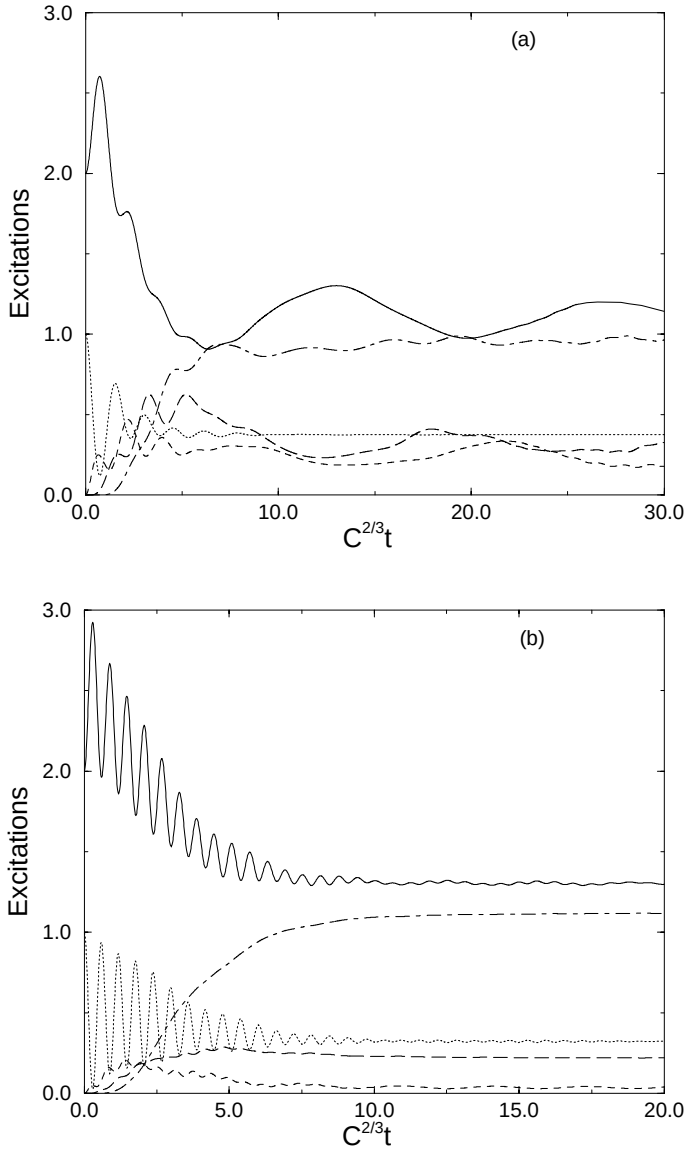

Fig. 7.6: The evolution of the system (atom + defect-mode + continuum) is plotted as a function of time. The dotted line is the population in the upper atomic state. The solid line is the mean number of photons in the defect-mode, the dashed line is the population in the one-photon sector of the reservoir Hilbert space, the long-dashed curve is the population in the two-photon sector of the reservoir Hilbert space and the dot-dashed curve is the population in the three-photon sector of the reservoir Hilbert space. Parameters: $N = 50$, $\omega_{up} = 10C^{2/3}$; (a) $g_d = C^{2/3}, \delta_e = \delta_d = -0.1C^{2/3}$; (b) $g_d = 3C^{2/3}, \delta_e = \delta_d = -1C^{2/3}$.

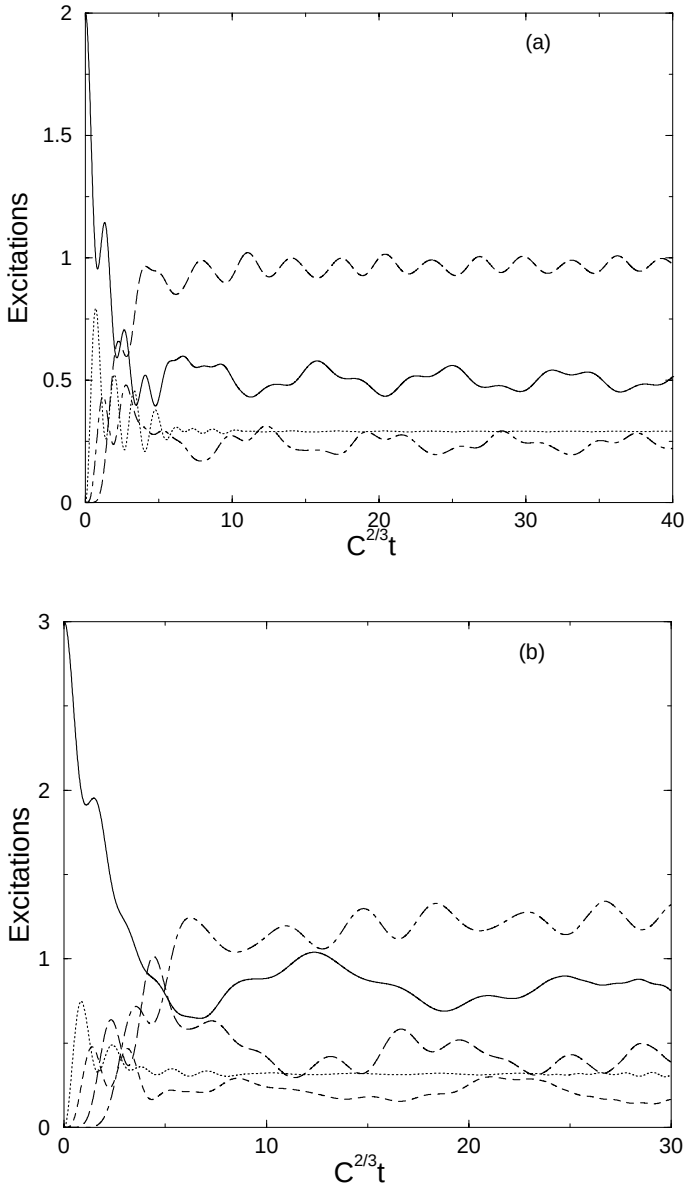

Fig. 7.7: The evolution of the system (atom + defect-mode + continuum) is plotted as a function of time. Initial state $|\psi(n,0)\rangle = |g;n_d,0\rangle$. (a) $n = 2$ and parameters as in Fig. 7.1(b). (b) $n = 3$ and parameters as in Fig. 7.6(a).

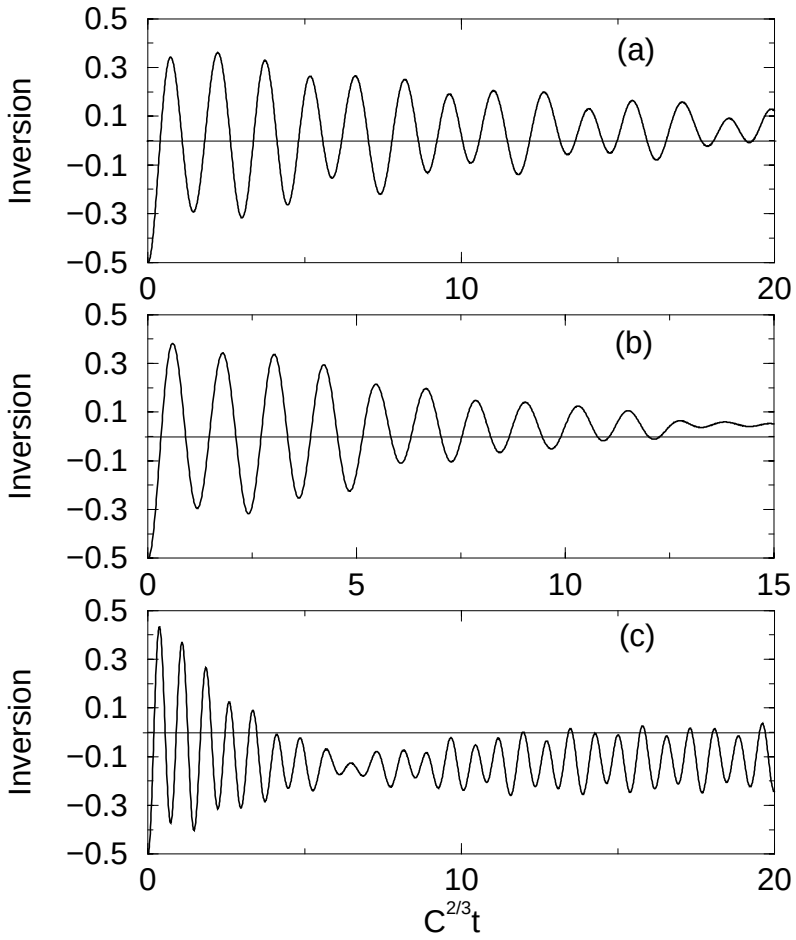

Fig. 7.8: The atomic inversion is plotted as a function of time for $\delta_e = \delta_d = -2.0C^{2/3}$. Parameters: (a) $N = 150$, $\omega_{up} = 10C^{2/3}$, $g_d = 1.5C^{2/3}$, $n = 2$; (b) $N = 50$, $\omega_{up} = 10C^{2/3}$, $g_d = 1.5C^{2/3}$, $n = 3$; (c)$N = 150$, $\omega_{up} = 10C^{2/3}$, $g_d = 3.0C^{2/3}$, $n = 2$.

is in a coherent superposition of Fock states (coherent state), the photon probabilities follow the Poissonian distribution (3.20), while for a thermal defect-field, the photon-number distribution is given by Eq. (3.22).

One of the properties of the Hamiltonian (7.1) is that each state-vector $|\psi(n,t)\rangle$ evolves independently. As a result, if the combined system (atom + defect-mode + continuum) is initially prepared in a state of the form

$$|\Psi(0)\rangle = \sum_{n=0}^{\infty} c_n |\psi(n,0)\rangle \equiv |e\rangle|F\rangle|0\rangle, \quad \mathcal{P}(n) = |c_n|^2, \tag{7.27}$$

the probability of finding the atom excited at time t, is given by

$$\Pi_{ee}(t) = \sum_{R} \sum_{n=0}^{\infty} \mathcal{P}(n) |\langle e; n_d, R|\psi(n,t)\rangle|^2 \tag{7.28}$$

where the first sum ($\sum_R$) is over all possible states of the PBG reservoir while the second one is over an infinite number of state-vectors for the defect-mode. If, however, the average number of photons $\bar{n}$ in the defect-mode is small, only terms involving small n will contribute significantly, making thus the computation feasible, as far as demands of the necessary number of discrete modes are concerned. Let's consider now such a case where the defect-field is initially prepared either in a coherent or a chaotic state with mean number of photons $\bar{n} = 0.5$. For this choice of mean number of photons, the contribution of state-vectors with $n > 3$ in the sum is negligible. Adopting the isotropic model of DOS, we have the time-evolution of each state-vector $|\psi(n,t)\rangle$, for a total of up to three excitations and thus the evaluation of $|\Psi(t)\rangle$ is feasible. Figs. 7.9(c), (d) show the time-evolution of the atomic population for a coherent and chaotic defect-field. Additionally, we plot the atomic population [Figs. 7.9(a), (b)] of an initially excited TLA resonantly coupled to a high-Q cavity-mode, which is given by

$$\langle \sigma_{ee} \rangle = \sum_{n} \mathcal{P}(n) cos^2 \left[\Omega \sqrt{n+1} t \right], \tag{7.29}$$

where Ω is the intrinsic Rabi frequency.

It is well known that the superposition of periodic oscillations such as Eq. (7.29), produces irregular fluctuations as is depicted in Figs. 7.9(a),(b). As the driving field becomes stronger, i.e., the mean number of photons becomes larger, the constructive interference between Rabi oscillations corresponding to different photon-numbers leads to collapse of the oscillations, which for a coherent state, will revive afterwards (see Sec. 3.4.2). Due to computational limitations for the time being, we restrict ourselves to weak fields ($\bar{n} < 1$) where such phenomena are not present. Even in this regime, however, the atom with transition frequency at the edge of a PBG, exhibits substantially different behavior from a TLA coupled to a high-Q cavity mode.

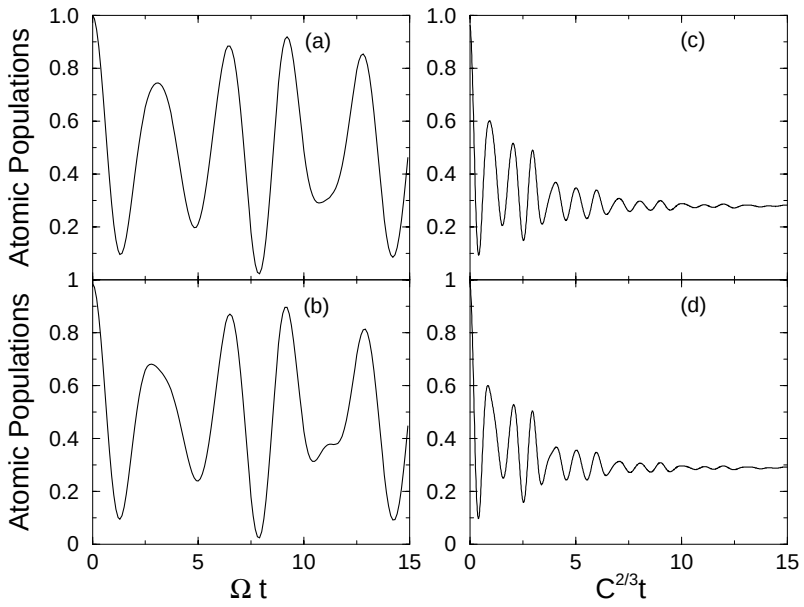

Fig. 7.9: (a) and (b): Population of an initially excited TLA interacting resonantly with the thermal (a) or coherent (b) field of a high-Q cavity-mode. (c) and (d): Population of an initially excited TLA with transition frequency close to the edge of a PBG, interacting with thermal (c) or coherent (d) field of a defect-mode. Parameters: $N = 150$, $\omega_{up} = 10C^{2/3}$; $\bar{n} = 0.5$, $g_d = 3C^{2/3}$, $\delta_e = \delta_d = -1C^{2/3}$.

Specifically, in contrast to Figs. 7.9(a),(b), the fluctuations in Figs. 7.9(c),(d) take place over short times. On a longer time scale the atom exhibits non-zero steady-state population. This behavior is not related to the so-called collapses in the Jaynes-Cummings model. On the contrary, as we have discussed in previous sections, it is intimately connected to the existence of the gap. Even for larger mean number of photons, the population trapping is expected to persist, since each state-vector $|\psi(n,t)\rangle$ exhibits such behavior [Figs. (7.3), (7.6)].

7.4 Summary

We have discussed the problem of resonance fluorescence in the context of PBG continua by means of the discretization approach. An atom with transition frequency near the edge of a gap is driven by a defect-mode centered at frequency inside the gap. Although the atom is coupled to a dissipative environment, for a wide range of parameters we found excitation trapping in the long-time limit, which persists even for atomic interactions with coherent or thermal defect-fields. For moderate values of the atomic coupling to the defect-mode, the atomic population may exhibit steady-state inversion.

We have also investigated some of the these features in the context of a Lorentzian, but still isotropic, DOS. For an atom and defect-mode slightly detuned from the band-edge we found that after some initial time, the atom becomes transparent to the defect-field. Although the defect-mode is not directly coupled to the reservoir but only through the atom, photons are exchanged between them while the atomic population remains practically constant.

Chapter 8

Collective Behavior of Few Atoms at the Edge of a PBG

In this chapter, we investigate the influence of the DDI on the radiative dynamics of a collection of two closely-spaced identical, or non-identical, initially excited TLAs. The atomic transitions are considered to be around the band-edge frequency of a gap. We thus have a problem involving two photons in a structured reservoir which can be solved by means of the discretization approach. Furthermore, a four-level configuration is adopted for the interpretation of the numerical results.

8.1 The system

We consider a system of two initially excited TLAs (A and B), separated by a distance R_{AB}. Both atoms are near-resonantly coupled to the edge of a PBG continuum. We denote by $|e_{A(B)}\rangle$ and $|g_{A(B)}\rangle$ the excited and ground states, respectively, of the atom $A(B)$, whose energy difference (atomic transition frequency) is $\omega_{A(B)}$. As a model for the description of the PBG reservoir, we adopt the isotropic DOS.

The near-resonant, fast-varying part of the continuum is treated using the discretization technique with ω_{up} being the upper cut-off frequency. The frequency of the j discrete mode is then obtained by Eq. (5.21), where $\delta\omega$ is chosen sufficiently small, while the atomic couplings $\mathcal{G}_{A,B}$ to each one of the discrete modes are determined by the following set of equations,

$$\mathcal{G}_A\mathcal{G}_A N = \int_{\omega_e}^{\omega_{up}} d\omega \mathcal{D}_I^{(A)}(\omega), \tag{8.1}$$

$$\mathcal{G}_B\mathcal{G}_B N = \int_{\omega_e}^{\omega_{up}} d\omega \mathcal{D}_I^{(B)}(\omega), \tag{8.2}$$

$$\mathcal{G}_A\mathcal{G}_B N = \int_{\omega_e}^{\omega_{up}} d\omega M_{AB}(\omega, R_{AB}), \tag{8.3}$$

where $\mathcal{D}_I^{(A,B)}(\omega)$ is the spectral response of the PBG continuum for atom A and B respectively,

$$\mathcal{D}_I^{(A,B)}(\omega) = \frac{C_{A,B}}{\pi}\frac{\Theta(\omega-\omega_e)}{\sqrt{\omega-\omega_e}}, \tag{8.4}$$

and $M_{AB}(\omega, R_{AB})$, is the spectral response of the PBG continuum for the system of the two atoms,

$$M_{AB}(\omega, R_{AB}) = \frac{C_M}{\pi}\frac{\Theta(\omega-\omega_e)}{\sqrt{\omega-\omega_e}}. \tag{8.5}$$

We denote by $C_{A(B)}$ the effective coupling of the atom $A(B)$ to the structured continuum, while the modified effective coupling of one of the atoms, say A, due to the presence of the second atom (B) at distance R_{AB}, is given by

$$C_M = \tau(r_{AB})\sqrt{C_A C_B}, \tag{8.6}$$

where r_{AB} is the normalized inter-atomic distance with respect to the band-edge wave-vector. In the Π atomic configuration, i.e., parallel atomic dipoles and aligned perpendicular to the inter-atomic separation axis, $\tau(r_{AB})$ reads

$$\tau(r_{AB}) = \frac{3}{2}\left[\frac{\sin(r_{AB})}{r_{AB}} + \frac{\cos(r_{AB})}{r_{AB}^2} - \frac{\sin(r_{AB})}{r_{AB}^3}\right]. \tag{8.7}$$

According to Eq. (8.6), C_M differs from $\sqrt{C_A C_B}$ by the factor $\tau(r_{AB})$, and thus Eqs. (8.1)-(8.3) can not be fulfilled simultaneously. For small interatomic distances, however, $\tau(r_{AB}) \approx 1$ and accordingly $C_M \approx \sqrt{C_A C_B}$. From Eqs. (8.1)-(8.5) we then obtain

$$\mathcal{G}_A \approx \sqrt{\frac{2C_A}{N\pi}\sqrt{\omega_{up}-\omega_e}}, \tag{8.8}$$

while the position-dependent coupling $\mathcal{G}_B$, is given by

$$\mathcal{G}_B = \frac{C_M}{C_A}\mathcal{G}_A. \tag{8.9}$$

The far off-resonant part of the continuum ($\omega > \omega_{up}$) can be treated perturbatively. As a result of this elimination, the upper atomic level of atom $A(B)$ is shifted by

$$S_{A(B)} = \frac{\mathcal{G}_{A(B)}^2 N}{\omega_{up}-\omega_e}, \tag{8.10}$$

towards the gap. We additionally have a coupling between the atoms due to their interaction through the eliminated part of the continuum, which is expressed by

$$S_M = \frac{\mathcal{G}_A \mathcal{G}_B N}{\omega_{up}-\omega_e}. \tag{8.11}$$

We thus obtain the effective Hamiltonian in an interaction picture rotating at the band-edge frequency ω_e ($\hbar = 1$), for the description of the radiative dynamics of the system

$$\mathcal{H} = \mathcal{H}_o + \mathcal{H}_{DD} + \mathcal{H}_{AR}, \tag{8.12}$$

where

$$\mathcal{H}_o = (\delta_A - S_A)|e_A\rangle\langle e_A| + (\delta_B - S_B)|e_B\rangle\langle e_B| + \sum_{j=1}^{N} \delta_j a_j^\dagger a_j, \tag{8.13}$$

is the unperturbed Hamiltonian of the combined system (atoms + field) with $\delta_{A(B)} = \omega_{A(B)} - \omega_e$, $\delta_j = \omega_j - \omega_e$, while

$$\mathcal{H}_{DD} = (V_{AB} - S_M)\left(|e_A g_B\rangle\langle e_B g_A| + |e_B g_A\rangle\langle e_A g_B|\right), \tag{8.14}$$

is the inter-atom interaction, with V_{AB} being the principal value part of the DDI integral for two atoms with transition frequencies close to the band-edge. As we have discussed in Sec. 4.4 the dipole-dipole coupling approaches its open-space value [Eq. (4.16)] for atomic transitions inside the gap, as well as around the edge. For large inter-atomic separations, with respect to the wavelength of the atomic transitions ($r_{AB} > 1$), $\tau(r_{AB}) \approx 0$ and $V_{AB} \approx 0$ and thus the two atoms are independent. On the contrary, for small inter-atomic distances ($r_{AB} < 1$), $\tau(r_{AB}) \approx 1$ while V_{AB} diverges as $1/r_{AB}^3$.

The third term in Eq. (8.12) describes the coupling of each atom to the near-resonant, fast-varying part of the continuum, which is modeled by N discrete modes, and in RWA is given by

$$\mathcal{H}_{AR} = \sum_{j=1}^{N} \left(\mathcal{G}_A a_j^\dagger |g_A\rangle\langle e_A| + \mathcal{G}_B a_j^\dagger |g_B\rangle\langle e_B| + H.c.\right), \tag{8.15}$$

where the sum is over all discrete modes. The creation(annihilation) operator $a_j^\dagger(a_j)$ in Eqs. (8.13)-(8.15), pertain to the j discrete mode, which is coupled to atom $A(B)$ with coupling constant $\mathcal{G}_{A(B)}$.

The relevant states of the problem are of the form

$$\begin{aligned} |E\rangle &= |e_A, e_B; 0\rangle, \\ |A_j\rangle &= |e_A, g_B; 1_j\rangle, \\ |B_j\rangle &= |g_A, e_B; 1_j\rangle, \\ |G_{j,m}\rangle &= |g_A, g_B; 1_j, 1_m\rangle, \end{aligned} \tag{8.16}$$

where, for instance, $|g_A, g_B; 1_j, 1_m\rangle = |g_A, g_B\rangle|1_j, 1_m\rangle$ denotes a state of the combined system (atoms + field), where both atoms (A and B) are in their ground states and two photons have been emitted into the structured

reservoir, populating the modes j and m respectively. Accordingly, the wavefunction of the complete system reads

$$|\psi(t)\rangle = a_0|E\rangle + \sum_j \left(a_j|A_j\rangle + b_j|B_j\rangle\right) + \sum_{\substack{j,m \\ (m\geq j)}} C_{jm}|G_{j,m}\rangle, \tag{8.17}$$

while, due to the fact that $|G_{j,m}\rangle \equiv |G_{m,j}\rangle$, we have $C_{jm} = C_{mj}$. Before proceeding to the numerical results, it is worth discussing the problem under consideration in the context of the so-called Dicke states.

It is evident from Eq. (8.14) that the DDI mixes only intermediate levels of the combined system, involving the same field state, i.e., $|e_A, g_B; 1_k\rangle$ and $|g_A, e_B; 1_k\rangle$. Diagonalizing thus the Hamiltonian in the absence of the atoms-field interaction term ($\mathcal{H}_{AR}$), and in the basis formed by the vectors (8.16), we obtain a new set of eigenstates

$$\begin{aligned} |\psi_{ee}\rangle &= |e_A, e_B; 0\rangle, \\ |\psi_j^{(+)}\rangle &= |\psi^{(+)}; 1_j\rangle, \\ |\psi_j^{(-)}\rangle &= |\psi^{(-)}; 1_j\rangle, \\ |\psi_{gg}\rangle &= |g_A, g_B; 1_j, 1_m\rangle. \end{aligned} \tag{8.18}$$

The symmetric ($|\psi^{(+)}\rangle$) and antisymmetric ($|\psi^{(-)}\rangle$) atomic states are

$$|\psi^{(\pm)}\rangle = \left(C_1^{\pm}|e_A, g_B\rangle + C_2^{\pm}|g_A, e_B\rangle\right), \tag{8.19}$$

and the corresponding eigenvalues are given by

$$\varepsilon_{\pm} = \frac{\delta_A + \delta_B}{2} \pm \frac{R}{2}, \quad R = \sqrt{(\delta_A - \delta_B)^2 + 4\tilde{V}_{AB}^2}, \tag{8.20}$$

where $\tilde{V}_{AB} = V_{AB} - S_M$. The coefficients in Eq. (8.19) are

$$C_1^{(\pm)} = \left[1 + \frac{\lambda_{\mp}^2}{\tilde{V}_{AB}^2}\right]^{-\frac{1}{2}}, \quad C_2^{(\pm)} = -\frac{\lambda_{\mp} C_1^{(\pm)}}{\tilde{V}_{AB}}, \tag{8.21}$$

with $\lambda_{\pm} = 0.5\left[(\delta_A - \delta_B) \pm R\right]$. The system of the two interacting TLAs can thus be treated as a single four-level atomic system of a cascade configuration, with upper state $|\psi_{ee}\rangle$, intermediate states $|\psi^{(+)}\rangle$, $|\psi^{(-)}\rangle$ and ground state $|\psi_{gg}\rangle$ (Fig. 8.1).

Before proceeding to the investigation of the dynamics for the two initially excited TLAs, let us test the validity of the discretization in the context of resonant DDI (see Sec. 4.4). Specifically, consider only one of the atoms, let's say A, initially excited and the other, which is identical to A, in its ground state. The problem involves a single excitation (relevant states $|\psi_{ee}\rangle$, $|\psi_j^{(+)}\rangle$, $|\psi_j^{(-)}\rangle$) and is amenable to the resolvent technique. In Fig.

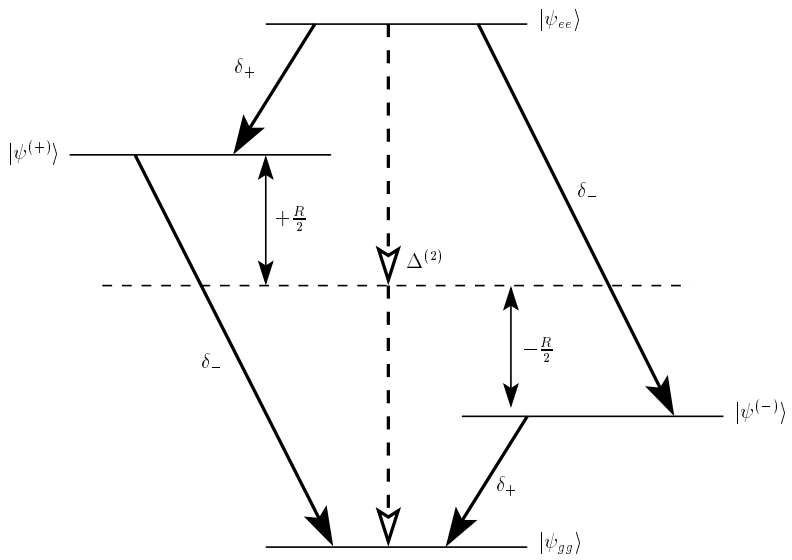

Fig. 8.1: Schematic representation of the collective atomic states and the possible transitions. The solid arrows denote the stepwise decay routes, while the dashed arrows denote the two-photon transition. The corresponding detunings from the band-edge frequency, as well as the shift of the symmetric and antisymmetric states are shown.

8.2, we plot the population in the upper state of atom A, for transition frequencies inside and outside the gap and two different values of $\tilde{V}_{AB}$. The solid lines correspond to the solution obtained by the direct solution of the Scrödinger equation, whereas the dashed lines correspond to the discretization approach for 50 modes. Clearly, although a relatively small part of the continuum has been discretized, the agreement with the exact solution is very good. Since, however, the phenomenon under consideration, that is DDI, results from virtual transitions, it is worth keeping a sufficiently wide range of frequencies in our simulations, to obtain reliable results.

8.2 Equations of Motion and Results

The time dependence of the amplitudes in Eq. (8.17) is governed by the Schrödinger equation with the Hamiltonian given by Eqs. [(8.12)-(8.15)], from which we obtain

$$\begin{aligned} \dot{a}_0 &= \frac{1}{i}\left(\Delta_A + \Delta_B\right) a_0 + \frac{1}{i}\sum_{j=1}^{N}\left(\mathcal{G}_B a_j + \mathcal{G}_A b_j\right), \qquad (8.22) \\ \dot{a}_j &= \frac{1}{i}\left(\Delta_A + \delta_j\right) a_j + \frac{1}{i}\tilde{V}_{AB} b_j + \frac{1}{i}\mathcal{G}_B a_0 \end{aligned}$$

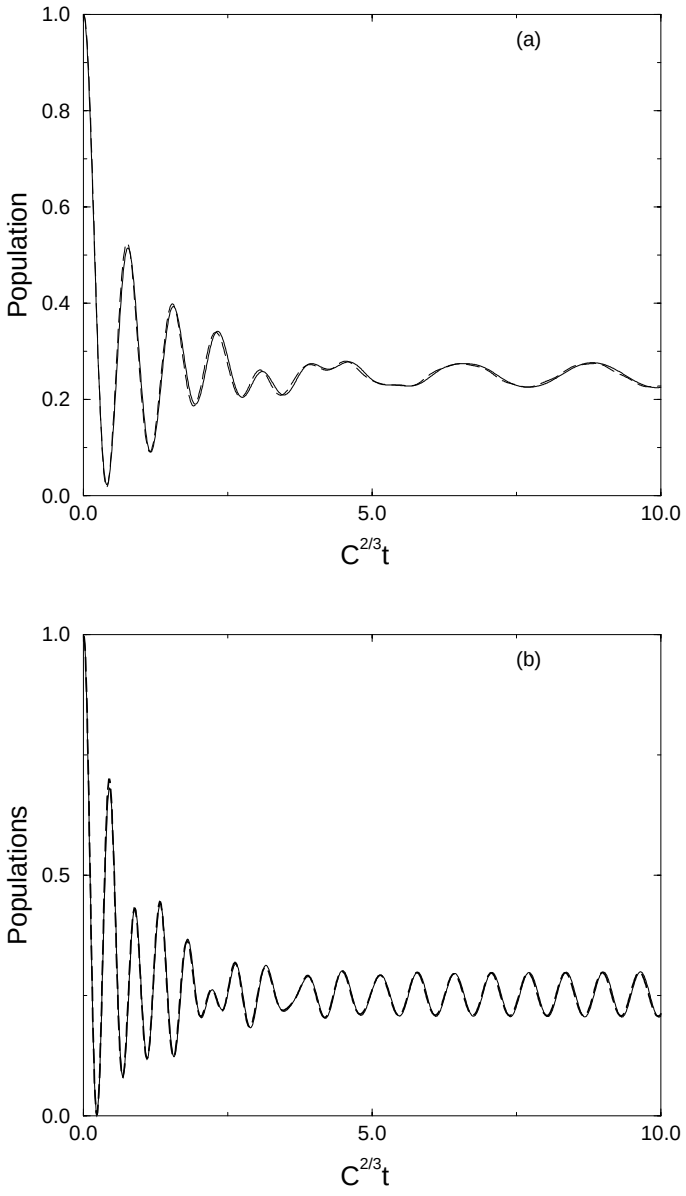

Fig. 8.2: The population in the upper state of atom A. The solid line is the exact solution and the dashed line corresponds to the discretization approach. Parameters: 50 modes, $\omega_{up} = 10C^{2/3}$; $C_B = C_A = C$, $C_M \approx C$; (a) $\delta_A = \delta_B = 1C^{2/3}$ and $V_{AB} = 4C^{2/3}$; (b) $\delta_A = \delta_B = -3C^{2/3}$ and $V_{AB} = 7C^{2/3}$.

$$+\frac{1}{i}\sum_{\substack{m=1\\(m\neq j)}}^{N}\mathcal{G}_A C_{jm}+\frac{1}{i}\sqrt{2}\mathcal{G}_A C_{jj}, \tag{8.23}$$

$$\dot{b}_j = \frac{1}{i}\left(\Delta_B+\delta_j\right)b_j+\frac{1}{i}\tilde{V}_{AB}a_j+\frac{1}{i}\mathcal{G}_A a_0 + \frac{1}{i}\sum_{\substack{m=1\\(m\neq j)}}^{N}\mathcal{G}_B C_{jm}+\frac{1}{i}\sqrt{2}\mathcal{G}_B C_{jj}, \tag{8.24}$$

$$\dot{C}_{jm} = \frac{1}{i}(\delta_j+\delta_m)C_{jm}+\frac{1}{i}(\mathcal{G}_A(a_j+a_m)+\mathcal{G}_B(b_j+b_m)), \tag{8.25}$$

$$\dot{C}_{jj} = \frac{2}{i}\delta_j C_{jj}+\frac{1}{i}\sqrt{2}(\mathcal{G}_A a_j+\mathcal{G}_B b_j), \tag{8.26}$$

where j,m are mode indexes running over all discrete modes and $\Delta_{A(B)} = \delta_{A(B)} - S_{A(B)}$. Throughout this section we restrict ourselves to the regime of small inter-atomic distances where C_M remains practically constant, i.e., $C_M \approx \sqrt{C_A C_B}$, while $\tilde{V}_{AB}$ increases rapidly as we reduce the inter-atomic separation.

8.2.1 Non-Identical Atoms

The set of differential equations (8.22)-(8.26) is solved for 170 discrete modes ($\omega_{up} \approx 13C_A^{2/3}, \delta\omega \approx 4.4\times10^{-4}C_A^{2/3}$) and the results are presented in Fig. 8.3. We plot the population in the fully excited state (solid line), the symmetric state (dashed line), the antisymmetric state (dot-dashed line) and the ground state (dotted line) of the system as functions of time, for various atomic detunings from the band-edge frequency, and different inter-atomic couplings.

In the picture of Dicke states, the system of the two TLAs resembles a double ladder system (Fig. 8.1). From the known dynamics of a cascade three-level atom with both its transitions at the edge of a PBG, we may expect three different decay channels. Specifically, the system can make the transition $|\psi_{ee}\rangle \rightarrow |\psi_{gg}\rangle$ either via one of the possible stepwise processes, i.e., $|\psi_{ee}\rangle \rightarrow |\psi^{(+)}\rangle \rightarrow |\psi_{gg}\rangle$ and $|\psi_{ee}\rangle \rightarrow |\psi^{(-)}\rangle \rightarrow |\psi_{gg}\rangle$ (solid arrows in Fig. 8.1), or via a direct two-photon process ($|\psi_{ee}\rangle \rightarrow |\psi_{gg}\rangle$) (dashed arrows in Fig. 8.1). The latter case involves a collective decay of the system and the corresponding effective detuning from the band-edge frequency is defined as $\Delta^{(2)} = \delta_A + \delta_B$. Which of the three routes the system will follow to arrive at $|\psi_{gg}\rangle$ depends on the position of the upper transitions, $|\psi_{ee}\rangle \rightarrow |\psi^{(+)}\rangle$ and $|\psi_{ee}\rangle \rightarrow |\psi^{(-)}\rangle$, with respect to the band-edge frequency. Let δ_+, δ_- be the relative detunings for $|\psi_{ee}\rangle \rightarrow |\psi^{(+)}\rangle$ and $|\psi_{ee}\rangle \rightarrow |\psi^{(-)}\rangle$, respectively. It can be shown that

$$\delta_\pm = \frac{\delta_A+\delta_B}{2} \mp \frac{\sqrt{(\delta_A-\delta_B)^2+4\tilde{V}_{AB}^2}}{2}, \tag{8.27}$$

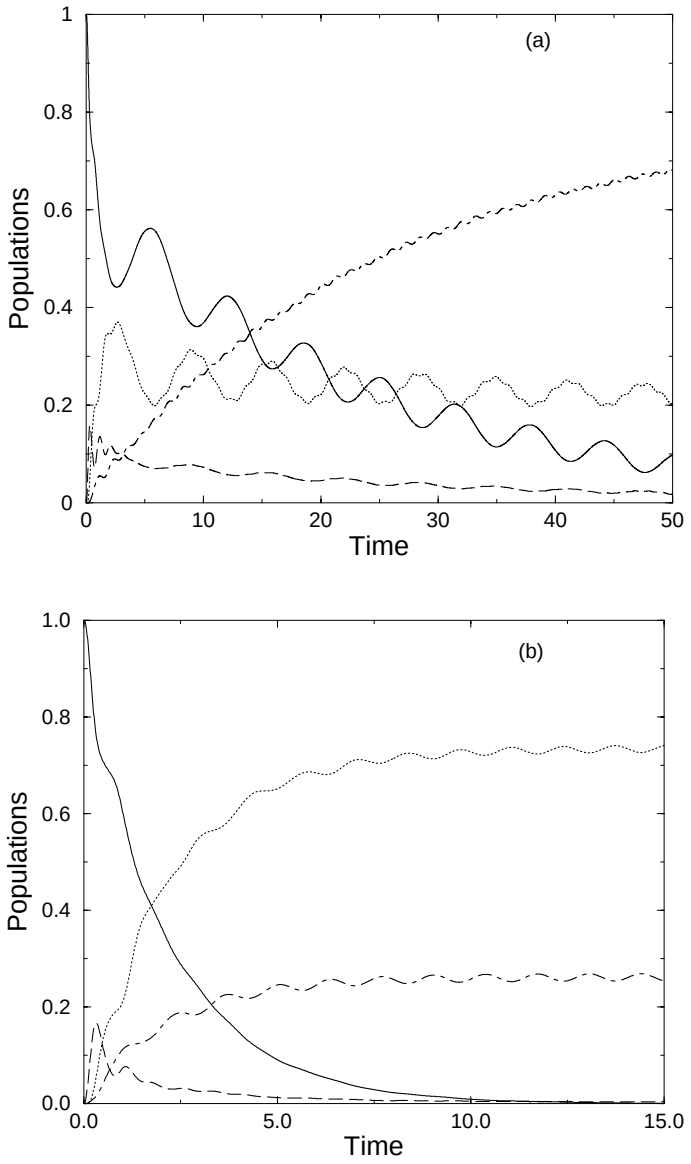

Fig. 8.3: The population in the Dicke states as function of time. The solid line is for $|\psi_{ee}\rangle$, the dashed line for $|\psi^{(+)}\rangle$, the dot-dashed line for $|\psi^{(-)}\rangle$ and the dotted line for $|\psi_{gg}\rangle$. Parameters: $C_B = 1.5C_A$; (a) $\delta_A = 2C_A^{2/3}$, $\delta_B = -2C_A^{2/3}$ and $\tilde{V}_{AB} = 5C_A^{2/3}$; (b) $\delta_A = 5C_A^{2/3}$, $\delta_B = -2C_A^{2/3}$ and $V_{AB} = 5C_A^{2/3}$. The time is in units of $C_A^{2/3}$.

while the corresponding couplings to each one of the discrete modes read

$$\mathcal{G}_{\pm} = \left(C_1^{\pm} \mathcal{G}_B + C_2^{\pm} \mathcal{G}_A \right), \tag{8.28}$$

with $\mathcal{G}_A$, $\mathcal{G}_B$ being defined in Eqs. (8.8) and (8.9). For the two remaining (subsequent) transitions, $|\psi^{(+)}\rangle \rightarrow |\psi_{gg}\rangle$ and $|\psi^{(-)}\rangle \rightarrow |\psi_{gg}\rangle$, the relative detunings from the band-edge are δ_- and δ_+ respectively.

Clearly, both $\delta_{\pm}$ depend on the DDI which, for given atomic detunings ($\delta_{A(B)}$), is the one that determines the atomic dynamics. For instance, if both atomic detunings $\delta_{A(B)}$ are positive or negative and $\tilde{V}_{AB}^2 < \delta_A \delta_B$, $\delta_{\pm}$ are also positive or negative respectively. This means that all transitions in the four-level configuration are inside or outside the gap. In the latter case, the system exhibits open-space behavior while in the former, all transitions are suppressed. On the contrary, if $\tilde{V}_{AB}^2 > \delta_A \delta_B$, irrespective of the atomic detunings, we have $\delta_- > 0$ and $\delta_+ < 0$. The transitions $|\psi_{ee}\rangle \rightarrow |\psi^{(-)}\rangle$ and $|\psi^{(+)}\rangle \rightarrow |\psi_{gg}\rangle$ therefore, are in the allowed part of the continuum, while $|\psi_{ee}\rangle \rightarrow |\psi^{(+)}\rangle$ and $|\psi^{(-)}\rangle \rightarrow |\psi_{gg}\rangle$ lie inside the gap.

In Fig. 8.3(a), we plot the populations in the Dicke states for $\delta_A = 2C_A^{2/3}$, $\delta_B = -2C_A^{2/3}$ and $\tilde{V}_{AB} = 5C_A^{2/3}$. First of all note that for this particular choice of parameters, $\tilde{V}_{AB}^2 > \delta_A \delta_B$ and $\Delta^{(2)} = 0$. Hence, the two-photon process dominates over the channel $|\psi_{ee}\rangle \rightarrow |\psi^{(+)}\rangle \rightarrow |\psi_{gg}\rangle$, which is suppressed since its upper transition is inside the gap ($\delta_+ < 0$). In analogy to the coupling of a cascade three-level atom to a PBG reservoir (Chap. 6), our four-level system evolves in time as if the fully excited state were coupled to the symmetric state via a single-photon process and simultaneously coupled to the ground state via a direct two-photon process. We have thus a counter-intuitive evolution of the system which is expressed through the oscillations in the populations of $|\psi_{ee}\rangle$, $|\psi^{(+)}\rangle$, $|\psi_{gg}\rangle$. On the other hand, the direct two-photon transition compete with the alternative stepwise decay route $\left(|\psi_{ee}\rangle \rightarrow |\psi^{(-)}\rangle \rightarrow |\psi_{gg}\rangle \right)$, which leads the system to a nearly exponential decay into $|\psi^{(-)}\rangle$ and finally the formation of a *"two-photon + two-atom" bound state* due to the fact that $\delta_+ < 0$. The oscillations between the populations in $|\psi^{(-)}\rangle$ and $|\psi_{gg}\rangle$ stem from the emission and reabsorption of photons in the transition $|\psi^{(-)}\rangle \rightarrow |\psi_{gg}\rangle$. If the atomic detunings are chosen such that both $\Delta^{(2)}, \delta_- > 0$, the oscillations between the populations of $|\psi_{ee}\rangle$ and $|\psi_{gg}\rangle$ disapear, indicating that the two-photon transition lies outside the gap, whereas the oscillations associated with the transition $|\psi^{(-)}\rangle \rightarrow |\psi_{gg}\rangle$ persist. Such a case is depicted in Fig. 8.3(b).

Choosing both atomic transition frequencies being well inside the gap and for relatively large values of $\tilde{V}_{AB}$, all the decay channels are practically forbidden (Fig. 8.4). In fact, the only allowed transition in our system is $|\psi_{ee}\rangle \rightarrow |\psi^{(-)}\rangle$, which falls in the allowed part of the continuum and as such, is purely Markovian and involves an exponential decay. Thus, the system

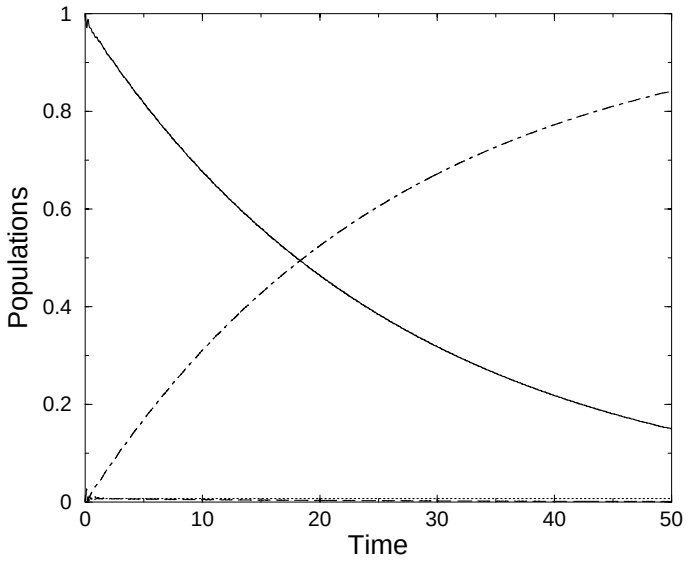

Fig. 8.4: The population in the Dicke states as function of time. The solid line is for $|\psi_{ee}\rangle$, the dashed line for $|\psi^{(+)}\rangle$, the dot-dashed line for $|\psi^{(-)}\rangle$ and the dotted line for $|\psi_{gg}\rangle$. Parameters: $C_B = 1.5C_A$, $\delta_A = -10C_A^{2/3}$, $\delta_B = -8C_A^{2/3}$ and $\tilde{V}_{AB} = 15C_A^{2/3}$. The time is in units of $C_A^{2/3}$.

will eventually end up in a purely antisymmetric atomic state of the form

$$|\psi_f\rangle = \alpha|e_A, g_B\rangle + \beta|g_A, e_B\rangle, \tag{8.29}$$

where there is no entanglement between the atoms and the field. Let $\mathcal{F}$ be the fidelity of the final state with respect to $|\psi^{(-)}\rangle$.

As long as the DOS is zero over a range of frequencies and $\delta_+ \ll 0$, the state of the atomic system in the long-time limit will be $|\psi_f\rangle = |\psi^{(-)}\rangle$ ($\mathcal{F} = \mathcal{F}_{max} = 1$) (Fig. 8.4). Furthermore, under such conditions, the two atoms will be entangled forever, which mathematically implies $t \to \infty$. In a real photonic crystal, however, the gap involves a range of frequencies over which DOS is several orders of magnitude smaller than its open-space value. As a result, the life-time of $|\psi_f\rangle$ is finite, while due to losses via the channel $|\psi_{ee}\rangle \to |\psi^{(+)}\rangle \to |\psi_{gg}\rangle$, the final state diverges from $|\psi^{(-)}\rangle$ ($\mathcal{F} < \mathcal{F}_{max}$). Nevertheless, even in this case, the decay rate for the transitions $|\psi_{ee}\rangle \to |\psi^{(+)}\rangle$ and $|\psi^{(-)}\rangle \to |\psi_{gg}\rangle$ is much smaller than open-space decay rate (since $\rho(\delta_+) \ll \rho_o$), and thus $\mathcal{F} \approx \mathcal{F}_{max}$ while the time scale over which the atomic system remains trapped in $|\psi_f\rangle$ can be so long that for all practical purposes is equivalent to $t \to \infty$.

Another point which should be also noted here is the dependence of the coefficients C_1^- and C_2^- in $|\psi^{(-)}\rangle$, on the inter-atomic coupling as well as the atomic detunings [Eq. (8.21)]. Hence, to prepare a desired entangled

state of the atoms, one actually needs a mechanism that controls either the inter-atomic separation or one of the atomic detunings, with the latter one being more feasible. For instance, one possibility is to use an external weak laser field with frequency outside the gap, which couples the upper state of one of the atoms, off-resonantly to higher atomic states. In this way we avoid population transfer to higher atomic levels, while simultaneously we are able to tune the atomic transition frequency, with respect to the band-edge. Alternatively, the same result can be achieved by means of an external static field. In conclusion, if we are able to control losses as well as the perfection of the gap, we may then have a way to entangle non-identical atoms in a controllable way.

8.2.2 Identical Atoms

Let's consider now the case of two identical atoms, i.e., $C_A = C_B = C$, $\delta_A = \delta_B = \delta_e$. The symmetric and antisymmetric atomic states read

$$|\psi^{(\pm)}\rangle = \frac{1}{\sqrt{2}}\left(|e_A, g_B\rangle \pm |g_A, e_B\rangle\right), \tag{8.30}$$

while the couplings $\mathcal{G}_\pm$ are given by

$$\mathcal{G}_\pm = \frac{1}{\sqrt{2}}\left(\mathcal{G}_B \pm \mathcal{G}_A\right), \tag{8.31}$$

and using Eqs. [(8.6)-(8.9)], we obtain

$$\mathcal{G}_\pm = \frac{1}{\sqrt{2}}\mathcal{G}_A\left(\tau(r) \pm 1\right). \tag{8.32}$$

For small inter-atomic distances we thus have $\mathcal{G}_- \approx 0$, which means that the antisymmetric state $|\psi^{(-)}\rangle$ is decoupled from the initially excited state $|\psi_{ee}\rangle$ and the four-level atomic system (Fig. 8.1) is effectively reduced to a three-level cascade with states $|\psi_{ee}\rangle$, $|\psi^{(+)}\rangle$ and $|\psi_{gg}\rangle$. In other words the evolution of the atomic system is restricted to a Hilbert subspace which involves only symmetrical superradiant, at least in open space, states.

The detunings for the upper and the lower transitions from the band-edge frequency, are δ_+ and δ_- respectively and are given by $\delta_\pm = \delta_e \mp \tilde{V}_{AB}$. Clearly, the effect of the dipole-dipole coupling is to shift the intermediate level towards the gap. Although in open space such shifts are responsible for the so-called frequency chirping effects in superradiance emission, their role near the edge of a gap seems to be rather crucial. In particular, they may be associated with suppression or enhancement of the collective decay. For relatively large values of the inter-atom coupling, ($\tilde{V}_{AB} > \delta_e$), the behavior of the system, resembles that of a single cascade three-level atom with both its transitions near resonantly coupled to the edge of a PBG (Chap. 6). Specifically, for $\delta_+ \leq 0$ and $\Delta^{(2)} \leq 0$ we expect the formation of a

"two-photon + two-atom" bound state which is associated with fractional population trapping in both upper levels, as well as a counterintuitive coherent evolution of all three levels. On the contrary, if $\Delta^{(2)} > 0$ a collective decay of both TLAs takes place.

On the other hand, for small interatomic coupling, i.e., $\tilde{V}_{AB} \ll \delta_e$ the dipole-dipole shift is negligible and the collective atomic levels are practically equidistant leading to problem of superradiance at the edge of a PBG. Introducing the Dicke notation, the Hamiltonian for the system in RWA and in the context of discretization, reads

$$\mathcal{H} = (\omega_o - S)\, J_z + \sum_k \omega_k a_k^\dagger a_k + \sum_k g_k (a_k^\dagger J^- + a_k J^+), \tag{8.33}$$

where the macroscopic atomic dipole and inversion operators $(J^\pm, J_z)$ have been defined in Sec. 3.7, while the shift terms stem from the adiabatic elimination of the off-resonant modes. Accordingly, the wavefunction of the total system can be written in terms of the Dicke states $|1, m\rangle$, where $m \in [-1, 1]$, as

$$|\psi(t)\rangle = bo|1,1\rangle|0\rangle + \sum_j b_j|1,0\rangle|1_j\rangle + \sum_{\substack{n,j \\ (n \geq j)}} b_{jn}|1,-1\rangle|1_j, 1_n\rangle \tag{8.34}$$

with $b_{jn} = b_{nj}$, and from Schrödinger equation we obtain:

$$i\dot{b}_o = (\delta_e - S) b_o + \sqrt{2} \sum_{j=1}^{N} \mathcal{G}_j b_j, \tag{8.35}$$

$$i\dot{b}_j = (\delta_j - S) b_j + 2\mathcal{G}_j b_{jj} + \sqrt{2} \sum_{\substack{n=1 \\ (n \neq j)}}^{N} \mathcal{G}_n b_{jn} + \sqrt{2}\mathcal{G}_j b_o, \tag{8.36}$$

$$i\dot{b}_{jn} = (-\delta_e + \delta_j + \delta_n) b_{jn} + \sqrt{2}\mathcal{G}_j b_n + \sqrt{2}\mathcal{G}_n b_j, \tag{8.37}$$

$$i\dot{b}_{jj} = (-\delta_e + 2\delta_j) b_{jj} + 2\mathcal{G}_j b_j, \tag{8.38}$$

where j, n are indexes over all discrete modes, while all transitions $|1, m\rangle \leftrightarrow |1, m \pm 1\rangle$ are identically coupled to each one of them with a coupling constant given by Eq. (6.9) and ω_{up} is the upper limit of the discretized part of the DOS. The detunings are defined with respect to the band-edge frequency, while the shift term S can be obtained from Eq. (5.19). It is worth noting here the appearance of the factor $\sqrt{2}$ in front of the couplings in Eqs. (8.35)-(8.38), which indicates that the collective radiative decay rate for the two-atom superradiant system in the isotropic PBG model is $2^{2/3}$ times larger than the decay rate of each individual atom. Propagating Eqs. (8.35)-(8.38), for $N = 50$ we obtain the evolution of the initially excited system.

In Fig. 8.5(a), we plot the atomic inversion $\langle J_z \rangle$ as a function of time for various detunings of the atomic resonant frequency from the band-edge.

For detunings far outside the gap (solid line), the dynamics resemble that of a superradiant system in open space; that is the system has completely decayed in the long-time limit. For detunings inside the gap, however, we note a substantially different behavior (dashed and dot-dashed line). After an initial transient regime where part of the population is lost, the superradiant behavior is turned-off and thus a significant part of the total initial excitation remains bound at the atoms, in the long-time limit. The atomic excitation at each time is given by

$$\langle \sigma_1^+ \sigma_1^- + \sigma_2^+ \sigma_2^- \rangle = 2|b_0|^2 + \sum_k |b_k|^2. \tag{8.39}$$

where $\sigma_1^+(\sigma_1^-)$ and $\sigma_2^+(\sigma_2^-)$ are the raising(lowering) atomic operators.

The quantum correlation between the two atoms (1 and 2), as is determined by $\langle \sigma_1^+ \sigma_2^- \rangle$, is plotted in Fig. 8.5(b). In open space, the correlation increases from zero at t=0 to a maximum value as the system cascades down the ladder of Dicke states. The maximum value corresponds to half-excited system and as the system keeps cascading down the ladder, the correlation between the atoms goes to zero. In the PBG case, however, the atoms are correlated in the long-time limit, with the degree of the final correlation being dependent on the atomic detuning from the band-edge. Note also the oscillatory behavior of both inversion and correlation, instead of the exponential decay of open space. Apparently, the behavior of the collection has the main features of the single atom dynamics at the edge of the gap. These oscillations stem from the strong interaction of the ensemble with its own localized radiation which leads to vacuum Rabi splitting of the atomic levels. As we have already discussed, in the isotropic model of DOS these oscillations are more pronounced than any other DOS model.

8.3 Summary

We have studied the radiative dynamics of two nearby TLAs interacting with a PBG continuum. Both atomic transitions have been considered to be near the band-edge frequency. A four-level configuration has been adopted for the description of the system. In analogy to a cascade three-level atom, the localization of the two emitted photons at the site of both atoms, leads to a competition between the two stepwise decay paths and the "direct" two-photon process. The dipole-dipole interaction has been shown to play a pivotal role in this competition. We have further found that the generation of any pure antisymmetric state of two non-identical atoms is possible. For two identical TLAs, the dynamics of the atomic superradiant system for atomic transitions inside the gap, is substantially different than in open space, in terms of the inversion as well as the correlation between the two atoms. Specifically, the system reaches a stable state in the long-time limit

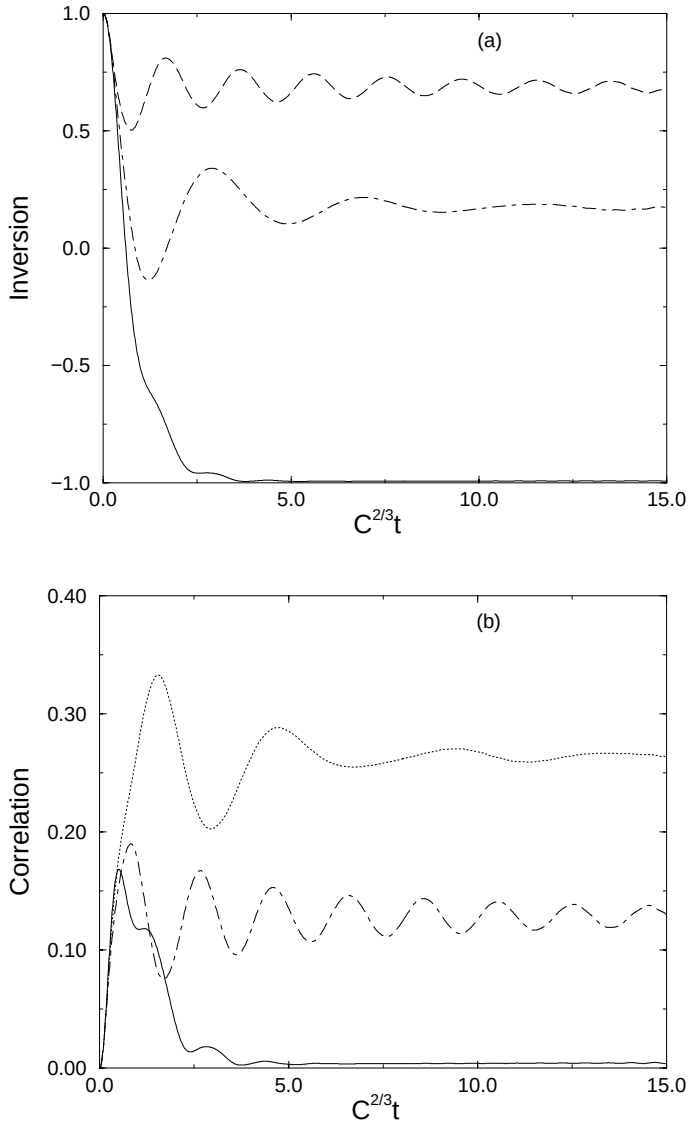

Fig. 8.5: The inversion (a) and the correlation (b) between the two atoms are plotted as functions of time, for various detunings from the band-edge: $\delta_e = -3C^{2/3}$ (dashed line), $\delta_e = -1C^{2/3}$ (dot-dashed line), $\delta_e = 3C^{2/3}$ (solid line). Parameters: $N = 50$, $\omega_u = 10C^{2/3}$.

where a significant part of the excitation remains bound at the atoms. As a result the atoms are correlated with degree of correlation being dependent on the atomic detunings from the band-edge frequency.

Chapter 9

Epilogue

9.1 Thesis summary

The main theme of this thesis is the interaction of small quantum systems with structured radiation reservoirs. This is a problem which emerges in many contexts of physics and the fundamental difficulty in its formulation stems from the invalidation of standard approximations. In particular we focused on the behavior of atomic systems with few quantal degrees of freedom, embedded in PBG materials. Mathematical difficulties had limited relevant investigations to problems involving one-photon fluorescence in the structured photonic continuum. In order to overcome the shortcomings of the Born and Markov approximations and thus be able to deal with multiple excitations in the structured reservoir, in Chap. 5, we proposed and implemented the discretization approach. The idea rests upon the substitution of the near-resonant strongly varying part of the continuum, by a relatively large number of discrete modes. The information about the structure of the continuum is thus incorporated, either in the couplings or the frequencies of these modes. The far off-resonant part of the continuum can be treated perturbatively, while the atomic dynamics can be obtained through the direct solution of a number of coupled differential equations for the amplitudes entering the wavefunction of the total system. Armed with the discretization technique, we then proceeded to address problems beyond single photon-emission at the edge of a PBG continuum.

Specifically, in Chap. 6 we investigated the dynamics of a ladder atomic system with both transitions coupled to the same structured reservoir and we found that this system supports a "two-photon + atom" bound state which leads to a fractional population trapping in both of the upper states. In addition we have shown that due to the localization of two photons at the site of the atom, a "direct" two-photon process coexists with a stepwise one. Which of the two dominates is determined mainly by the detuning of the upper transition from the band-edge.

In Chap. 7, we elaborated on certain aspects of resonance fluorescence close to the edge of a PBG. An atom with transition frequency near the edge of a gap is driven by an initially populated defect-mode centered at a frequency inside the gap. Irrespective of the state of the defect-field, the splitting of the atomic levels due to the coupling between the atom and the defect-mode, may lead to a significant excitation trapping in the long-time limit, while the atomic population may exhibit inversion. Furthermore, if both atom and defect-mode are slightly detuned from the band-edge we have shown that after some initial time, the atom may become transparent to the defect-field.

Finally, in Chap. 8, we studied the radiative dynamics of two nearby TLAs interacting with a PBG continuum. In analogy to the ladder system, the localization of the two emitted photons at the site of both atoms, leads to a competition between the stepwise decay path(s) and the "direct" two-photon process. The dipole-dipole interaction has been shown to play a pivotal role in this competition, and accordingly in the enhancement of the collective atomic decay. On the other hand, dipole-dipole interaction may lead the atomic system to a pure antisymmetric state. If both atomic transitions lie far inside the gap, the system reaches a stable state where a significant part of the excitation remains bound at the collection and the atoms are correlated in the long-time limit.

9.2 Outlook

To the best of our knowledge, no experiments probing the atomic dynamics in PBG structures have been carried out so far, since large-scale PCs exhibiting full 3D band gap in optical regime are not available yet. There have been only some experimental verifications of inhibition and suppression of fluorescence by dye molecules embedded in opal structures [93, 99, 106, 129, 132]. For this reason, throughout this thesis we have not considered any specific atomic transition or a real DOS for the photonic continuum and our studies had a model character. Nevertheless, as we have alluded to Sec. 4.1, the LDOS (the DOS at the location of the atom) is the one that is expected to play a pivotal role in any quantum optical experiment and not the total DOS [112]. Furthermore, even if the existed PCs do not exhibit a full PBG, their LDOS may exhibit pseudogaps as well as Van-Hove singularities, providing thus the appropriate "colored vacuum" for many of the novel phenomena we have discussed to be observed. It is thus likely that the first quantum optical experiments will be performed in the near future and at that time, in order to compare theory with experiment, realistic parameters for both the atom and the photonic DOS will be necessary.

From that point of view, discretization is a rather promising approach, in the sense that it allows a direct incorporation of realistic band-structure

calculations into investigations of the dynamics of atoms embedded in PCs. Specifically, the coupling constants and frequencies corresponding to each one of the discrete modes can be obtained from band-structure calculations and thus the discretization provides a way of interpreting experimental results. On the other hand, as we have shown in this thesis, the discretization is capable of handling at least few photons in structured radiation reservoirs of any DOS. The limitation on the number of photons that can be treated through the discretization comes from purely computational considerations, at least in the present form of the approach. Whether an alternative form may improve the efficiency and the accuracy of the approach in terms of the CPU time and computer memory, remains to be seen.

The doors are, therefore, open for the development of new theoretical methods, and the improvement of the already existing ones, to deal with many-excitation non-Markovian problems in the context of radiation reservoirs of any DOS. As we have seen, by adding one and two photons to the systems we have discussed in this thesis, a variety of unexpected phenomena has emerged. We may thus say with certainty that their many-photon extension will introduce considerable further richness in the behavior of few-level atomic systems coupled to strongly modified radiation reservoirs.

Appendix A

Application of QMC and QSD

A general idea of QMC and QSD methods has been given in Chap. 3. In this appendix, we apply the methods to the problem of resonance fluorescence by a single TLA, in open space [81]. The atom-laser Hamiltonian in an interaction picture rotating at the laser frequency and in RWA is:

$$\mathcal{H}_s = \Delta_L \sigma_z + \frac{\Omega}{2}(\sigma^+ + \sigma^-), \tag{A.1}$$

while we have only one Lindbland operator $L^\dagger = \sqrt{\gamma_a}\sigma^+$, where γ_a is the atomic decay rate, and the master equation describing the dynamics of the system is given by Eq. (3.74). Let's assume that the combined system (atom + field) at time t is described by the wave function

$$|\psi(t)\rangle \equiv (a_e|e\rangle + a_g|g\rangle)|\{0_\lambda\}\rangle, \tag{A.2}$$

and let dt be a time interval such that $dt << \gamma_a^{-1}, \Omega^{-1}, \Delta_L^{-1}$. This ensures that at most one photon can be emitted within this interval.

In the context of QMC approach, the wavefunction at time $t + dt$ can be obtained by evolving $|\psi(t)\rangle$ during the interval dt, with the non-Hermitian Hamiltonian

$$\mathcal{H}_u = \mathcal{H}_s - \frac{i\gamma_a}{2}\sigma^+\sigma^-. \tag{A.3}$$

Simultaneously, we compare the probability of having spontaneous emission during dt, which is $dp = \gamma_a|a_e|^2 dt$, with a random number ε uniformly distributed within $[0, 1]$. We have thus two possibilities:

- If $dp > \varepsilon$, the new normalized wave-function at $t + dt$ is

$$|\psi(t + dt)\rangle = \frac{e^{-i\mathcal{H}_u t}|\psi(t)\rangle}{\sqrt{1 - dp}}. \tag{A.4}$$

- If $\varepsilon < dp$ a *quantum jump* occurs which is associated with the projection of the wavefunction onto the ground state $|g\rangle$ and the detection of

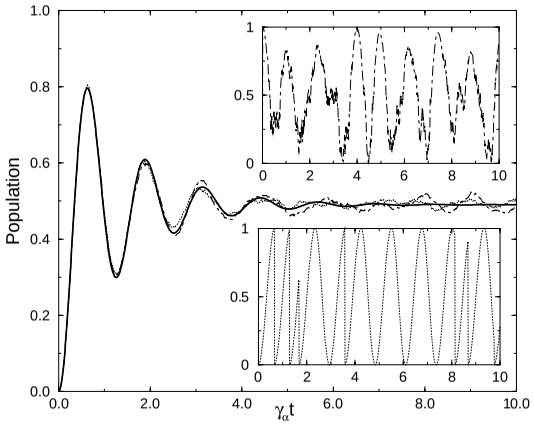

Fig. A.1: The population in the upper state of a two-level atom, driven by a classical field is plotted as function of the dimensionless time $\gamma_a t$. The solid line corresponds to the solution obtained by a master equation. The dotted and dot-dashed lines correspond to the solutions obtained by QSD and QMC methods respectively, for 1000 simulations. The insets show the solutions obtained by a single simulation. Parameters: $\Omega = 5\gamma_a$, $\Delta_L = 0$.

a photon. Assuming that after each *gedanken measurement* the photon is annihilated, the wave-function at $t + dt$ reads

$$|\psi(t + dt)\rangle = |g\rangle|\{0_\lambda\}\rangle. \tag{A.5}$$

The QSD equation for the problem at hand reads,

$$\frac{d|\psi(t)\rangle}{dt} = -i\mathcal{H}_s|\psi(t)\rangle + \frac{\gamma_a}{2}(2\langle\sigma^+\rangle\sigma^- + \sigma^+\sigma^-)|\psi(t)\rangle + \sqrt{\frac{\gamma_a}{2}}\sigma^-|\psi(t)\rangle d\xi, \tag{A.6}$$

where $d\xi$ is a complex differential random variable such that

$$\langle d\xi\rangle = 0 = \langle d\xi^2\rangle, \quad \langle d\xi d\xi^*\rangle = 2dt. \tag{A.7}$$

As in the QMC method, Eq. (A.6) does not preserve the norm and thus the state vector $|\psi(t)\rangle$, needs to be renormalized at each step. In Fig. A.1, we show the convergence of the QMC and QSD methods with respect to the result obtained by the master-equation approach.

Appendix B

A Photonic Band-Gap in the Scalar Approximation

The propagation of a monochromatic electromagnetic wave in an inhomogeneous, non-dissipative dielectric medium is governed by the following equation

$$-\nabla^2\mathbf{E} + \nabla(\nabla\cdot\mathbf{E}) - \frac{\omega^2}{c^2}\epsilon_f(\mathbf{r})\mathbf{E} = \bar{\epsilon}\frac{\omega^2}{c^2}\mathbf{E}, \tag{B.1}$$

where ω and c are the frequency and the speed of light in the medium, whose dielectric constant has been written as its average value $\bar{\epsilon}$, plus a fluctuating part, i.e., $\epsilon(\mathbf{r}) = \bar{\epsilon} + \epsilon_f(\mathbf{r})$, while $\epsilon(\mathbf{r}) > 0$. The term $\frac{\omega^2}{c^2}\bar{\epsilon}$ on the right hand side of Eq. (B.1) can be viewed as an energy eigenvalue, whereas the term $\frac{\omega^2}{c^2}\epsilon_f(\mathbf{r})$, as a "potential". From this point of view, Eq. (B.1) is the electromagnetic analogue of the Schrödinger equation.

Let us consider now an 1D crystal, consisting of periodically arranged dielectric scatterers of radius a and refractive index n. Setting $\bar{\epsilon} = 1$, the wave-equation (B.1) reads

$$-\nabla^2\psi(x) + \Phi(x)\psi(x) = \frac{\omega^2}{c^2}\psi(x), \tag{B.2}$$

where $\Phi(x) = -\frac{\omega^2}{c^2}\epsilon_f(x)$ is the periodic "potential", and

$$\epsilon_f(x) = \sum_{m=-\infty}^{m=\infty} u(x - mL), \tag{B.3}$$

with $L = 2a + b$ being the lattice constant and

$$u(x) = \begin{cases} n^2 - 1, & |x| < a \\ 0, & \text{otherwise.} \end{cases} \tag{B.4}$$

The "potential" can thus be viewed as a sequence of "potential-barriers" $u(x)$, of width $2a$ (Fig. B.1). Restricting ourselves to a unit cell of the

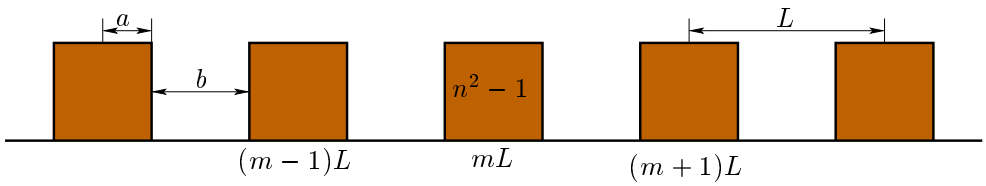

Fig. B.1: The periodic "potential" in the isotropic model

crystal, the wave function can be written as

$$\psi(x) = \begin{cases} Ae^{i\kappa x} + Be^{-i\kappa x}, & x < -a \\ Ce^{i\kappa' x} + De^{-i\kappa' x}, & |x| < a \\ Ee^{i\kappa x} + Fe^{-i\kappa x}, & x > a \end{cases} \tag{B.5}$$

where $\kappa = \omega/c$ and $\kappa' = n\omega/c$. According to the Floquet theorem, $\psi(x)$ must satisfy the following relation

$$\psi(x+L) = e^{ikL}\psi(x), \tag{B.6}$$

for suitable k and accordingly

$$\frac{d\psi(x+L)}{dx} = e^{ikL}\frac{d\psi(x)}{dx}. \tag{B.7}$$

Furthermore, both $\psi(x)$ and $d\psi/dx$ must be continuous at $x = \pm a$. Applying all these conditions, we may obtain the coefficients entering the wavefunction, as well as the following transcendental equation:

$$\cos(kL) = cos\left(\frac{2na\omega}{c}\right) cos\left(\frac{b\omega}{c}\right) - \frac{n^2+1}{2n} sin\left(\frac{2na\omega}{c}\right) sin\left(\frac{b\omega}{c}\right), \tag{B.8}$$

which for $b = 2na$ can be solved analytically, yielding the dispersion relation for the 1D crystal,

$$\omega_k = \frac{c}{4na} arccos\left[\frac{4ncos(2ka(1+n)) + (1-n)^2}{(1+n)^2}\right]. \tag{B.9}$$

List of Figures

Bibliography

[1] G. S. Agarwal. *Quantum Statistical Theories of Spontaneous Emission and their Relation to other Approaches*, volume 70 of *Springer Tracts in Modern Physics*. Springer, Berlin, 1974.

[2] L. Allen and J. H. Eberly. *Optical Resonance and Two-Level Atoms*. Dover Publications, New York, 1987.

[3] A. V. Andreev, V. I. Emel'yanov, and Yu A. Il'inskiĭ. *Cooperative Effects in Optics: Superradiance and Phase Transitions*. Malvern Physics Series. Institute of Physics Publishing, Bristol and Philadelphia, 1993.

[4] S. Bay. *Quantum Optics In Structured Radiation Reservoirs*. PhD thesis, Institute of Physics and Astronomy, University of Aarhus, 1998.

[5] S. Bay and P. Lambropoulos. *Opt. Comm.*, 146:130, 1998.

[6] S. Bay, P. Lambropoulos, and K. Mølmer. *Phys. Rev. A*, 55:1485, 1997.

[7] S. Bay, P. Lambropoulos, and K. Mølmer. *Phys. Rev. Lett.*, 79:2654, 1997.

[8] S. Bay, P. Lambropoulos, and K. Mølmer. *Phys. Rev. A*, 57:3065, 1998.

[9] J. M. Bendickson, J. P. Dowling, and M. Scalora. *Phys. Rev. E*, 53:4107, 1996.

[10] A. Blanco, E. Chomski, S. Grabtchak, M. Ibisate, S. John, S. W. Leonard, C. Lopez, F. Meseguer, H. Miguez, J. P. Mondia, G. A. Ozin, O. Toader, and M. van Driel. *Nature*, 405:437, 2000.

[11] V. N. Bogomolov, S. V. Gaponenko, A. M. Kapitonov, A. V. Prokofiev, A. N. Ponyavina, N. I. Silvanovich, and S. M. Samoilovich. *Appl. Phys. A*, 63:613, 1996.

[12] S. Brattke, B. T. H. Varcoe, and H. Walther. *Opt. Express.*, 8:131, 2001.

[13] H. P. Breuer, B. Kappler, and F. Petruccione. *Phys. Rev. A*, 59:1633, 1999.

[14] M. Brune, F. Schmidt-Kaler, A. Maali, J. Dreyer, E. Hagley, J. M. Raimond, and S. Haroche. *Phys. Rev. Lett.*, 76:1800, 1996.

[15] K. Busch and S. John. *Phys. Rev. E*, 58:3869, 1998.

[16] K. Busch and S. John. *Phys. Rev. Lett.*, 83:967, 1999.

[17] V. P. Bykov. *Sov. Phys. JETP*, 35:269, 1972.

[18] A. O. Caldeira and A. J. Leggett. *Ann. Phys. (N.Y.)*, 149:374, 1994.

[19] H. Carmichael. *An Open Systems Approach to Quantum Optics*, volume 18 of *Lecture Notes in Physics*. Springer-Verlag, Berlin, 1993.

[20] C. C. Cheng, V. Arbet-Engels, A. Scherer, and E. Yablonovitch. *Phys. Scripta*, 68:17, 1996.

[21] C. Cohen-Tannoudji, J. Dupont-Roc, and G. Grynberg. *Atom-Photon Interactions*. Wiley, New York, 1992.

[22] S. Curtis. *Vacuum Solutions*, page 19, 1999.

[23] J. Dalibard, Y. Castin, and K. Mølmer. *Phys. Rev. Lett.*, 68:580, 1992.

[24] R. H. Dicke. *Phys. Rev.*, 93:99, 1954.

[25] L. Diósi, N. Gisin, and W. T. Strunz. *Phys. Rev. A*, 58:1699, 1998.

[26] J. P. Dowling and C. M. Bowden. *Phys. Rev. A*, 46:612, 1992.

[27] J. P. Dowling, M. Scalora, M. J. Bloemer, and C. M. Bowden. *J. Opt. Soc. Am. B*, 75:1896, 1994.

[28] R. Dum, A. S. Parkins, P. Zoller, and C. W. Gardiner. *Phys. Rev. A*, 46:4382, 1992.

[29] S. Fan, P. R. Villeneuve, J. D. Joannopoulos, and H. A. Haus. *Opt. Express.*, 3:4, 1998.

[30] S. Fan, P. R. Villeneuve, J. D. Joannopoulos, and H. A. Haus. *Phys. Rev. Lett.*, 80:960, 1998.

[31] J. G. Fleming and S. Y. Lin. *Opt. Lett.*, 24:49, 1999.

[32] I. S. Fogel, J. M. Bendickson, M. D. Tocci, M. J. Bloemer, M. Scalora, C. M. Bowden, and J. P. Dowling. *Pure and Appl. Opt.*, 7:393, 1998.

[33] C. W. Gardiner. *Handbook of stochastic methods in physics, chemistry and natural sciences*. Springer-Verlag, Berlin, 1985.

[34] C. W. Gardiner, A. S. Parkins, and P. Zoller. *Phys. Rev. A*, 46:4363, 1992.

[35] C. W. Gardiner and Zoller. *A Handbook of Markovian and non-Markovian quantum stochastic methods, with applications to quantum optics*. Springer-Verlag, Berlin, 2000.

[36] B. M. Garraway. *Phys. Rev. A*, 55:2290, 1997.

[37] B. M. Garraway. *Phys. Rev. A*, 55:4636, 1997.

[38] H. Giessen, J. D. Berger, G. Mohs, P. Meystre, and S. F. Yelin. *Phys. Rev. A*, 53:2816, 1996.

[39] N. Gisin and I.C. Percival. *J. Phys. A*, 25:567, 1992.

[40] N. Gisin and I.C. Percival. *J. Phys. A*, 26:2233, 1993.

[41] N. Gisin and I.C. Percival. *J. Phys. A*, 26:2245, 1993.

[42] M. L. Goldberger and K. M. Watson. *Collision Theory*. Wiley, New York, 1964.

[43] E. V. Goldstein and P. Meystre. *Phys. Rev. A*, 56:5135, 1997.

[44] M. Gross and S. Haroche. *Phys. Rep.*, 93:301, 1982.

[45] K. M. Ho, C. T. Chan, and C. M. Soukoulis. *Phys. Rev. Lett.*, 65:3152, 1990.

[46] K. M. Ho, C. T. Chan, C. M. Soukoulis, R. Biswas, and M. Sigalas. *Solid State Comm.*, 89:413, 1994.

[47] A. Imamoglu. *Phys. Rev. A*, 50:3650, 1994.

[48] M. W. Jack, M. J. Collet, and D. F. Walls. *J. Opt. B*, 1:452, 1999.

[49] J. D. Joannopoulos. *Photonic Crystals:Molding the Flow of Light*. Princeton University Press, Princeton, 1995.

[50] J. D. Joannopoulos, P. R. Villeneuve, and S. Fan. *Nature*, 386:143, 1997.

[51] S. John. *Phys. Rev. Lett.*, 58:2486, 1987.

[52] S. John. *Phys. Today*, page 32, May 1991.

[53] S. John and T. Quang. *Phys. Rev. A*, 50:1764, 1994.

[54] S. John and T. Quang. *Phys. Rev. A*, 52:4083, 1995.

[55] S. John and T. Quang. *Phys. Rev. A*, 54:4479, 1995.

[56] S. John and T. Quang. *Phys. Rev. Lett.*, 74:3419, 1995.

[57] S. John and T. Quang. *Phys. Rev. Lett.*, 76:2484, 1996.

[58] S. John and T. Quang. *Phys. Rev. Lett.*, 78:1888, 1997.

[59] S. John and J. Wang. *Phys. Rev. Lett.*, 64:2418, 1990.

[60] S. John and J. Wang. *Phys. Rev. B*, 43:127772, 1991.

[61] D. Kleppner. *Phys. Rev. Lett.*, 47:233, 1981.

[62] A. G. Kofman, G. Kurizki, and B. Sherman. *J. Mod. Opt*, 41:353, 1994.

[63] G. I. Kweon and N. M. Lawandy. *J. Mod. Opt*, 41:311, 1994.

[64] P. Lambropoulos, G. M. Nikolopoulos, T. R. Nielsen, and S. Bay. *Rep. Prog. Phys.*, 63:455, 2000.

[65] B. G. Levi. *Phys. Today*, page 17, 1999.

[66] B. G. Levi. *Phys. Today*, page 20, 1999.

[67] M. Lewenstein and T. W. Mossberg. *Phys. Rev. A*, 37:2048, 1988.

[68] M. Lewenstein, J. Zakrzewski, and T. W. Mossberg. *Phys. Rev. A*, 38:808, 1988.

[69] Z. Y. Li and Y. Xia. *Phys. Rev. B*, 63, 2001.

[70] H-B. Lin, R. J. Tonucci, and A. J. Campillo. *Opt. Lett.*, 23:94, 1998.

[71] S-Y. Lin, E. Chow, S. G. Johnson, and J. D. Joannopoulos. *Opt. Lett.*, 25:1297, 2000.

[72] S-Y. Lin, J. G. Fleming, M. M. Sigalas, R. Biswas, and K. M. Ho. *Phys. Rev. B*, 59:15579, 1999.

[73] S-Y. Lin, V. M. Hietala, S. K. Lyo, and A. Zaslavsky. *Appl. Phys. Lett.*, 68:3233, 1996.

[74] R. Loudon. *The quantum theory of light.* Clarendon Press Oxford, 1983.

[75] W. H. Louisell. *Quantum Statistical Properties.* Wiley New York, 1990.

[76] S. L. McCall, P. M. Platzman, R. Dalichaouch, D. Smith, and S. Schultz. *Phys. Rev. Lett.*, 67:2017, 1991.

[77] M. Megens, J. E. Wijnhoven, A. Lagendijk, and W. L. Vos. *Phys. Rev. A*, 59:4727, 1999.

[78] A. Mekis, J. C. Chen, I. Kurland, S. Fan, P. R. Villeneuve, and J. D. Joannopoulos. *Phys. Rev. Lett.*, 77:3787, 1996.

[79] P. Meystre and M Sargent. *Elements of Quantum Optics*. Springer Verlag, Berlin, 1999.

[80] P. W. Milloni and P. L. Knight. *Phys. Rev. A*, 10:1096, 1974.

[81] K. Mølmer, Y. Castin, and J. Dalibard. *J. Opt. Soc. Am. B*, 10:524, 1993.

[82] T. W. Mossberg and M. Lewenstein. *J. Opt. Soc. Am. B*, 10:340, 1993.

[83] G. M. Moy, J. J. Hope, and C. M. Savage. *Phys. Rev. A*, 59:667, 1999.

[84] G. M. Moy and C. M. Savage. *Phys. Rev. A*, 56:1087, 1997.

[85] R. F. Nabiev, P. Yeh, and J. J. Sanchez-Mondragon. *Phys. Rev. A*, 47:3380, 1993.

[86] G. M. Nikolopoulos, S. Bay, and P. Lambropoulos. *Phys. Rev. A*, 60:5079, 1999.

[87] G. M. Nikolopoulos and P. Lambropoulos. *Phys. Rev. A*, 61:053812, 2000.

[88] G. M. Nikolopoulos and P. Lambropoulos. submitted to. *J. Mod. Opt*, 2001.

[89] G. M. Nikolopoulos and P. Lambropoulos. to appear in. *J. Opt. B*, 2001.

[90] S. Noda, N. Yamamoto, and An. Sasaki. *Japn. J. Appl. Phys.*, 36:909, 1996.

[91] G. Noga, A. Rauschenbeutel, S. Osnaghi, M. Brune, J. M. Raimond, and S. Haroche. *Nature*, 400:239, 1999.

[92] O. Painter, R. K. Lee, A. Scherer, A. Yariv, J. D. O'Brien, P. D. Dapkus, and I. Kim. *Science*, 284:1819, 1999.

[93] E. P. Petrov, V. N. Bogomolov, I. I. Kalosha, and S. V. Gaponenko. *Phys. Rev. Lett.*, 81:77, 1998.

[94] B. M. Plenio and P. L. Knight. *Rev. Mod. Phys.*, 70:101, 1998.

[95] H. Plöhn, M. Thoss, M. Winterstetter, and W. Domcke. *Phys. Rev. A*, 58:1152, 1998.

[96] T. Quang, M. Woldeyohannes, S. John, and G. S. Agarwal. *Phys. Rev. Lett.*, 79:5238, 1997.

[97] G. Rempe, H. Walther, and N. Klein. *Phys. Rev. Lett.*, 58:353, 1987.

[98] M. Rippin and P. L. Knight. *J. Mod. Opt*, 43:807, 1996.

[99] S. G. Romanov, T. Maka, C. M. Torres, M. Müller, and R. Zentel. *Appl. Phys. Lett.*, 75:1057, 1999.

[100] J. J. Sakurai. *Advanced Quantum Mechanics.* Addison-Wesley, New York, 1995.

[101] M. Sargent, M. O. Scully, and W. E. Jr. Lamb. *Laser Physics.* Addison-Wesley, Reading, Mass., 1974.

[102] M. Scalora, J. P. Dowling, C. M. Bowden, and M. J. Bloemer. *J. Appl. Phys.*, 76:2023, 1994.

[103] M. Scalora, J. P. Dowling, C. M. Bowden, and M. J. Bloemer. *Phys. Rev. Lett.*, 73:1368, 1994.

[104] M. Scalora, J. P. Dowling, M. D. Tocci, M. J. Bloemer, C. M. Bowden, and J. W. Haus. *Appl. Phys. B*, 60:57, 1995.

[105] M. Scalora, R. J. Flunn, S. B.Reinhardt, R. L. Fork, M. J. Bloemer, M. D. Tocci, C. M. Bowden, H. S. Ledbetter, J. M. Bendickson, and R. P. Leavitt. *Phys. Rev. E*, 54:1078, 1996.

[106] H. P. Schriemer, H. M. vanDriel, A. F. Koenderink, and W. L. Vos. *Phys. Rev. A*, 63:011801, 2001.

[107] M. O. Scully and M. S. Zubairy. *Quantum Optics.* Cambridge University Press, 1997.

[108] R. Shankar. *Principles of quantum mechanics.* Plenum Press New York, 1994.

[109] B. Sherman, A. G. Kofman, and G. Kurizki. *Appl. Phys. B*, 60:99, 1995.

[110] B. Shore. *The Theory of Coherent Excitation.* John Wiley and Sons, New York, 1990.

[111] B. Shore and P. L. Knight. *J. Mod. Opt*, 40:1195, 1993.

[112] R. Sprik, B. A. van Tiggelen, and A. Lagendijk. *Europhys. Lett.*, 35:265, 1996.

[113] P. Stenius and A. Imamoglu. *Quantum and Semiclass. Opt.*, 8:283, 1996.

[114] W. T. Strunz, L. Diósi, and N. Gisin. *Phys. Rev. Lett.*, 82:1801, 1999.

[115] M. D. Tocci, M. J. Bloemer, M. Scalora, J. P. Dowling, and C. M. Bowden. *Appl. Phys. Lett.*, 66:2324, 1995.

[116] M. D. Tocci, M. Scalora, M. J. Bloemer, J. P. Dowling, and C. M. Bowden. *Phys. Rev. A*, 53:2799, 1996.

[117] B. T. H. Varcoe, S. Brattke, M. Weidinger, and H. Walther. *Nature*, 403:743, 2000.

[118] N. Vats and S. John. *Phys. Rev. A*, 58:4168, 1998.

[119] P. R. Villeneuve, S. Fan, and J. D. Joannopoulos. *Phys. Rev. B*, 54:7837, 1996.

[120] W. L. Vos, R. Sprik, A. Blaaderen, A. Imhof, A. Lagendijk, and G. H. Wegdam. *Phys. Rev. B*, 53:16231, 1996.

[121] D. F. Walls and G. J. Milburn. *Quantum Optics*. Springer Verlag, Berlin, 1994.

[122] H. Wang, J. Shan, T. C. Damen, and L. N. Pfeiffer. *Phys. Rev. Lett.*, 74:3065, 1995.

[123] J. E. Wijnhoven and W. L. Vos. *Science*, 281:802, 1998.

[124] M. Woldeyohannes and S. John. *Phys. Rev. A*, 60:5046, 1999.

[125] E. Yablonovitch. *Phys. Rev. Lett.*, 58:2059, 1987.

[126] E. Yablonovitch. *J. Opt. Soc. Am. B*, 10:283, 1993.

[127] E. Yablonovitch, T. J. Gmitter, and K. M. Leung. *Phys. Rev. Lett.*, 67:3380, 1991.

[128] E. Yablonovitch, T. J. Gmitter, R. D. Meade, K. D. Brommer, A. M. Rappe, and J. D. Joannopoulos. *Phys. Rev. Lett.*, 67:2295, 1991.

[129] T. Yamasaki and T. Tsutsui. *Appl. Phys. Lett.*, 72:1957, 1998.

[130] Y. Yang and S. Y. Zhu. *Phys. Rev. A*, 62:013805, 2000.

[131] Y. Yang and S. Y. Zhu. *Phys. Rev. A*, 62:043809, 2000.

[132] K. Yoshimo, S. B. Lee, S. Tatsuhara, Y. Kawagishi, and M. Osaki. *Appl. Phys. Lett.*, 73:3506, 1998.

[133] T. Yu, L. Diosi, N. Gisin, and W. T. Strunz. *Phys. Rev. A*, 60:91, 1999.

[134] S. Y. Zhu, H. Chen, and H. Huang. *Phys. Rev. Lett.*, 79:205, 1997.

[135] S. Y. Zhu, Y. Yang, H. Chen, H. Zheng, and M. S. Zubairy. *Phys. Rev. Lett.*, 84:2136, 2000.